Universidade de Aveiro Departamento de Engenharia de Materiais e Cerâmica
Ano 2017/2018

Sílvia Tatiana Sá Paiva

SCAFFOLDS DE HIDROGEL/FIBRAS ELECTROFIADAS COM GRADIENTES 3D PARA ORIENTAÇÃO CELULAR EM ENGENHARIA DE TECIDOS ÓSSEOS

HYDROGEL/ELECTROSPUN SCAFFOLD WITH 3D GRADIENTS INTENDED FOR CELL GUIDANCE IN BONE TISSUE ENGINEERING

Universidade de Aveiro Departamento de Engenharia de Materiais e Cerâmica
Ano 2017/2018

Sílvia Tatiana Sá Paiva

SCAFFOLDS DE HIDROGEL/FIBRAS ELECTROFIADAS COM GRADIENTES 3D PARA ORIENTAÇÃO CELULAR EM ENGENHARIA DE TECIDOS ÓSSEOS

HYDROGEL/ELECTROSPUN SCAFFOLD WITH 3D GRADIENTS INTENDED FOR CELL GUIDANCE IN BONE TISSUE ENGINEERING

Dissertação apresentada à Universidade de Aveiro para cumprimento dos requisitos necessários à obtenção do grau de Mestre em Materiais e Dispositivos Biomédicos, realizada sob a orientação científica do Professor José Maria Ferreira do Departamento de Engenharia de Materiais e Cerâmica e da Doutora Ana Sofia Duarte do Departamento de Biologia da Universidade de Aveiro.

Dedico este trabalho à minha mãe.

o júri

presidente	Professora Doutora Maria da Piedade Moreira Brandão professora adjunta da Escola Superior de Saúde da Universidade de Aveiro
arguente	Professora Doutora Catarina Rodrigues de Almeida professora auxiliar em regime laboral do Departamento de Ciências Médicas da Universidade de Aveiro
orientador	Doutora Ana Sofia Direito dos Santos Duarte professora auxiliar convidada do Departamento de Biologia da Universidade de Aveiro

agradecimentos

Agradeço a todos os professores, técnicos, amigos e colegas de curso que acompanharam a minha formação, quer na Universidade de Aveiro, quer na Università degli Studi di Padova, especialmente aos responsáveis pela supervisão da minha dissertação. À Professora Monica Dettin por me ter dado a oportunidade de desenvolver este projecto no seu laboratório, à Doutora Annj Zammuner por me ter guiado nas tarefas laboratoriais. Ao Professor José Maria Ferreira e à Professora Ana Sofia Duarte por terem aceite co-supervisionar o trabalho.

Palavras-chave *Scaffolds* para regeneração óssea, electrofiação, hidrógeis de péptidos auto-agregantes, adesão celular.

Resumo

Scaffolds para a Engenharia de Tecidos (ET) representam hoje em dia a principal estratégia nas terapias de reparação e regeneração óssea. Estas estruturas, actuam essencialmente como materiais de suporte à formação de tecido. São tipicamente semeadas com células e ocasionalmente com factores de crescimento, proporcionando desta forma uma matriz extra-celular (MEC) artificial e temporária para as células formadoras de osso, os osteoblastos.

Nano-fibras de policaprolactona (PCL) obtidas por eletrofiação e hidrogéis à base de péptidos auto-agregantes (*self-assembling peptides - SAPs*), já demonstraram o seu potencial para funcionarem como MECs artificiais, capazes de promoverem a adesão e a captação celular. A combinação de ambos os sistemas na forma de um material compósito para suporte de células em engenharia de tecido ósseo revelou ser bem-sucedida.

Este trabalho descreve a produção de um novo substituto ósseo poroso destinado a promover a penetração de osteoblastos. O substituto consiste numa arquitectura 3D com camadas alternadas de fibras de PCL com hidrogel, e decorado com sinalizadores químicos para favorecer a orientação celular. Esta estrutura explora a capacidade das nano-fibras de PCL para imobilizar moléculas adesivas, após um tratamento superfical apropriado, com a possibilidade de introduzir moléculas solúveis, tais como factores de crescimento, no hidrogel.

O tratamento superficial foi realizado por plasma à pressão atmosférica, para reduzir a hidrofobicidade das fibras de PCL, resultando num ângulo de contacto com a água de 0º, demonstrando assim a sua eficácia. Este tratamento permitiu a deposição de grupos amina capazes de interagir com os grupos aldeído presentes no fragmento da vitronectina humana (351-359), uma sequência adesiva que promove a adesão específica de osteoblastos. Os resultados da viabilidade celular demonstraram que a adesão celular dependia da concentração de HVP, não dependendo do tratamento superficial por plasma. Um *scaffold* decorado com moléculas bioactivas ordenadas de forma a fornecer um gradiente de sinalizadores químicos para as células foi montado e comparado com um *scaffold* para controlo, o qual não incluiu nenhuma espécie de moléculas bioactivas. Ambos resultaram numa espessura total de cerca de 0,30 mm. A análise por microscopia confocal revelou que as células migraram ao longo da espessura dos *scaffolds* até, pelo menos, 50 µm de profundidade, e a utilização de moléculas bioactivas mostrou-se benéfica em termos de proliferação celular.

Keywords Scaffolds for bone regeneration, electrospinning, hydrogels from self-assembling peptides, cell adhesion.

Abstract

Scaffolds for Tissue Engineering (TE) represent nowadays the leading strategy for bone reconstruction and regeneration therapies. The scaffolds essentially act as templates for tissue formation and are typically seeded with cells and occasionally with growth factors, providing a temporary and artificial extra cellular matrix (ECM) for bone-formation cells - the osteoblasts.

Polycaprolactone (PCL) nanofibres obtained by electrospinning and hydrogels from self-assembling peptides (SAPs) have already demonstrated their potential as artificial ECM capable to promote cell attachment and uptake; and the combination of both systems as a composite material has been shown to provide successful results in supporting cells functions in bone TE.

In this work, the bottom-up production of a novel bone substitute construct intended to promote osteoblasts penetration is described. The substitute is composed by a multi-layer scaffold with alternated layers of electrospun PCL fibres and hydrogels from SAPs in a 3D architecture decorated with appropriate chemical guidance cues. This structure explores the advantages of PCL nanofibres to immobilize adhesive molecules after an appropriate surface treatment, and the possibility of hydrogels to incorporate soluble molecules, such as growth factors.

Surface treatment done by atmospheric pressure plasma efficiently reduced the hydrophobicity of the PCL matrices, resulting in a water contact angle of 0º. This treatment allowed the deposition of functional amino groups able to interact with the aldehyde groups presented in the fragment of human vitronectin (351-359), an adhesive sequence that promotes the specific adhesion of osteoblast-like cells. Cell adhesion results, demonstrated that cell attachment is concentration-dependent of the HVP molecule, and does not depend on the plasma surface treatment itself. A functionalized scaffold decorated with bioactive molecules orderly disposed in a gradient, was assembled and compared with a control scaffold, which did not comprise any type of biofunctionalization. Both resulted in a thickness of around 0.30 mm. Confocal microscope analysis showed that cells could migrate, at least, to a depth of 50 µm for both scaffolds, presenting a higher proliferation in the functionalized one, suggesting the efficiency of the bioactive molecules to sustain the cellular viability.

TABLE OF CONTENTS

INDEX OF FIGURES

INDEX OF TABLES

INDEX OF ABBREVIATIONS

3D: Three-Dimensional

A: Alanine

APP: Atmospheric Pressure Plasma

APPJ: Atmospheric Pressure Plasma Jet

APTES: (3-aminopropyl)triethoxysilane

AU: Adimensional Unit

BSA: Bovine Serum Albumin

Boc: tert-(Butyloxycarbonyl)

DCM: Dichloromethane

DIPEA: N,N-diisopropylethylamine

DMF: Dimethylformamide

D-MEM/F12: Dulbecco's Modified Eagle's Medium/Ham's F-12 Nutrient Mixture

E: Glutamic acid

ECM: Extra Cellular Matrix

FBS: Fetal Bovine Serum

Fmoc: 9-Fluorenylmethyloxycarbonyl

HATU: 1-[Bis(dimethylamino)methylene]-1H-1,2,3-triazolo[4,5-b] pyridinium 3-oxid hexafluorophosphate

HBTU: 2-(1H-Benzotriazole-1-yl)-1,1,3,3-tetramethyluronium hexafluorophosphate

HF: High-frequency

HFIP: Hexafluoroisopropanol

HOBt: 1-Hydroxybenzotriazole

HV: High-voltage

HVP: HVP-G$(7)_3$F-(CHO), Human Vitronectin Peptide

IL-6: Interleukin-6

K: Lysine

MALDI: Matrix-assisted laser desorption ionization

MTT: 3-(4,5-dimethylthiazole-2-yl)-2,5-diphenyl tetrazolium bromide

NMP: N-methyl-2-pyrrolidone

PBS: Phosphate *Buffered* Solution

PCL: Poly(ε-caprolactone)

Phe: Phenylalanine

RF: Radio-frequency

rhFGF: Human recombinant Fibroblast Growth Factor

RRM: Regenerative and Reparative Medicine

RP-HPLC: Reverse-phase High Performance Liquid Chromatography

SAPs: Self-assembling peptides

SDS: Sodiumdodecyl sulfate

SP: Semi-Preparative

SPPS: Solid-phase peptide synthesis

TBS: Tris-*Buffered* Saline

TE: Tissue Engineering

TFA: Trifluoracetic acid

UV: Ultra-violet

CHAPTER 1 – INTRODUCTION

1.1 Theoretical Framework

The twentieth century was marked by extraordinary social and medical achievements. With the gain of life expectancy, the need for new therapies becomes fundamental to respond to age-related widespread conditions such as obesity, bone disorders, and allied pathologies.[1] Respecting to bone disorders, osteoporosis is by far the most common bone disease, representing worldwide a huge personal and economic toll. This problem is characterized by compromised bone strength predisposing to an increased risk of fracture that, converted in numbers, represents more than 8.9 million fractures annually, portraying one of the major causes for disability in Europe.[2] The capability for bone to regenerate and repair itself represents an important mechanism to overcome these adversities. However, the bone structure gradually loses its valence over time, requiring even surgical interventions when the fractures reach a critical size. Traditionally, surgery for bone tissue reconstruction opts for the most common reconstructive and repair strategies – the use of bone grafts or implants. There are three main types of bone grafts: autografts, allografts, and bone graft substitutes. Nonetheless, despite the success of these therapeutic solutions, some drawbacks have been pointed out. Concerning the autografts, it disadvantages lays in the limited availability and the fact of mandating an additional surgical procedure with associated donor-site morbidity, risk of infection, and additional cost. In its turn, allografts lack the osteoactive capacity of autografts and carry the risk of infectious agents or immune rejection. To overcome these limitations, Tissue Engineering (TE) appears as an outstanding alternative for the treatment of traumas that can lead damage and degeneration of tissues in the human body.[3,4]

Regenerative and Reparative Medicine (RRM) encompasses tissue engineering and biomaterials in the search for new health solutions. The principle of TE relies extensively on the use of three-dimensional (3D) porous matrices, commonly known as scaffolds. Nowadays, TE scaffolds are the leading technique of repair and regeneration of bone defects. These scaffolds essentially act as a template for tissue formation and are typically seeded with cells and occasionally growth factors. They should allow cell's rapid integration and coalescence into the needed tissue and, hence, start the bone regeneration process. Apart from serving as a temporary and artificial extra cellular matrix (ECM) for growing cells which degrade overtime; scaffolds can be used as a reservoir to deliver bioactive agents to promote regeneration of the injured tissues. An ideal bone graft or scaffold should be made of biomaterials that imitate the structure and properties of natural bone ECM, include osteoprogenitor cells and provide all the necessary environmental cues found in natural bone.[5] Even though the advances in developing new biomaterials for applications in bone substitutes has been steeply increasing, yet none biomaterial hold all the ideal characteristics. A successful bone substitute must exhibit biocompatibility and bioresorbability, possess other essential biologic properties, including selective osteogenic potential, high levels of osteoinductivity and vascularization, good osteoconductivity and integration with host tissue, also known as osseointegration, and be cost-effective. The problems with the current scaffolds and tissue engineered constructs are usually related with their limited osseointegration and lack of vascularity.[4,6]

Converging nanotechnology into TE has provided the ability for materials to be tailored to tune with ECM mechanical and physical properties, and to be designed at their molecular level. It represents an important factor in constructing and processing the future composite and integrated materials. Materials with appropriate physical characteristics such as high porosity and interconnectivity have been designed and engineered to facilitate material/cell interactions, nutrient/oxygen infiltration, and vascularization. Furthermore, the incorporation of ECM proteins or ECM-derived peptides or protein fragments which engage integrins and direct osteoblast adhesion and differentiation, has given biomaterials a fundamental tool to signal and manipulate cell behaviours towards tissue formation.

One of the most evolving strategies for producing bone substitutes is through the using of composite scaffolds. Electrospun fibres and hydrogels are examples of polymeric structures commonly used as scaffolds. Electrospun fibres have been widely used in TE as scaffolds for cell culture due to their unique biomimetic properties characterized by interconnected porous structure with high porosity, high surface area, fibre diameters in the sub-micron range, variable pore size distribution, versatility in materials selection, reproducibility, and the ability to be tailored into a variety of sizes and shapes.[7] Hydrogels greatest property relates with their degree of flexibility very similar to natural tissue due to their large water content. They are capable to mimic the physiochemical and biological properties of natural ECM of tissues such as cartilage and bone. The low level of bioactivity of electrospun fibres represents its major disadvantage, while hydrogels most common problem is regarding their poor mechanical properties.[8] Hydrogels reinforced with electrospun fibres represents an outstanding strategy with potential for bone regeneration due to the merging of both unique properties. Moreover, combining these two systems into a scaffold provides a solution to overcome their individual limitations.

Electrospun fibres can be produced through a wide range of materials. Polycaprolactone (PCL) nanofibres are now commonly used due to their properties viable for biomedical applications.[9] PCL fibres in its origin offer a hydrophobic environment that cannot favour cell functions. Since osseointegration and long-term success of the implant are determined by the complex reactions taking place at the tissue-material interface, PCL fibres require surface modifications. Molecular processes driving cell adhesion and growth have focused the treatment of implant surfaces on improving the surface-to-cells interaction, complying with the new approach of “biochemical functionalization”. Most promising approach involves the decoration of surfaces of the implant with adhesive sequences or osteogenic growth factors.[1] In its turn, hydrogels can be produced using self-assembling peptides (SAPs). Hydrogels from self-assembled peptides have a potential to serve as synthetic extra cellular matrices.[10] Their excellent properties can offer three-dimensional supports for cell growth, and can become vehicles for the delivery of stem cells, drugs, or bioactive proteins. This can be explained by the unusual stable structures that some peptides form when self-assembled, such as β-sheets structures. Many SAPs have been designed as β-sheet peptides. SAPs with β-sheet structures have repeated alternating hydrophobic and hydrophilic amino acids along a linear sequence. After β-sheet formation, this results in two distinct faces of hydrophobic and hydrophilic character. It is believed that is this hydrophobic character between two β-sheets

that gives the ability to encapsulate guest molecules that also impart in hydrophobic environments (like cells and some drugs), making SAPs hydrogels viable for cell-penetration and uptake.[11]

1.2 Aim of this thesis

The aim of this thesis is to provide a novel bone substitute construct intended to promote osteoblast penetration. Exploring the advantages of electrospun fibres and hydrogels from SAPs, we aim to design a multi-layer composite scaffold by alternating both systems in a 3D structure. The multi-layered scaffold should be produced to mimic the natural bone tissue with appropriate porosity to allow all the necessary transport within, and a suitable environment for cell growth and migration. The design of a nano-fibrous/nano-porous structure mimicking an ECM environment must be able to reproduce the typical biochemical stimuli characteristic of lifelike bone regeneration process. These stimuli will be generated through the insertion of matrix-bound bioactive molecules, such as adhesive molecules, in the nanofibres, and the incorporation of soluble molecules, such as growth factors, in the hydrogels. These two approaches combined along the scaffold aim to create a 3D gradient intended to signalize and guide bone-forming cells (osteoblasts), when seeded in our structure, to the places needed for ossification. This gradient will be disposed in an orderly manner in such a way to give viability to cells and sustain their proliferation and migration functions. By addressing these points, besides offering an *in vitro* validated prototype for the *in vivo* studies, we expect to build an innovative multi-layered porous scaffold decorated with gradient of appropriate bioactive molecules to foster the adhesion and the spread of osteoblasts throughout the entire volume of the bony support, and, finally, ensure osseointegration, immediate loading, and long-term success of the implant.

1.2.1 Objectives of this thesis

- Produce and morphologically characterize layers of micro- and nanofibres of PCL obtained by electrospinning;
- Graft specific functional groups through atmospheric pressure plasma and evaluate their availability in the chemoselective ligation with adhesive sequences;
- Compare the cellular adhesion on surfaces functionalized with adhesive molecules at different concentrations;
- Build manually a multi-layered porous scaffold decorated with a gradient of appropriate adhesive cues and growth factors embedded in hydrogel.

1.3 Structure of the thesis

This report will be duly organized into six chapters. Chapter 1 provides a framework for the theme to be developed, exposes the problem in need for a solution, and summarizes the main objectives to be achieved.

In chapter 2 will be briefly presented a bibliographic review, which explains the importance of this work, what has already been done and investigated, and what can be eventually improved. Chapter 3 focuses on the materials and methods used for the experimental work described in the following Chapter 4. Chapter 5 will present the obtained results accompanied by a careful and critical discussion. Chapter 6 will resume the main achievement of this master's project, presenting a visionary view of possible future work.

CHAPTER 2 – BIBLIOGRAPHIC REVIEW

2.1 Bone Tissue and Cells

Bone is a tissue characteristic of the vertebrate animal's class. Being a specialized tissue in the loading of forces and stress, bone is an essential supportive structure of the body, characterized by its rigidity, hardness and regeneration ability. It serves to guard necessary organs, produces blood cells, acts as a mineral reservoir for calcium, and maintains acid-base balance. Bone is also responsible to convert the muscle contraction in movement of whole body through the formation of the lever system of the body.[12] It is a composite material consisting of crystals of mineral bound to proteins. This provides both strength and resilience so that the skeleton can absorb impact without breaking.[13] It is a kind of tissue composed by bone cells and a bone matrix comprising organic and inorganic components. The mineral-inorganic phase of bone consists of small crystals containing calcium and phosphate ions, called hydroxyapatite ($Ca_{10}(PO_4)_6(OH)_2$), and this inorganic component constitutes about 50% of the total bone weight. This mineral is bound in an orderly manner to a matrix that is made up largely of a single protein, type I collagen. Bone consists of 70% inorganic component (mainly hydroxyapatite), 20% organic component, and 10% of water. Collagen type I represents around 90% of the organic content.[14,15] To provide the body with a frame that is both light and strong, bones are hollow. Due to the connection of the collagen fibres and hydroxyapatite, dense bone is formed. The outer dense shell is called cortical bone, which makes up roughly 75% of the total skeletal mass. Inside the cortical shell is a fine network of connecting plates and rods called trabecular bone, that makes up the remaining 25 percent.[13]

Bone is a dynamically and highly vascularized metabolized tissue hosting osteocytes (entrapped within the bone matrix), osteoblasts (the bone-forming cells) and osteoclasts (cells committed to bone resorption) hierarchically and spatially organized within the ECM.[14] ECM is present in all living tissues. The ECM in bone is distinguished from the others because of its mineralization. It confers a structural support for tissues, serves as a site for cell adhesion and determines the mechanical properties of the skeleton. However, it has been recently recognized that ECM plays far more dynamic role in regulating cell function and tissue morphogenesis. In the context of bone, ECM components can play a role in modulating the assembly of the structural matrix, particularly in organizing the process of matrix mineralization. As well, the ECM can bind to extracellular growth factors; cell bound ligands and receptors, and proteases. Bone matrix consists of amorphous and fibrillary components. The amorphous component is formed by proteoglycans (glycosaminoglycan chondroitin sulphate and keratin sulphate) and structural glycoproteins (osteonectin, sialoprotein, osteocalcin, binding calcium ions). The fibrillary component corresponds to the already mentioned collagen-organic part of the bone.[16] Bone is covered by collagenous connective tissue called periosteum and its inner cavity is lined by endosteum. Both structures are composed of outer connective tissue layer and inner cellular layer formed by osteoprogenitor cells (that differentiate into osteoblasts) and pre-osteoblasts. Endosteum is much thinner that

periosteum and ensures the nutrition of bone. It is also source of new osteoblasts which are used for growth and remodelling of bone.[17]

Throughout life, bone is constantly changing in size, shape and position. Two processes guide these changes – modelling and remodelling. Both modelling and remodelling involve the cells that form bone, osteoblasts, and the cells that break down bone, osteoclasts. In remodelling, there is an important local interaction between osteoblasts or their precursors (the cells that will develop into osteoblasts by acquiring more specialized functions – a process called differentiation), and osteoclasts or their precursors. The differentiation and function are regulated by osteotropic hormones and cytokines.[14] Osteogenesis is roughly assumed to ossification by the medical dictionary, i.e., the natural formation of bone. This, together with the modelling and remodelling stages, encompasses the processes involved in bone's life span. All these processes are mediated by osteoblasts, which work in tight cooperation with bone-resorbing osteoclasts.[18,19]

Osteoclasts are the principal cells involved in the reabsorption of bone. As bone as being destroyed, these cells are committed to remove it, and to make deposition of new bone. This process is named bone remodelling, and occurs with calcium release.[20] When bone is in resorption stage, osteoclasts are located at the bone surface. They provoke the losing of tissue, creating depressions nominated as re-entrances or Howship's lacunaes. Besides the osteolytic function, osteoclasts play an important role in the bone development and growth by releasing growth factors from the mineralized ECM. Osteoclasts differentiate in contact with the bone throughout mononuclear hematopoietic progenitor cells. They can be found in the bone marrow together with the cells that generate osteoblasts.

Osteoblasts are engaged in bone formation, i.e., the production of bone matrix. During the functional remodelling process of bone structure, regarding the adaption to mechanical forces and stresses, these cells play a fundamental role. They derive from precursor cells that can also be stimulated to become muscle, fat or cartilage; however, under the right conditions, these cells change (or differentiate) to form new bone. Osteoblasts are responsible for the process of mineralization of the osteoid tissue.[21] They are mononuclear cells that synthesize the organic ECM of bone, including collagen type I alpha 1, osteocalcin, osteopontin, osteonection, alkaline phosphatases, proteoglycans, as well as growth factors, stored within the bone matrix and in charge of the regulation of bone growth.[20,22] Osteoblasts lay down bone in orderly layers that add strength to the matrix. Generally, they line on the bone surface and are called as bone lining cells. Some of the osteoblasts are buried in the matrix as it is being produced and these are now called osteocytes.[14]

Osteocytes are the most numerous cells in bone and are extensively connected to each other – osteocyte perilacunar matrix - and to the surface of osteoblasts by a network of small thin extensions. They represent the mature form of the osteoblast. Very small changes in the shape of the bone can act on the osteocytes, which produce chemical signals that allow the skeleton to respond to changes in mechanical loading.[23] Figure 2.1 illustrates all the compartments of bone matrix as well as the cells involved in the bone remodelling process.

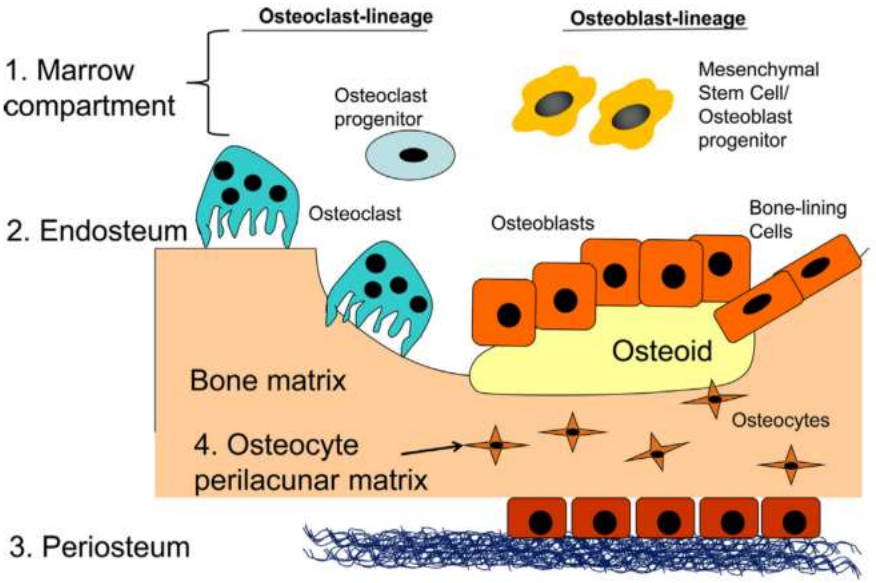

Figure 2.1 Overview of the cells involved in bone remodelling and the matrix compartments of bone.[101]

The recruitment of osteoblasts to the injured sites represents the key to the development of new anabolic bone remodelling strategies. The principle of this process involves an understanding of molecular mechanisms that accommodate the functioning of bone-producing osteoblasts. The recruitment of osteoprogenitors to the bone surface is an indispensable aspect of bone formation, and modulating this process could offer unique properties for anabolic treatment of osteoporosis and other metabolic bone disorders.[18] Skeletal morphogenesis involves highly coordinated sequential steps of cell migration, aggregation, condensation and organogenesis. Cell migration is a dynamic process that requires the coordinated formation and disassembly of focal adhesions and rearrangements of the actin cytoskeleton. Although the underlying mechanisms in osteoblast lineage cells are still poorly understood there is evidence that the osteoprogenitors are attracted, together with blood vessels, by chemotactic factors released from the mould, a process known as chemotaxis.[24]

Chemotaxis is a fundamental process in which cells migrate directionally when they are exposed to external chemical gradients. Recruitment of osteoblast lineage cells to the sites programmed for ossification or in need of new bone formation conceivably relies on precisely controlled temporal and spatial chemotactic navigation signals. Molecules attracting cells are called chemoattractant or chemokines. Chemotaxis can be positive or negative respectively whether the cell moves toward an increasing or decreasing concentrations of chemokines.[25] For example, the balance between bone formation and degradation is normally tightly controlled; however, it becomes deregulated, shifting towards more degradation under pathological conditions or during aging, thereby leading to osteoporosis. This tight balance implies the existence of mechanisms coordinating the differentiation of osteoblasts and osteoclasts as well as their migration to locations where they function. This mechanism is known as osteoclastogenesis and can be described as a process in which the presence of specific cues can control the differentiation of both precursor cells, avoiding over-degradation. Likely, in inflammatory response, chemotaxis is crucial for macrophages migration in the site of inflammation. In this case, chemo-

attractants are released by the tissue in the previous phase of coagulation and clot degradation. There are multiple candidate guidance cues that may be involved in the directional migration of osteoblasts and their precursors: constituents of the bone matrix, such as fragments of collagen or osteocalcin, complement fragments, inflammatory cytokines and growth factors that are typically released, activated or produced at sites of matrix resorption.[26]

Growth factors are polypeptides that can either stimulate or inhibit cellular proliferation, differentiation, migration, adhesion, and gene expression. Growth factor's effects are concentration-dependent. Due to their control of many biological processes, growth factors are finding widespread use in the regeneration of many tissue types such as musculoskeletal, neural, hepatic and vascular systems.[27,28] Enhance the *in vitro* and *in vivo* efficacy of growth factors passes through incorporating them into polymeric biomaterials (such as hydrogels) to maintain their stability and control their release kinetics. The release of these factors is then controlled by diffusion and/or scaffold erosion or degradation mechanisms. The application of growth factor in delivery systems are of utmost importance in the field of tissue engineering, namely, bone and cartilage regeneration.[29]

2.2 Designed Materials for Bone Tissue Engineering

The term 'Tissue Engineering' was officially coined at a National Science Foundation workshop in 1988. TE aims to "regenerate damaged tissues instead of replacing them, by developing biological substitutes that restore, maintain or improve tissue function". The regeneration of a whole (or partial) tissue or organ requires a complete understanding of the tissue/organ properties. Knowing their characteristics and transferring them to a structure that will be biologically accepted, constitutes the first criteria to develop a biological substitute with predictable success. Nowadays, TE scaffolds are the leading strategy of repair and regeneration of bone defects. Their construction is mostly based in the advances in materials science, especially in the field of biomaterials, where structures are specifically designed for specific purposes.[5]

Biomaterials play a pivotal role towards the design of ideal bone grafts substitutes. Biomaterials can be polymer-based (natural or synthetic), ceramic-based, metallic-based, and composites. The most accepted definition of biomaterials is currently the one employed by the American National Institute of Health that describes biomaterial as "any substance or combination of substances, other than drugs, synthetic or natural in origin, which can be used for any period of time, which augments or replaces partially or totally any tissue, organ or function of the body, in order to maintain or improve the quality of life of the individual".[30] Biomaterials have passed through an evolution process over time. Three major generations of biomaterials can be found: first generation, second generation and third generation. Briefly, the first generation of biomaterials relies on the capability of the material to be biologically inert, or bio-inert. They were intended for mechanical support and the major functionality of preventing rejection. This class include metals (e.g., titanium and titanium alloys), certain synthetic polymers (e.g., PMMA, PEEK), and some ceramics (e.g., alumina, zirconia). The second generation evolved to the new concept of bioactive/bio-resorbable materials. This class is categorized by materials that, besides the advantages of the 1st generation, can also stimulate regeneration and adopt a strongly biomaterial-bone interface form. Synthetic and naturally derived biodegradable polymers, calcium phosphates, carbonates and sulphates, and bioactive glasses are included in this class. Lastly, the third generation presents the outstanding and widely studied strategy emerging continuously in the field of regenerative medicine. Third generation bone grafts substitutes try to get close to the autograft standard. Integrating the bioactivity and biodegradability achieved in the second generation, third generation improvements motivate the development of biomaterials in modulating the response of host osteoblast and osteoprogenitor cells to the implant, inducing biological responses at molecular level. In this category are included the high porous scaffolds, nanotechnology based strategies, and the cell/gene/growth factor/loaded scaffolds.[4]

The design of 3D biomaterials able to mimic the complex structural and biochemical functions of the ECM is the current and most challenging aim of TE studies. For that reason, the selection of a biomaterial able to induce and enhance osseointegration, and bone formation is of utmost importance in bone TE. A successful orthopaedic biomaterial must support the adhesion, organization, differentiation and matrix mineralization of osteoblasts and osteoprogenitor cells, key factors for optimal osseointegration. The limited osseointegration in the current orthopaedic biomaterials represents the major drawback for the success of the current bone

substitutes. Also, the lack of vascularity in scaffolds and TE constructs is of major concern. The ability for materials to be molecularly designed represents an important factor in constructing and processing the future composite and integrated materials. Bioinspired strategies have included functionalizing implants with ECM proteins or ECM-derived peptides or protein fragments which engage integrins and direct osteoblast adhesion and differentiation. Different peptides can be designed to promote cell adhesion to the implanted biomaterial, proliferation, differentiation, angiogenesis or a combination of effects, what makes them highly versatile tools.[15] The design of materials still allows the tune with the desired mechanical and physical properties. Materials with appropriate physical characteristics such as high porosity and interconnectivity have been designed and engineered to facilitate material/cell interactions, nutrient/oxygen infiltration and vascularization. The capacity to control the porosity and pore size within a scaffold is of major importance. The porosity should be high enough to provide sufficient space for cell adhesion, ECM regeneration and minimal diffusional constraints during culture. The pore structure should allow even spatial cell distribution throughout the scaffold to facilitate homogeneous tissue formation. Ideally, the structures of the scaffold must be highly porous, with open pores and fully interconnected. Micro-porosity with pores less than 10 μm is needed for capillary ingrowth and cell-matrix interactions. Macro-porosity with pore sizes of 150−900 μm allows for nutrient supply and waste removal of cells grown on the scaffold. Depending upon the cell type, the optimal pore diameters are 20−100 μm.[6,31,32]

One of the most evolving strategies for producing bone substitutes is through the using of polymeric scaffolds. Electrospun fibres have been widely used in TE as scaffolds for 3D cell culture due to their unique biomimetic properties characterized by interconnected porous structure with high porosity, high surface area, fibre diameters in the sub-micron range (tuneable between 50 nm and 5 μm), variable pore size distribution, versatility of materials selection, reproducibility, and the ability to be tailored into a variety of sizes and shapes. The production of 3D network structures from electrospun fibres is intended for mimicking the characteristics of ECM, where cells can anchor, grow and perform their multiple functions, to bring back to the tissue it natural functionality.[33,34] Electrospun fibres can be produced through a wide range of polymers. Various synthetic and natural polymers, such as proteins, and the blend of both types can be used. Examples of natural polymers include collagen, chitosan, cellulose acetate, silk protein, chitin, fibrinogen, among others. Typical synthetic polymers are hydrophobic biodegradable polyesters, such as poly(ε-caprolactone) (PCL), poly(lactic acid) (PLA), poly(glycolic acid) (PGA), polyurethane (PU), the copolymer poly(lactide-co-glycolide) (PLGA), and the copolymer poly(L-lactide-co–caprolactone) [P(LLA-CL)].[7] Normally, the fibre diameter of the matrices conform to the structural properties of the ECM are on the order of 80-500 nm. It has also been reported that biocompatibility of a material improves with decreasing fibre diameter. Fibrous scaffolds can be designed combining micro- and nano-fibres unto stratified architecture. Alternating micro- and nano-fibres, it can be easily created an environment to facilitate cellular infiltration into the scaffolds. It has been reported that cells are able to easily migrate to a depth of about 100 μm.[32]

Another emerging strategy in the field of TE involves the use of hydrogels. Hydrogels are promising materials for bone and cartilage regeneration. Equally, hydrogels present very particular characteristics that allow them to be used in the biomedical and pharmaceutical applications. It greatest property relates with their degree of flexibility very similar to natural tissue due to their large water content. They are capable to mimic the physiochemical and biological properties of natural ECM of tissues such as cartilage and bone. Hydrogels represent a group of polymeric materials that can be either from synthetic and natural origins. The porous structure of hydrogels enables the transfer of low molecular weight nutrients and cellular waste, which is vital for cellular life. In addition, biocompatible and biodegradable hydrogels can direct the migration, growth, and arrangement of cells during regeneration processes.[8,35] However, the major drawbacks regarding the use of hydrogels lays in their poor mechanical properties and low bioactivity, making them inappropriate for hard tissue.[36] To improve their bioactivity, is taken the advantage of hydrogel's ability to recreate the natural mechanisms by using synthetic low-molecular weight peptides able to aggregate by spontaneous self-assembling. SAPs hydrogels are nano-structural materials that can act as nano-fibrous scaffolds with an average of 10 nm in fibre diameter with pores between 5-200 nm. These structures can be easily functionalized with chemotactic factors, growth factors or adhesive peptides, providing favourable environments for culturing cells, triggering tissue regeneration, and for releasing drugs.[37] Moreover, when mixed together with other porous polymer scaffolds, the peptide scaffolds enhanced osteoblast growth and differentiation.[38]

Hydrogels reinforced with electrospun fibres represent a revolutionary strategy with potential for bone regeneration due to the merging of both unique properties. However, only few studies have been reported on fibrous scaffolds for application in bone TE. In literature is reported a combination where SAPs hydrogels were mixed with PCL in solution to produce electrospun fibres. This presents a path to assess the potential of modulating the excessive softness of those hydrogels and to add biomimetic molecules to PCL scaffolds. Indeed, these scaffolds can emulate the natural ECM (for its porosity and water content) and possess improved mechanical properties due to the fibres ability to reorient under deformation, stiffening, strengthening and toughening the system. Danesin, R. *et al*, proved that the enrichment of fibres with peptides produced higher surface wettability, and enhanced *h*-osteoblast adhesion to maintain osteoblast differentiation and to stimulate the expression of several genes.[36,39] Khorshidi, S. *et al*, prepared a hydrogel/fibre scaffold for osteochondral regeneration, possessing gradient in both phases. In this experiment, they had come with the idea of amalgaming hydrogel and fibres to obtain composites encompassing gradient features to restore osteochondral matrix. This idea aims at overcoming the inherent limitations of both individual scaffold systems - the innately scarce cell migration of fibres and poor mechanical properties of hydrogels. Mehdi-Sahad *et al*, fabricated a 3D cell-laden three-layered hybrid scaffold incorporating a 2D mat layer of poly(hydroxybutyrate) and nano-hydroxyapatite fibres (diameter 2.0±0.2 μm) between two layers of methacrylated gelatin/Hap. All the results showed an improvement in the mechanical properties when compared to the hydrogel itself; however, they were still inferior to the natural tissue. To overcome this problem, it has been suggested an increasing in the thickness of the electrospun mat located at the centre of the scaffold. But, this approach would lead to a denser

electrospun mat, with decreased porosity that would potentially hindered cell penetration into the electrospun centre.[40]

A scaffold designed as the one planned to obtain in this work, presents an original and innovative idea. First, assembling alternating layers of hydrogel/electrospun fibres onto a stratified architecture allows controlling the nano-fibrous structure of both systems in terms of fibre morphology, since their production is done individually. The mechanical properties of hydrogels are expected to be improved whatsoever, although knowing that the loading of the substitute will be far from the mechanic loading exhibited by natural bone. This type of combination permits the incorporation of different kind of bioactive molecules:

(1) Matrix-bound bioactive molecules, as adhesive sequences, decorating the surfaces of the electrospun matrices, intended to promote cells' attachment along the scaffold;

(2) Soluble molecules, as growth factors, embedded in hydrogels, essential for cell growth and sustainability, where their release will occur mainly by bulk degradation of the material.

2.2.1 Biofunctionalization of surfaces

Osseointegration and long-term success of the implant are determined by its ability to communicate with surrounding biological environment. It is of major importance for an implant to be recognized by the host biological system and initiate the functions for which it is intended as a part of the natural process. In the design of a biomaterial, the surface properties should be tailored to maximize the tissue-implant reciprocity, i.e., the interaction of the material with proteins. For this reason, bone grafts/substitutes have received specially attention in surface treatments to improve surface-to-cells interaction. Currently, the most promising approach involves the decoration of surfaces of the implant with adhesive sequences or osteogenic growth factors, a process named biochemical functionalization, or bio-functionalization, where the presence of these molecules at the surface of the implant triggers a series of molecular processes driving cell adhesion and growth.[1,41]

Activity and behaviour of osteoblasts contacting material surface, both *in vitro* and *in vivo*, are influenced by surface properties such as hydrophilic/hydrophobic nature of the scaffold, surface wettability, roughness and deformability. Many mechanical and chemical treatments, and combination of both, are thus performed to modify surface with opportune characteristics to optimize its biological and mechanical properties. ECM proteins, such as fibronectin and vitronectin, are examples of cell adhesion proteins and are known to promote osteoblasts adhesion, and, therefore, bone growth. The attachment of osteoblasts to the bone matrix is mediated by vitronectin receptor.[14] In the literature is reported that the FRHRNRKGY peptide mapped on human vitronectin (HVP) selectively promotes osteoblast-like adhesion.[42] The peptide reproducing the 351–359 sequence of human vitronectin increases osteoblast adhesion through a specific mechanism of interaction between cell membrane heparin sulphate proteoglycans and heparin-binding sites of ECM proteins.[43]

There are several advantages and disadvantages when using peptides instead of whole proteins. Proteins offer higher activity, they are well characterized molecules and are commercially available. However, the immobilization of an entire protein on a surface can lead to protein denaturation and loss in the bioactivity. They

are more expensive and, biologically, more immunogenic and sensitive, which make them bind with a range of biological ligands, losing it specificity. The immobilization of short biomimetic peptides, reproducing the receptor binding site of the protein, offers a convenient alternative route. When compared to proteins, peptides provide less activity and are poorly characterized, and there aren't many commercialized products available. However, peptides can be synthesize in a cost-effective way, offering more stable molecules, with high specificity and less immunogenic reactions.[44] Peptides can be attached to a bioactive surface either by physicochemical adsorption or by covalent immobilization. The first method is the simplest one but lacks control on the quantity and orientation of the adsorbed peptide; this disadvantage can be overcome by covalent binding of the selected peptide to the surface through an optimized synthetic procedure. One of the favourite techniques for covalent immobilization involves deposition of a silane carrying a reacting functional group that can be used to anchor another different molecule. Usually, a further bifunctional molecule (cross-linker or spacer) is subsequently added to maintain the peptide flexibility. Several authors reported the covalent immobilization of RGD-containing peptides on various surfaces by reaction with different silanes and cross-linkers.[43]

2.3 Hydrogels

Hydrogels were first reported by Czech chemists Otto Wichterle and Drahoslav Lím in 1960. They invented polyhydroxyethylmethacrylate, the synthetic material that was later used for soft contact lenses.[45] Hydrogel products constitute a group of polymeric materials with interest to biomaterial scientists for many years because of their hydrophilic character and potential to be biocompatible. Hydrogels are hydrophilic 3D networks that are recognized by their capability to swell and retain significant amounts of water within it structure. During the swollen and water storage process, hydrogel's structure can be maintained due to chemical or physical crosslinking of individual polymer chains. Water must constitute at least 10% of the total weight (or volume) for a material to be a hydrogel. Hydrogels also possess a degree of flexibility very similar to natural tissue due to their significant water content. The hydrophilicity of the network is due to the presence of hydrophilic groups attached to the polymeric backbone, such as $-NH_2$, $-COOH$, $-OH$, $-CONH_2$, $-CONH$, and $-SO_3H$, while their resistance to dissolution arise from crosslinking between network chains. Thanks to their notable properties such as versatility in fabrication, tuneable physical, chemical and biological characteristics, high biocompatibility, and similarity to living tissues, hydrogels have been widely used in biomedical/pharmaceutical applications.[46,47]

Hydrogels are mainly formed from biopolymers and/or polyelectrolytes.[46] They can be either from synthetic or natural polymers. Synthetic polymers that forms hydrogels are traditionally prepared using chemical polymerization methods. Usually they have well-defined structures that can be modified to yield tailor able degradability and functionality. On the other hand, natural hydrogels present long service life, high capacity of water absorption, and high gel strength, being the reasons for the gradually replace of the synthetic ones.[8,48] One of the way to produce hydrogels is through the combination with molecular units, like peptides and proteins, as the emerging case of hydrogels from SAPs.

2.4 Hydrogels from self-assembling peptides

Peptides are very versatile building blocks for fabricating supramolecular architectures. Their ability to adopt specific secondary structures, as prescribed by amino acids sequence, provides a unique platform for the design of self-assembling biomaterials with hierarchical 3D macromolecular architectures, nanoscale features and tuneable physical properties.[49] Peptides offer a great diversity of biochemical (specificity, intrinsic bioactivity, biodegradability), and physical (small size, conformation) properties to form self-assembled structures with different molecular configurations. Self-assembly is a spontaneous process of organization of chaotic molecular units into ordered structures because of intramolecular/intermolecular interactions, normally using processes driven by enthalpy that include Van der Waals, electrostatic, hydrogen bonding, and π-π stacking interactions.[50] Self-assembly involve the formation of a wide variety of complex biological structures such as actin filaments in the cytoskeleton, the fibrous proteins components of the ECM, DNA, among others.

These molecules can spontaneously assemble into various nanostructures in aqueous media such as fibres, tubes, sheets, and spheres.[51]

SAPs are highly biocompatible and versatile structures. They may vary in the number of amino acids starting from 2 to as high as 20. Once there are the amino acids that form the building blocks, designed SAPs present the advantage to incorporate functional molecules on the carboxyl or amine terminal groups, opening a wide range of possibilities for chemical interactions and modifications. This fact, besides enhancing the design opportunities when compared to individual components, also leads to functional specificity, since the supramolecular organization of the hybrid materials is driven mainly by the bio-recognition of peptide segments.[52,53] Self-assembling peptide systems undergo a sol-gel transition when brought to neutral pH and ionic concentration. These systems do not use crosslinking agents; hence, they can safely encapsulate cells and/or drugs without exposing them to toxic agents. Applications of SAPs as nano-biomaterials include carriers for drug delivery, hydrogels for cells culture, and tissue repair. Hydrogels from SAPs have a potential to serve as synthetic extracellular matrices. Their excellent properties can offer 3D supports for cell growth and can become vehicles for the delivery of stem cells, drugs or bioactive proteins. Despite the numerous advantages of self-assembling peptides, there are several challenges associated with their use in biomedical applications, which include problems related to process, control of size, functionalization, and stability in aqueous medium.[10]

Zhang, S. first demonstrated the use of SAPs systems in the design of soft materials. Three types of SAPs have been systematically studied thus far and can be distinguished based on the final secondary molecular structure, that can result in β-sheet peptide, α-helix peptides, and peptide amphiphiles.[42,43] These categories are numbered in type I, II and III. Type I self-assembling peptides, also known as “Molecular Lego”, are the ones of utmost interest for the current report. They form β-sheet structures in aqueous solution because they contain two distinct surfaces, one hydrophilic and one another hydrophobic. The unique structural feature of these peptides is that they form complementary ionic bonds with regular repeats on the hydrophilic surface. The complementary ionic sides are classified according to the amino acid ionic pairing and charge distribution of the residues. The discovery of such a class of ionic-complementary peptides by Zhang S. was remarkable and caught the attention for the fields of biotechnology. The origins of the discovery date many years of investigation in the field of molecular biology. However, the rising interest dates back in the early 1990s when Zhang showed the importance of the Z-DNA, with the discovery of a Z-DNA binding protein, zuotin, in yeast. Analysis of the Z-DNA binding protein revealed an unusual 16-amino acid sequence (EAK 16-II) with repetitive polar and nonpolar residues suggesting a new class of SAPs.[54] These peptides have been reported to support mammalian cell attachment and have been used as a scaffold for neurite outgrowth and synapse formation.[55,56]

2.4.1 β-Sheet peptide

The β-sheet is a common motif, and second major type, of regular secondary structure in proteins. β-sheets consist of multiple peptide chains that have an extended backbone arrangement that permits hydrogen bonding between the backbone amides (–NH) and carbonyls. The interactions do not involve side chains thus many different sequences can form a β-sheet, such as self-assembly of peptides into hydrogels. Although these interactions are relatively weak when compared to covalent bonds, they form thermodynamically stable structures through self-assembly due to lower values of Gibbs free energy when compared to that of the individual components (building blocks). Since the underlying interactions are rather weak, any external stimulus can alter the self-assembled structures. However, once the stimulus is removed, they can revert to their original structure.

Many SAPs have been designed as β-sheet peptides, for example, KLD−12 (Ac–$(KLDL)_4$–NH_2), RADA 16−I (Ac–$(RARADADA)_2$–NH_2), EAK 16−II (Ac–$(AEAEAKAK)_2$–NH_2), among others. Each of these oligopeptides can form a polymeric network of nanofibres rich in β-sheet secondary structures under well-defined conditions, for example, pH and temperature. Alanine-based sequence were the pioneering sequences and serve as the best model for creating hydrogel-forming systems.[10,50,57] SAPs with β-sheet structures have repeated alternating hydrophobic and hydrophilic amino acids along a linear sequence (Figure 2.2A). This results in two distinct surfaces of hydrophobic and hydrophilic character. Hydrophobic interactions play an important role as a primary driving force for self-assembly. Electrostatic interactions and hydrogen bonds derived from hydrophilic amino acids contribute to structural specificity. The alternating hydrophobic-hydrophilic residues assembled into sheets, where two sheets came together to bury this hydrophobic face from the surrounding water (Figure 2.2B). Thus, depending on the number of packed sheets, a variety of different hierarchical structural arrays can be designed, including tapes, ribbons, fibrils and fibres (Figure 2.2C).

Peptides that form β-sheets have applications in drug delivery as nanowires, nanofibres or hydrogel scaffolds, where the ability to encapsulate hydrophobic guest molecules between two β-sheets enhanced their cell-penetration and uptake. A β-sheet is a regular and rigid structure often represented as a series of flattened arrows (Figure 2B). Each arrow points towards the protein C-terminus. β-sheets can be orientated so that all their C-terminus are at one end of a structure, described as a parallel structure, or so that the N and C terminus alternates, described as an anti-parallel structure. In both positions, the β-strands become oriented in such a way that alternate amino acid side chains remains at opposite sides of the sheet. Sometimes, the electrostatic and hydrophobic forces among the amino acids chains stabilize the sheets.[57] This has an important impact on the orientation of hydrogen bonds between sheets and side chain orientations and interactions.[58]

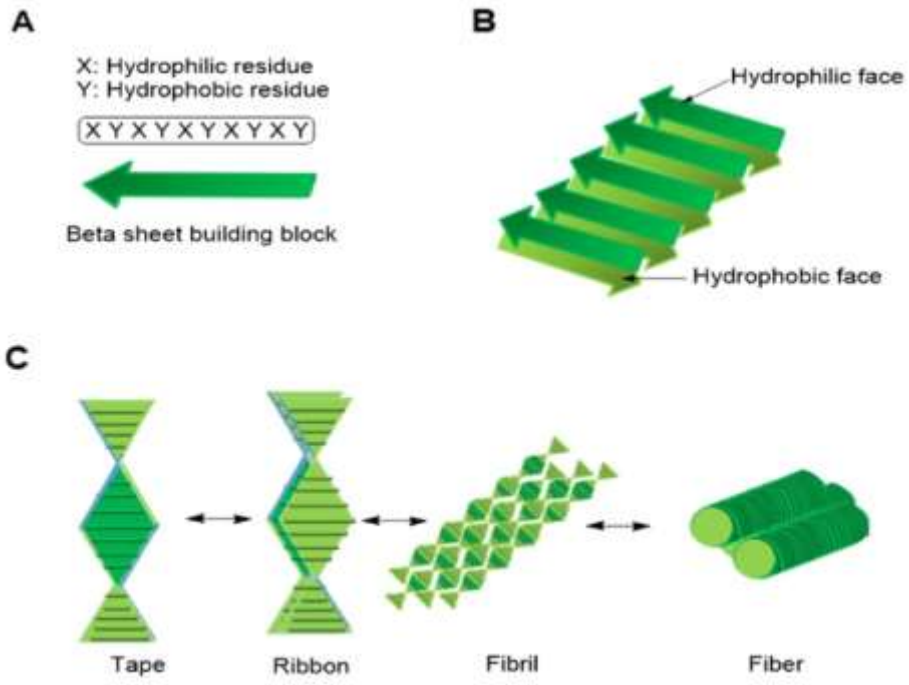

Figure 2.2 Schematic representations of peptides able to form β-sheets and of the resulting self-assembled structures (adapted from Loo, Y., Zhang, S. & Hauser, C. A. E. From short peptides to nanofibres to macromolecular assemblies in biomedicine. *Biotechnol. Adv.* 30, 593–603 (2012)).[50]

EAK 16-II is a typical example of "Molecular Lego" peptide that forms fibrillary assemblies at physical pH values. This peptide sequence is composed by a conjugation of 16 amino acids: two charged residues, involved in charge-charge interactions - Glutamic acid (Glu, E) with acidic properties, and Lysine (Lys, K) with basic properties; and one aliphatic hydrophobic residue, providing a hydrophobic environment – Alanine (Ala, A) (Figure 2.3).

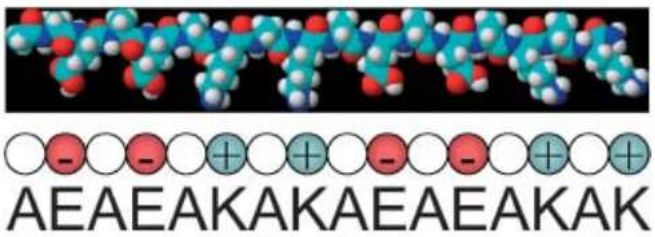

Figure 2.3 Schematic 3D molecular model of EAK 16-II. Carbon atoms are cyan, oxygen atoms are red, nitrogen are blue, and hydrogen atoms are white.[102]

EAK 16 contains alternating hydrophobic and hydrophilic amino acid residues. In this conformation, all the hydrophobic Alanine residues side chain face in one direction. While the opposite polar face is composed by Glutamic acid and Lysine residues, negatively and positively charged, respectively. This conformation creates two distinct faces. When protonated, the amine groups of the Lysine residues will link with the carboxylic groups present in the Glutamic acid residue through ionic complementarity. On the other hand, the nonpolar side chain establishes hydrophobic interactions, Figure 2.4. This repetitive anti-parallel arrangement

of amino acids imparts an amphiphilic property to the peptide. Instead of exhibiting a hydrophobic tail and a hydrophilic head like usual surfactants, EAK 16 has a hydrophobic side and a hydrophilic side. This peptide turns out to form unusual stable form β-sheets and further stable membrane-like structures upon an addition of salts in solution.[56]

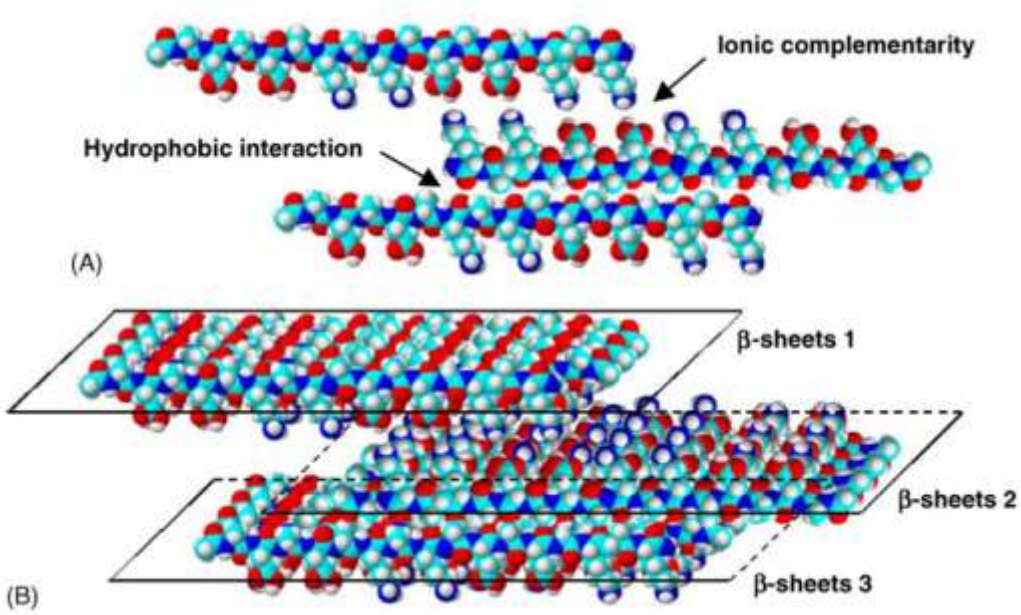

Figure 2.4 Schematic of EAK 16-II self-assembly through hydrophobic interaction and ionic-complementary.[56]

Upon the introduction of milli molar amounts of monovalent cations (such as Na^+, Cs^+), either through the addition of salt solution, cell culture media or injection of the material *in vivo*, EAK 16-II undergoes self-assembly into nanofibres, ~10 nm in diameter, on a scale like the *in vivo* ECM. EAK 16–II can form a macroscopic nano-fibrous membrane resistant to high temperatures, extreme pH values as well as chemical denaturants. The resulting EAK 16–II hydrogel exhibits the ability to foster mammalian cell attachment.[59] The physical size relative to cells and proteins, the amphiphilic peptide's charge density, and water-structuring abilities mimic the *in vivo* ECM as well. These well-ordered nanofibres create 3D porous scaffolds that are very difficult or impossible to synthetically produce by other manufacturing techniques. Comparing to Matrigel™, these scaffolds have been shown to be more effective in promoting the bone regeneration of calvaria bone defects in mice.[60] The nanofibre density and average pore size, ~5–200 nm, correlates with the concentration of peptide solution that is used to produce the material, which can be varied from 0.1 to 3% in water (1–30 w/v (%)) depending on the application. EAK 16-II not only can be used as a coating or to encapsulate cells similar to the ECM, but can also be tailor-made for particular cells, tissues and therapies.[61]

2.5 Electrospinning and Nanofibres

Fibres are defined, from a geometrical standpoint, as a slender, elongated threadlike object or structure. Joining this term with the prefix “nano” it can be easily perceptible that the word nanofibres stands for fibres whose fabrication technology in which they are designed and built, by the specification and placement of individual atoms or molecules, has, at least, one dimension on a scale of nanometers.[62]

Electrospinning is a cost-effective attractive technique to synthesize nanofibres from various biodegradable polymers due to the simplicity of the technique, ability to effectively control the process, and potential for scale-up production.[32] Although electrospinning has just became a topic of interest to produce polymeric nanofibres in the lately years, it was observed more than one century ago by Rayleigh (1897) and firstly patented by Formhals (1934). The main advantages of electrospinning is it capability to produce long and continuous fibres with micro- and nano-diameters, and their ability to be manipulated to form 3D structures during deposition.[33,63]

2.5.1 Electrospinning Process

The most basic electrospinning setup consists of three major components: a high voltage power supply, an electrically conducting spinneret and a collector separated at a defined distance, Figure 2.5.[64] The most common setup used in laboratory comprise a syringe that holds the polymer solution with a blunt tip needle as spinneret. The solution can be fed at a constant and controllable rate using the syringe pump.[7]

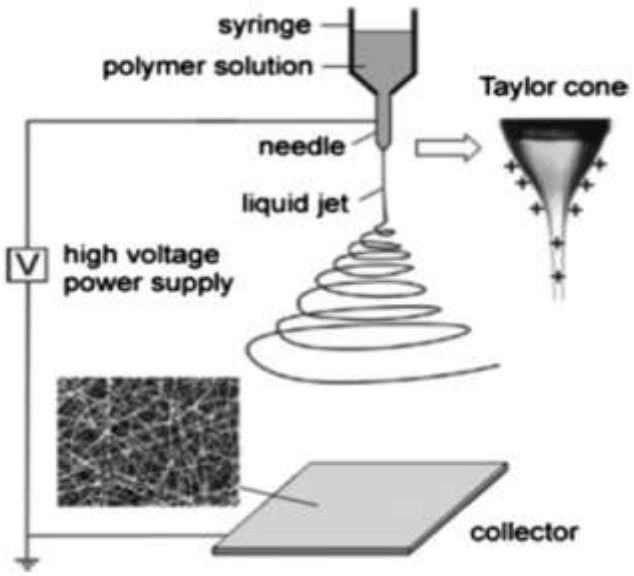

Figure 2.5 Basic electrospinning setup (adapted from D. Li and Y. Xia, Adv. Mater. Weinheim, Ger. 16, 1151, 2004).[64]

Electrospinning is a process of creating nanofibres and/or microfibres through the action of an external electric field imposed on a liquid polymer solution. The polymer solutions can be either from natural or synthetic polymers.[7,64] When a high voltage (typically in the range of 5-30 kV) is applied to a polymer, the surface of the

fluid droplet held by its own surface tension gets electrostatically charged at the spinneret tip. When charges within the fluid reaches a critical amount, a fluid jet will erupt from the droplet at the tip of the needle resulting in the formation of a Taylor cone, see Figure 6, and a fine jet ejects from its surface toward the collection plate.

Electrospinning process comprises three stages: jet initiation, jet elongation and jet solidification.[64] The jet initiation stage is characterized by the formation of the already referred "Taylor Cone". The conical surface is due to the application of the electric field, inducing a charge on the surface of the drop. This charge offsets the forces of surface tension and the droplet changes shape from spherical to conical. When the intensity of the electric field attains an adequate value, the electrostatic forces overcome the surface tension of the polymer solution and force the ejection of the liquid jet from the tip of the Taylor cone. The electrospinning jet will travel towards the region of lower potential which, in most cases, is a grounded collector. Along this drive, elongation stage occurs. Before reaching the collector screen, the liquid jet elongates, and the solvent evaporates, leading to the formation of a randomly oriented, non-woven mat of thin polymeric fibres on the collector. The liquid jet is electrically charged, and the charge causes the fibres to bend in such a way that every time the polymer fibre loops, its diameter is reduced, Figure 2.6. This fact, known as bending instability, is due to the shifts in the balance between surface tension and electrical forces, and changes in the jet trajectory. Initially, the solution jet follows a linear trajectory but, at some critical distance from the spinneret orifice, the jet begins to whip out, and starts following a diverging helical path. The repulsive forces between the charges carried with the jet, elongate the jet in the direction of its axis until it solidifies.

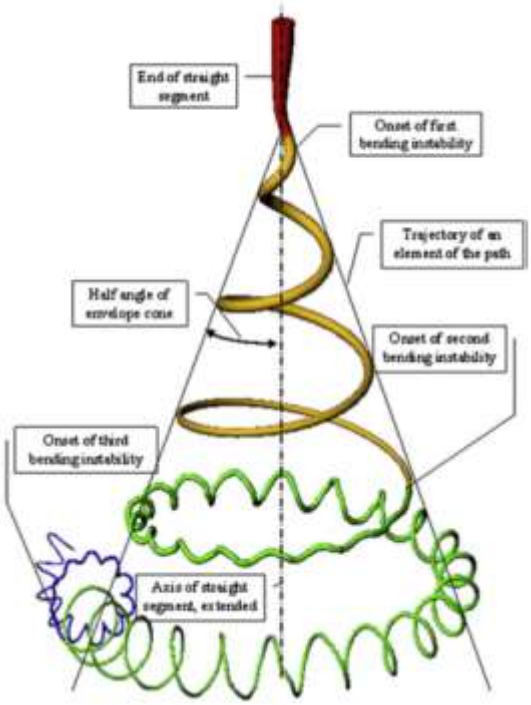

Figure 2.6 Diagram showing onset and development of bending instabilities (adapted from D. H. Reneker and H. Fong, Polymeric Nanofibres, American Chemical Society, Washington DC, 2005).[64]

The solidification of the jet results in the deposition of a dry nanofibre on the collector. The solidification rate varies with the polymer concentration, electrostatic field and gap distance. With the evaporation of the solvent and posterior solidification of the fluid jet, it is normally observed a mass decrease and a volume variation. This stage is characterized by strong attachments at crossing points that hence stiffen the mat. This is an important factor since it determines the mechanical properties of the structure. After the onset of bending instability, the jet path may follow a very complicated path, and successive loops of coil may touch in flight and form permanent connections, Figure 2.7.

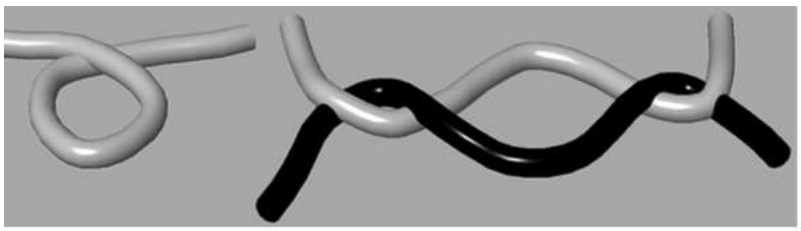

Figure 2.7 A diagram of a loop in a segment of one fibre and another loop (adapted from Reneker et al., Polymer 43, 6785, 2002).[64]

There are many parameters that will influence the morphology of the resultant electrospun fibres from beaded fibres to fibres with pores on its surface. Performing electrospinning comprises the understanding of several features which will directly influence that resulting fibre morphology. These features are usually related to the working conditions in which the technique is undertaken.

2.5.2 Effects of working parameters on electrospinning

Working parameters are very important to understand not only the nature of electrospinning but also the conversion of polymer solutions into nanofibres through electrospinning. The parameters affecting electrospinning and the fibres may be broadly classified into polymer solution parameters, processing conditions which include the applied voltage, temperature, and effect of collector, and ambient conditions. Each of these parameters can affect the fibres morphologies, and by proper control of these parameters we can fabricate electrospun fibres with desired morphologies and diameters.[62]

A. Polymer Solution Parameters

i. Concentration

The polymers concentration is an important parameter in the solution aspects because it affects both surface tension and viscosity of the solution, and the deposition area. For very low concentration, polymeric micro- and nanoparticles will be obtained. At this point, electrospray occurs instead of electrospinning because the low entanglement of polymer chains cannot withstand the electrostatic charge. As the concentration is gradually increased, a mixture of beads and thin fibres will be formed along the fibre axis. When the

concentration is suitable, smooth and more uniform nanoFibres can be obtained. If the concentration is too high, the fibre formation will not occur.[9]

ii. Molecular Weight and Solution Viscosity

The molecular weight of the polymer represents the length of the polymer chain, which in turn influence the viscosity of the solution. One of the conditions necessary for electrospinning to occur where fibres are formed is that the solution must consists of polymer of sufficient molecular weight and the solution must be of sufficient viscosity. As the jet leaves the needle tip during electrospinning, the polymer solution is stretched as it travels towards the collection plate. During the stretching of the polymer solution, it is the entanglement of the molecule chains that prevents the electrically driven jet from breaking up thus maintaining a continuous solution jet. As a result, monomeric polymer solution does not form fibres when electrospun.[65] Keeping the concentration fixed and lowering the molecular weight of the polymer tends to form beads rather than smooth fibres. Increasing the molecular weight, smooth fibres will be obtained. When the viscosity of the solution is too low, electro-spraying may occur. A way to increase the viscosity of the solution is to increase the polymer concentration. During electrospinning, there may be secondary jet erupting from the main electrospinning jet which is stable enough to yield fibres of smaller diameter at certain viscosity. This may explain the differential fibre diameter distribution observed in some cases. However, when the viscosity is high enough, it may discourage secondary jets from breaking off from the main jet which may contribute to the increased fibre diameter.[7]

iii. Surface Tension

The initiation of electrospinning requires the charged solution to overcome its surface tension. The jet stretching already reported is caused by the influence of solution surface tension in the drops and, consequently, the cause of fibres formation. As the jet travels towards the collection plate, the surface tension may cause the formation of beads along the jet. Surface tension has the effect of decreasing the surface area per unit mass of a fluid and is directly affected by the temperature. For a pure liquid system, the surface tension of the liquid would decrease with increasing temperature.[33,66]

iv. Polymer Solubility

The structure of the polymer has an impact on its solubility in the solvent. Generally, a polymer with higher molecular weight is less soluble and takes much longer to dissolve than one with a lower molecular weight using the same solvent. Crystallinity of the polymer measures the degree of orderliness of the polymer chain packed within the bulk. Polymers of higher crystallinity has lower solubility as the solvent molecules have difficulty in penetrating the interior of the polymer bulk.[62,67]

v. Volatility (Evaporation) of the solution

The type of solvent is important to determine the ability of fibre forming. When most of the solvents have evaporated when the jet reaches the collector, individual fibres are formed. If the ejected fibres are collected before the complete evaporation of the solvent, the fibres will either flatten or adhere to other fibres causing interconnected network of fibres. Moreover, if the rate of evaporation of the solvent is too low such that the solution has not evaporated sufficiently when the electrospinning jet reaches the collector, fibres may not be formed at all, and a thin film of polymer solution are deposited on the collector. The evaporation rate of a solvent is dependent on many factors: vapour pressure, boiling point, specific heat, enthalpy and heat of vaporization of the solvent, rate of heat supply, interaction between solvent molecules and between solvent and solute molecules, surface tension of liquid, and air movement above the liquid surface.[9,62]

B. Processing Conditions

i. Voltage

A crucial element in electrospinning is the application of a high voltage (HV) to the solution. The high voltage will induce the necessary charges on the solution and together with the external electric field, will initiate the electrospinning process. Generally, both high negative or positive voltage of more than 6kV can cause the solution drop at the tip of the needle. Depending on the feed rate of the solution, a higher voltage may be required so that the Taylor Cone is stable. In most cases, a higher voltage will lead a reducing in the diameter of the fibres and encourage faster solvent evaporation to yield drier fibres. The effect of high voltage is not only on the physical appearance of the fibre, it also affects the crystallinity of the polymer. The electrostatic field may cause the polymer molecules to be more ordered during electrospinning, thus inducing a greater crystallinity in the fibre. Another factor that may influence the diameter of the fibre is the flight time of the electrospinning jet. A longer flight time will allow more time for the fibres to stretch and elongates before it is deposited on the collection plate. Thus, at a lower voltage, the reduced acceleration of the jet and the weaker electric field may increase the flight time of the electrospinning jet which may favour the formation of finer fibres. Both AC and DC voltage supply can be used in electrospinning, although DC is more commonly used.[62]

ii. Feed rate

The feed rate will determine the amount of solution available for electrospinning. For a given voltage, there is a corresponding feed rate if a stable Taylor Cone is maintained. When the feed rate is increased, there is a corresponding increase in the fibre diameter or beads size, Figure 2.8.[9]

iii. Effect of Collector

The collector plate is made of conductive material such as aluminium foil which is electrically grounded so that there is a stable potential difference between the source and the collector. In the case when a non-conducting material is used as a collector, charges on the electrospinning jet will quickly accumulate on the collector which will result in fewer fibres deposited with lower packing density compared to those collected on

a conducting surface. For a conducting collector, charges on the fibres are dissipated thus allowing more fibres to be attracted to the collector.[62]

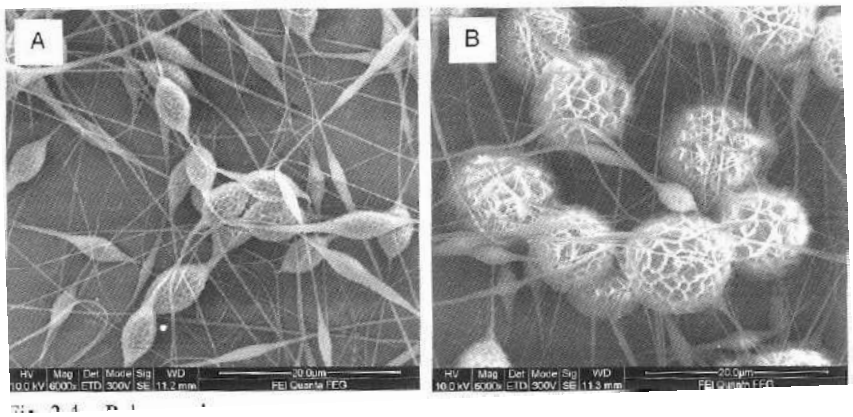

Figure 2.8 Polycaprolactone fibres with increasing beads size with increasing feed rate at A. 0.5mL/h and B. 2mL/h (courtesy of Teo and Ramakrishna, National University of Singapore).[62]

iv. Nozzle (needle) diameter

A smaller internal diameter of the needle was found to reduce the clogging as well as the number of beads on the electrospun fibres. The reduction in the clogging could be due to less exposure of the solution to the atmosphere during electrospinning. Decrease in the internal diameter of the orifice causes a reduction in the diameter of the electrospun fibres. In any case, if the diameter of the orifice is too small, it may not be possible to extrude a droplet of solution at its tip.[62]

v. Distance between Tip and Collector

Varying the distance between the tip and the collector will have a direct influence in both the flight time and the electric field strength. Increasing collecting distance cause fibre diameter decrease as the jet will have a longer distance to travel. It gives enough time for the solvents to evaporate before reaching the collector. When the distance is too low, excess solvent may cause the fibres to merge where they contact to form junctions resulting in inter and intra layer bonding, Figure 2.9. This interconnected fibre mesh may provide additional strength to the resultant scaffold.[9]

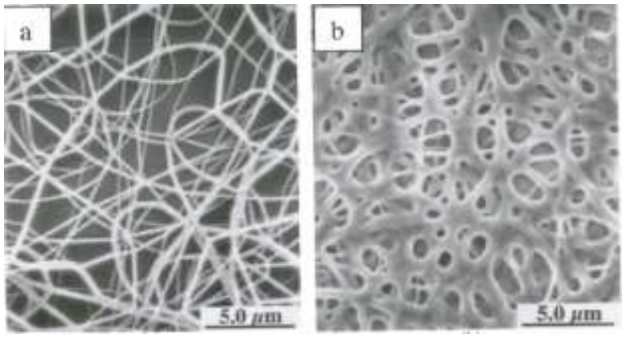

Figure 2.9 Nylon 6,6 at a) 2 cm deposition distance and b) 0.5 cm deposition distance (adapted from Buchko et al., 1999).[62]

C. Ambient Parameters

i. Humidity

The humidity of the environment determines the rate of evaporation of the solvent in the solution. There are no ideal values for humidity to improve the morphology of the fibres. However, at a very low humidity, a volatile solvent may dry rapidly.[62]

ii. Type of Atmosphere

Different gases have different behaviour under high electrostatic field. For example, helium will break down under high electrostatic field and thus electrospinning is not possible. When gas with higher breakdown voltage is used, the fibres obtained have twice the diameter of those electrospun in air, given all other conditions equal.[62]

iii. Pressure

Generally, reduction in the pressure surrounding the electrospinning jet does not improve the process. When the pressure is below atmospheric pressure, the polymer solution in the syringe will have a greater tendency to flow out of the needle and there cause unstable jet initiation. As the pressure decreases, rapid bubbling of the solution will occur at the needle tip. At very low pressure, electrospinning is not possible due to direct discharge of the electrical charges.[62]

2.5.3 Properties of electrospun nanofibres

A. Porosity

For a variety of applications, porous fibre surfaces are desired. In electrospun nanofibres, two types of pores can be identified: pores on/within each fibre and pores between the fibres of a nanofibrous membrane. A high density of pores can be formed due to the entanglement of fibres. When compared to mesoporous materials (e.g., molecular sieves), the specific surface area of the electrospun fibres is lower, but the pores are relatively large and fully interconnected to form a 3D network. The knowledge of pore size and porosity is essential in determining the membrane's performance. Pore size determines the type of substance or species that can permeate through, whereas porosity is a measure of the flow across the membrane.[64,68]

B. Surface structure

The surface of electrospun fibres is generally smooth. The use of low concentration solution or high electrical potential produces beaded electrospun structures that are considerably rougher than completely fibrous structures, Figure 2.10. The cross-sectional shape of electrospun fibres is usually circular. However, in some cases, a skin forms on the polymeric jet and then collapses into a ribbon as the solvent evaporates. This results in flattened nanofibres, which are created with high molecular weight polymers and high polymer concentration. The solvent evaporation reduces with higher solution viscosity, resulting in wet fibres that reach the collector

and are flattened by the impact. The flat ribbon shape can be attributed to the collapse of an outer skin formed on the surface of the jet.[64]

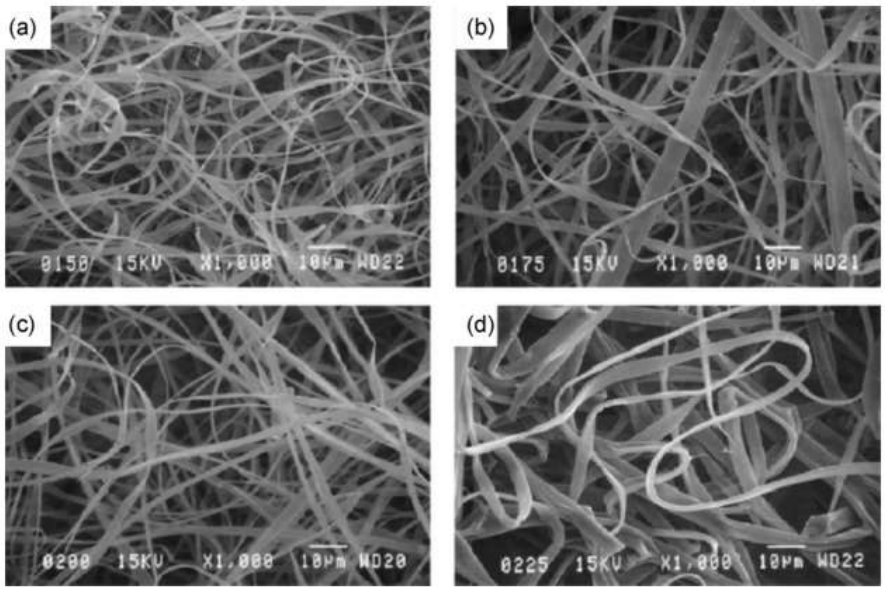

Figure 2.10 SEM images of electrospun haemoglobin in 2,2,2-Trifluoroethanol at the following concentration: (a) 150 mg/ml, (b) 175 mg/ml, (c) 200 mg/ml and (d) 225 mg/ml (courtesy of Barnes et al., Journal of Engineered Fibers and Fabrics, JEFF, 1, 16, 2006).[64]

C. Chain conformation and crystallinity

Due to rapid stretching of the electrified jet and the rapid evaporation of the solvent, the polymer chains are expected to experience an extremely strong shear force during the electrospinning process. This rapid stretching and solidification can prevent the polymer chains from relaxing back to their equilibrium conformations. As a result, more molecular orientation is found. The rapid stretching and solidification of the polymer chains lead to another important effect, the retardation of the crystallization process. The time is not enough for stretched chains to crystallize. Although the polymer chains are noncrystalline in the nanofibres, they are highly oriented. Thus, the defects in crystallization are minimal.[64]

2.6 Potential of electrospun PCL fibre mats for biomedical applications

Poly (ε-caprolactone), (PCL) or simply polycaprolactone is a hydrophobic semi-crystalline polymer. Its biodegradability, biocompatibility, chemical and thermal stability, and good mechanical properties present the viability in the usage of this polyester in the emerging field of biomedical applications.[9,69] Biodegradable synthetic polymers as PCL are widely used as scaffolds for TE. The electrospun PCL fibre mats act as temporary substrates for promoting adhesion, proliferation and differentiation of various types of cultured cells, carriers for biological agents, and wound decreasing materials.[6] PCL is synthetized by ring opening polymerization of the cyclic monomer ε-caprolactone, using various anionic, cationic and co-ordination catalysts.

The good solubility and blend compatibility of PCL has been making it useful in biomedical applications. Because PCL can be degraded in slower rate than other polymers such as polyglycolide, poly D,L-lactide and its copolymers, thus it is suitable for use in applications that require slow degradation. PCL can be blended and modified with other polymers to improve its physical, chemical, and mechanical properties. Moreover, it is approved by the Food and Drug Administration for use in humans.[69] In addition, PCL can be formed as continuous ultrafine fibres by electrospinning to give excellent characteristics such as high porosity and surface area.[9] The degradation of PCL nanofibres has received a great deal of attention when used as an implantable biomaterial. PCL can be degraded by hydrolysis of its ester linkages in physiological conditions (such as in the human body).[69] Biodegradability of PCL is important; thus, the sub-products of degradation could not evoke any inflammatory reaction. Depending on the molecular weight, PCL as a homopolymer has degradation times ranging from 2 to 4 years. As a semi-crystalline material, the degradation initiates in the amorphous regions. When the amorphous phases are fully degraded, it results in a highly crystalline but with low molecular weight polymer. Water molecules will permeate further into the implant. Further degradation of the crystalline phase is carried out by cellular activity, and will result in fragmentation and decreased mechanical properties.[41,70]

The hydrophobic nature of PCL limits protein absorption and consequently cell attachment. To improve the hemocompatibility and endothelization of PCL nanofibres, usually the polymer surface is submitted to a chemical modification. This should enhance the subsequent immobilization of various bioactive substances.[71,72] Several approaches have been developed to modify polymer surfaces, such as plasma modification, wet chemical method, surface graft polymerization, blending of synthetic polymers with natural ones, or physical adsorption of proteins.[73,74]

CHAPTER 3 – MATERIALS AND METHODS

3.1 Materials

3.1.1 Synthesis of EAK 16–II

The solid support, Rink Amide MBHA resin LL (100–200 mesh) (4–(2Æ,4Æ–Dimethoxyphenyl–Fmoc-aminomethyl)–phenoxyacetamido norleucyl–MBHA), was provided by Novabiochem® (Merck KGaA, Darmstadt, Germany). The Fmoc (9–Fluorenylmethyloxycarbonyl) protected amino acids: Fmoc–Glu(OtBu), Fmoc–Ala and Fmoc–Lys(Boc) were from Novabiochem®. The coupling reagents 2–(1H–Benzotriazole–1–yl)–1,1,3,3-tetramethyluronium hexafluorophosphate (HBTU), 1–Hydroxybenzotriazole (HOBt) and 1–[Bis(dimethylamino)methylene]–1H–1,2,3–triazolo[4,5–b] pyridinium 3–oxid hexafluorophosphate (HATU) were from Advanced Biotech® (Seveso, Italy) and the coupling reagent Oxyma Pure (Ethyl cyano(hydroxyimino)acetate) was from Novabiochem®. Solvents as trifluoracetic acid (TFA) and N-methyl–2–pyrrolidone (NMP) were from Biosolve® (Leenderweg, Valkenswaard, Netherlands), *N*,*N*–dimethylformamide (DMF) was from AnalaR NORMAPUR® (VWR International, Milan, Italy) and (triethoxysilane) (TES) was from Sigma-Aldrich® (Merck KGaA, Darmstadt, Germany). N,N–diisopropylethylamine (DIPEA), piperidine and ninhydrin (2,2–Dihydroxyindane–1,3–dione) were from Biosolve®.

3.1.2 Synthesis of HVP-CHO

The solid support, H–Phe–H NovaSyn® TG resin, was provided by Novabiochem® (Merck KGaA, Darmstadt, Germany). The Fmoc protected amino acids: Fmoc–Gly–OH, Fmoc–L–His(Trt)–OH, Fmoc–L–Tyr(tBu)–OH and Fmoc–L–Arg(Pbf)–OH were from Novabiochem® (Merck KGaA, Darmstadt, Germany). The Fmoc-protected amino acids: Fmoc–L–Asn(Trt)–OH, Fmoc–L–Lys(Boc)–OH and Fmoc–L–Phe–OH were from Novabiochem® (Merck Schuchardt OHG, Hohenbrunn, Germany). The Fmoc–protected amino acid Fmoc–(7-aminoheptanoic acid) was from Bachem AG (Bübendorf, Switzerland). The coupling reagents 2–(1H–Benzotriazole–1–yl)–1,1,3,3–tetramethyluronium hexafluorophosphate (HBTU) and 1–Hydroxybenzotriazole (HOBt) were from Advanced Biotech® (Seveso, Italy). Solvents as trifluoracetic acid (TFA) and N-methyl–2–pyrrolidone (NMP) were from Biosolve® (Leenderweg, Valkenswaard, Netherlands), *N*,*N*–dimethylformamide (DMF) was from AnalaR NORMAPUR® (VWR International, Milan, Italy) and (triethoxysilane) (TES) was from Sigma-Aldrich® (Merck KGaA, Darmstadt, Germany). N,N–diisopropylethylamine (DIPEA), piperidine and ninhydrin were from Biosolve®.

3.1.3 Peptide purification

The purification used MilliQ H_2O, the organic solvent acetonitrile (CH_3CN) provided by VWR International s.a.s (Fontenay-sous-Bois, France) and the ion-pair reagent trifluoracetic acid (TFA). These reagents were used to produce two eluents for the analysis.

Eluent A: 0.05% TFA in MilliQ H_2O;

Eluent B: 0.05% TFA in CH_3CN (acetonitrile).

3.1.4 Mass analysis

Mass analysis used matrix-assisted laser desorption ionization (MALDI) matrix (H_2O MilliQ/CH_3CN, 0.1% TFA, 10μg/μl α-cyano-4-hydroxycinnanic acid), prepared in the laboratory.

3.1.5 PCL electrospun fibres

The polymer Polycaprolactone (PCL) Mn. 60000 was from Sigma-Aldrich® (Steinheim, Germany). The solvent Hexa-fluoroisopropanol (HFIP) was from Sigma-Aldrich® (Steinheim, Germany) and the solvent dichloromethane (DCM) was from Biosolve Chimie (France).

3.1.6 Plasma Polymer Deposition

The chemical precursor (3-aminopropyl)triethoxysilane (3-APTES, ≥98%) was from Sigma-Aldrich® (Merck KGaA, Darmstadt, Germany).

3.1.7 Biological assays

The culture medium Dulbecco's modified Eagle's Medium/Ham's F-12 Nutrient Mixture (D-MEM/F12), the Fetal Bovine Serum (FBS), sodium pyruvate, nonessential amino acids, antibiotic-antimycotic solution, insulin, and Trypsin-EDTA were all provided by Gibco® (Invitrogen, Milan, Italy). Ascorbic acid, dexamethasone, β-glycerophosphate and (3–(4,5–dimethylthiazole–2–yl)–2,5–diphenyl tetrazolium bromide) (MTT) were from Sigma-Aldrich® (Milan, Italy).

3.2 Methods

3.2.1 Fmoc - Solid Phase Peptide Synthesis

Solid-Phase Peptide Synthesis (SPPS) was introduced by Bruce Merrifield in 1959 and has now become the method of choice to produce peptides because of the facility to obtain the final product rapidly and in a less expensive way. Solid-phase is a powerful strategy for multi-step reactions and it means that the desired molecule will be synthesized on the surface of a solid polymeric support. It changed the strategy of peptide synthesis by allowing the isolation of the intended products out of each step and simplifying the tedious and demanding steps of purification associated with solution phase synthesis. Moreover, it permitted the development of automation and the extensive range of robotic instrumentation, saving lots of time during the procedure and dramatically improving the yields of product. In SPPS two main strategies are used: the *Boc/Bzl* and the *Fmoc/tBu* approaches for N-terminal/side chain protecting groups. In this work, the focus is the Fmoc strategy for SPPS. The *Fmoc/tBu* method is based upon an orthogonal protecting group strategy.[75]

SPPS is performed from the C-terminus to the N-terminus of the peptide (opposite to direction in nature) with the introduction of N^{α}-protected amino acids. In *Fmoc*-SPPS, the peptide chain is assembled stepwise, one amino acid at a time, while attached to an insoluble resin support. Amino acids are protected at their amino terminus by the *Fmoc* group. *Fmoc* is a special protecting group which is used to protect amine functional groups from reacting. This approach uses the base-labile *Fmoc* group for protection of the α-amino function from the acid-labile linkers that constitute the C-terminal amino acid protecting group. This amino group acts as a linker in the amino acids coupling reactions and is responsible for the activation reaction between the first amino acid and the resin. Before every coupling reaction, the amino acid needs to be *Fmoc*-de-protected, resulting in a free amine group available for coupling. The amino acids coupling reaction, and the consequent chain grow, occurs after activation of the carboxylic acid terminus. This procedure is repeated doing *n*-de-protections and *n*-couplings during *n*-cycles until the desired sequence is complete. Once chain elaboration is accomplished, the final *Fmoc* should be equally removed and the N-terminus can be either left as a free amine or it can be capped with a subtle group. The peptide is then cleaved from the resin and side chain protections are removed. In this synthesis, a process of washing and filtration of the sample is performed at the end of each step. Thus, excess of reagents, solvents, and any other compounds not bound to the resin are removed. This procedure can prevent unwanted reactions, allowing higher yields, and producing cleaner synthesis.[76] Figure 3.1 summarizes the SPPS method.

i. Solid support

The solid support is a plastic polymer functionalized with a linker molecule. These are often referred to as resins. The resin is an insoluble and inert support. The function of the linkers is to link the peptide to the resin during SPPS. The linker also defines the C-terminal functional groups that can be either an acidic or an amidic group, formed, respectively, via an ester or an amide bond. For the synthesis of C-terminal peptide amides the

commonly used resins are Rink amide resin, Pal resin, and Sieber resin. These resins are compatible with *Fmoc* chemistry and final acidic cleavage. These resins are usually *Fmoc*-protected and should be deprotected before incorporation of the first residue.[77]

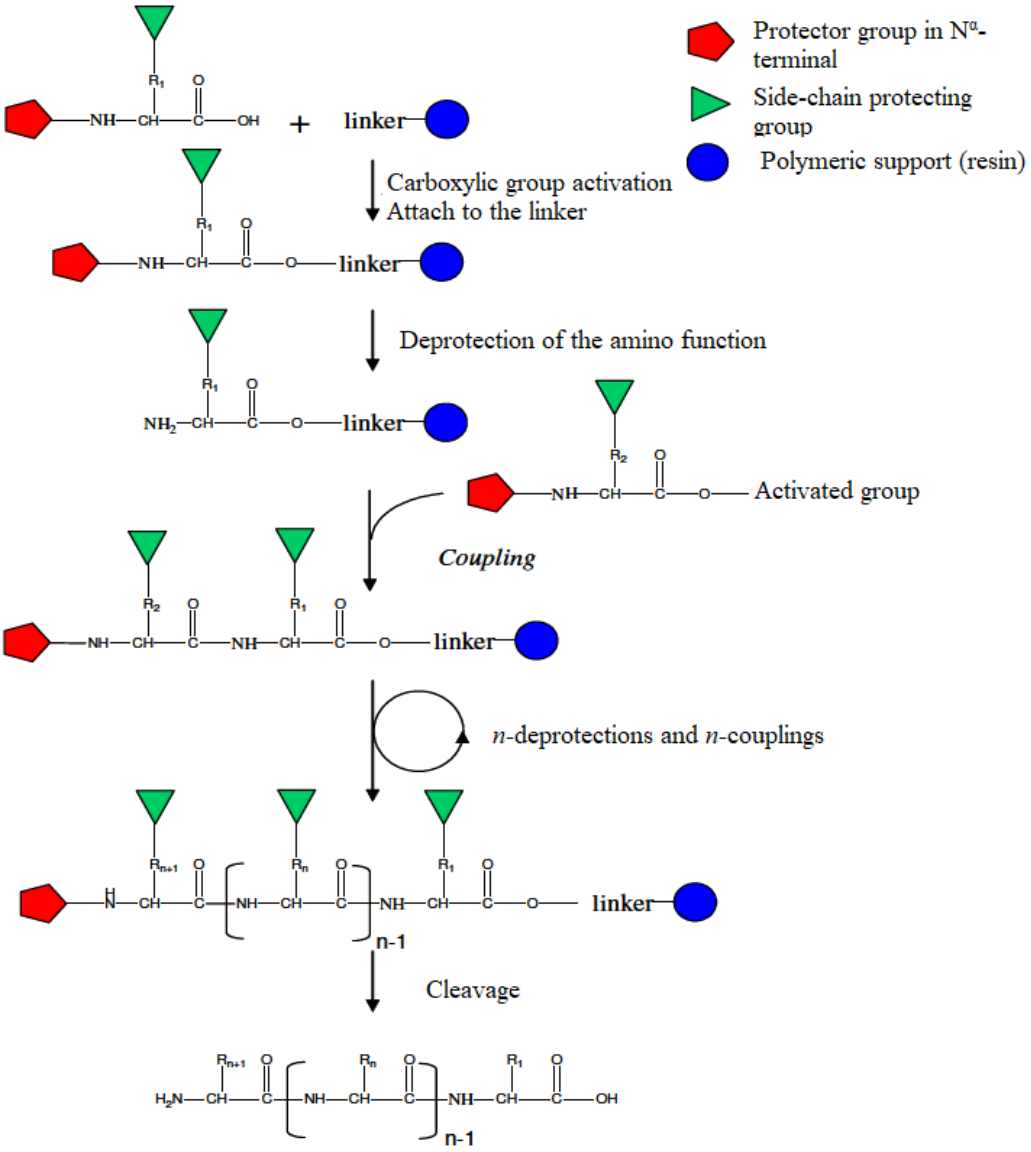

Figure 3.1 Scheme of SPPS method, (adapted).[77]

ii. Solvents

Prior to beginning a synthesis, the resin should be swelled in the synthesis solvent. The most common solvents for *Fmoc*-SPPS are dimethylformamide (DMF) or N-methylpyrolidone (NMP). Swelling the resins allows them to expand and maximize the exposure of their functional groups to the incoming reactants. NMP and DMF are common used solvents. They efficiently solvate the resin and, in many cases, improves coupling

yield. Most common peptide reagents are very soluble in NMP; however, DMF is cheaper that NMP, so it is more frequently used even despite its tendency to release reactive amines.

iii. *Fmoc*-deprotection and Piperidine test

Fmoc is stable in acidic conditions but it is easily removed by a weak base. Typically, piperidine is used as the base for this de-protection reaction. The result is an unprotected or free amine which can undergo a coupling reaction with the carbonyl of the next amino acid. *Fmoc* de-protection is a very critical step since it determines the yield and quality of reaction due to deleted residues and even capped peptides. *Fmoc* group removal in SPPS proceeds through a two-step mechanism, where the unprotected amino acids, or resin, are protonated resulting in the final product with a free -NH_2 group. The first step is the removal of the acidic proton at the 9-position of the fluorene ring system by a mild base, preferably a secondary amine, like piperidine. The use of cyclic secondary amines is more convenient due to their nucleophilicity (capacity to attack any other atom than hydrogen). The second step is the subsequent β-elimination that yields a highly reactive dibenzofulvene (DBF) intermediate which is immediately trapped by the secondary amine to form stable adducts, Figure 3.2. This step occurs with the formation of CO_2. These reactions work better in an electron donor and relative polar medium, such as DMF.[78] To ensure the correct coupling of the first amino acid, a piperidine test is performed. This test is also known as resin functionalization test and is used to quantify the functionalization of the resin with the first amino acid. *Fmoc* removal can be monitored by UV spectroscopy. The de-protection results in formation of a DBF-piperidine adduct that strongly absorbs in the UV range. This is a common procedure with automatic synthesizers. The piperidine test must result in a functionalization of, at least, 98%.

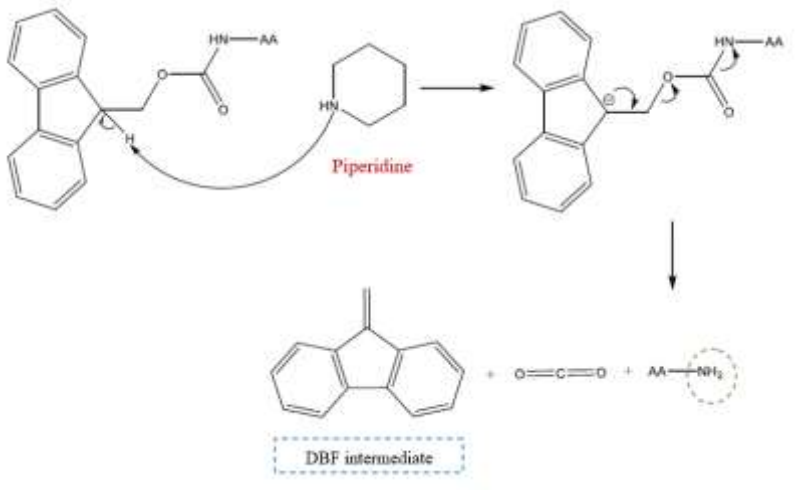

Figure 3.2 Mechanism of removal of *Fmoc* protecting group using piperidine, (adapted).[103]

iv. Carboxylic activation and coupling reagents

The activation reaction involves the binding of the carboxyl terminal of the amino acid to the solid support, and to the consequent amino acids. The carboxylate here is not very reactive, thus the carbonyl needs to be activated. The activation of the carboxylic group passes through making it more electrophilic. Normally, this step is performed using the coupling reagents promoting the activation *in situ*. Coupling reagents activate the carbonyl group for substitutions by converting the anionic oxygen into an acceptable leaving group. The carboxylic activation is described as an acceleration of carbodiimide-mediated couplings, a suppression of racemization and an inhibition of dehydration of the carboxamide side chains. In other words, it is the chemical process responsible to remove the carboxylic group present in the amino acid nomenclature and to form an amidic group, sustaining the chirality of the molecule. Activation occurs very rapidly in DMF. Excellent results have been obtained for *Fmoc*-SPPS using the activating reagent HBTU combined with HOBt, in the presence of a base such as the tertiary amine DIPEA. HATU is also typically used in cases of difficult coupling reactions and its rather combined with Oxyma Pure.[79]

v. Kaiser test (ninhydrin test)

The *Kaiser* test is a quantitative and very sensitive test where it uses ninhydrin to detect the presence or absence of free primary amino groups. It is a widespread colorimetric assay commonly used in SPPS to monitor the N-terminus de-protection, to determine if coupling reactions are complete, and gives the overall yield of the reaction. This test is responsible to determine the percentage of free amine groups present in the synthesis, i.e., the amine groups that didn't react with the C-terminus of the following amino acid, resulting in short chains of peptide. Ninhydrin reacts with the de-protected N-terminal amine group of the peptide-resin. Ninhydrin is a white solid which is soluble in ethanol and acetone at room temperature. When reacting with free amines, a deep blue or purple colour known as Ruhemann's purple is produced, Figure 3.3. However, when amino acids residues are attached with their N-terminus protected, so if the next residue has been successfully coupled onto the chain, the test gives as colourless or yellow result.[80] Depending on the colour obtained the synthesis can either proceed or undergo the repetition of some previous steps. The actions followed according to the obtained colour are described in the table 1. In the end, the yield of reaction needs to be more than 97% to assume completion of the coupling reaction and for the synthesis to proceed.

Table 1 Actions available according to the colour results obtained from reacting ninhydrin with free amines.[81]

Colour	Result	Action
Colourless or faint blue	Complete coupling	Proceed with synthesis
Dark blue, colourless beads	Nearly complete coupling	Extend coupling or cap unreacted chains
Light blue, dark blue beads	Incomplete coupling	Recouple
Intense blue, all beads are blue	Failed coupling	Check amino acids, reagents Recouple

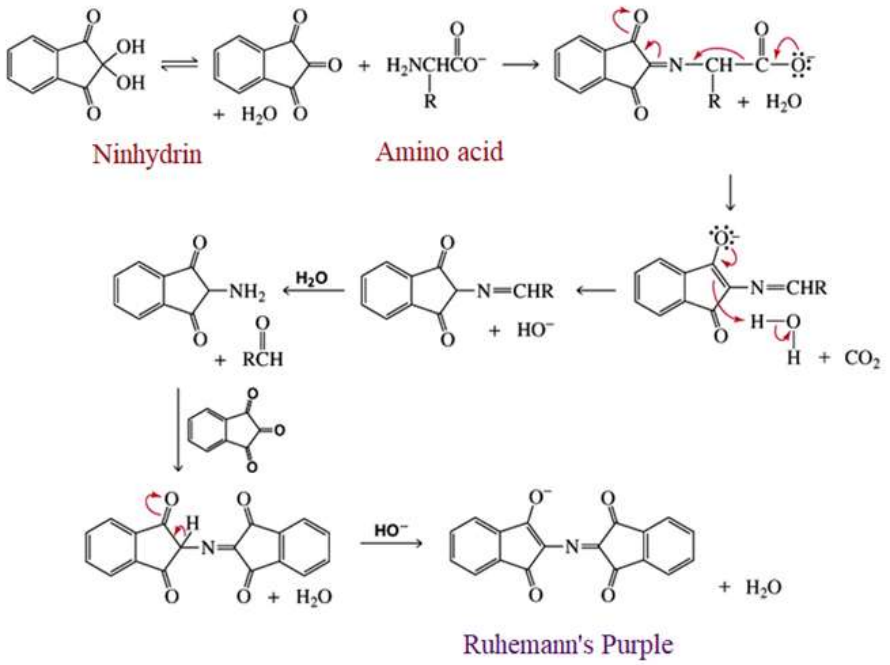

Figure 3.3 Mechanism describing the reaction of ninhydrin with free amines, resulting in the formation of the Ruhemann's Purple compound (adapted).[80]

vi. Side chain protecting groups

In the *Fmoc* strategy, it is important that the side chain protecting groups are not sensitive to base, so that these groups remain on the side chains throughout all coupling steps and do not fall off during the piperidine de-protection steps. Some of the most commonly used side-chain protecting groups are *Boc* and *OtBu*. Both aren't reactive with piperidine and can be removed under acidic conditions, commonly using TFA, at the final cleavage of the peptidyl-resin linkage. Both permanent and temporary protector will ensure the reaction of *Fmoc*-amino acids, only in the site of interest for the formation of the peptide bond. It helps to prevent secondary reactions, such as the incorporation of dipeptides derivatives instead of an amino acid derivative. In addition, it may help in the final purification of the product due to reduced number of undesired products.[75]

vii. Final De-protection and Cleavage

After performing the coupling of all amino acids of the peptide sequence, the synthesis proceeds to peptide cleavage. Peptide cleavage consists in the separation of the peptide from the resin and in the removal of the side chain protecting groups and, thus, in obtaining the desired peptide, free of any protecting groups or structural modification. When using the orthogonal protection *Fmoc/tBu* strategy, the peptidyl-resin linkage and the side chain protecting groups are removed in an acidic environment, normally using TFA. The process of deprotection in an acid environment can, however, generate highly reactive species (e.g. carbocations). These carbocations are very reactive electrophilic species, capable of reacting with some side chains with nucleophilic characteristics, causing covalent modifications of some amino acid residues. The use of nucleophilic reagents, called scavengers (reactive with properties like those of the species to be protected), together with TFA during

the release, allows to significantly reduce unwanted side reactions. The cleavage is then performed using the so-called cleavage *cocktail*. The *cocktail* consists in a mixture of a solution composed mainly by TFA and appropriated scavengers such as water, trialkylsilanes, thiols. The choice of the release mixture, the type of scavengers and the time required by the de-protection, depend on the amino acid sequence, and on the nature and number of the protecting groups used in the side chain. Cleavage reactions typically take 0.5 to 3 hours depending on the linkers and protecting groups used. After the cleavage reaction, the cleavage solution is filtered from the resin and the peptide is obtained by precipitation with ice-cold ether. Peptides should be washed at least 3 times with ice-cold ether following precipitation to remove the scavengers as much as possible. Afterwards, peptides may be left in a hood to air-dry overnight, or lyophilized for storage.[75]

3.2.2 Peptide purification and chromatographic characterization

The crude peptide obtained from stepwise SPPS will often contain a variety of by-products in addition to the desired product. These products include peptides containing deletion or addition sequences generated during the synthesis itself and a series of peptides containing chemical modifications usually generated during the cleavage and de-protection steps. Crude peptides of less than 30 residues can be expected to be between 80-95% target peptide, all that is required is an effective purification protocol, where the other components can be successfully removed. In general, mostly of the peptides fewer than 50 residues in length can be purified using Reversed Phase - High Performance Liquid Chromatography (RP-HPLC). RP-HPLC is the most widely used analytical technique for the separation, identification and quantification of organic compounds in mixtures, such as biomedical samples. HPLC can be performed with or without prior clean-up steps, although time-consuming clean-up and fractioning steps are crucial to its success.[82] Molecules that possess some degree of hydrophobic character, such as proteins and peptides, can be separated by RP-HPLC with excellent recovery due to its high resolution.

i. Components of a basic RP-HPLC

A basic RP-HPLC system comprises the following components: a reservoir, a high-pressure pump, an injector, a column, and a detector, Figure 3.4. The reservoir is responsible to hold the solvent, called the mobile phase. The motion of the solvent is generated using a high-pressure pump that also serves to determine it specific flow rate. The sample is injected into the continuously flowing mobile phase stream by the injector, carrying the sample into the HPLC column. The column contains the chromatographic packing material needed to affect the separation. This packing material is called the stationary phase because it is held in place by the column hardware. A detector is needed to see the separated compound bands as they elute from the HPLC column. Commonly, UV detector with fixed or variable wavelength is used for liquid chromatographic analysis. The mobile phase exits the detector and can be sent to waste, or collected, as desired.[83]

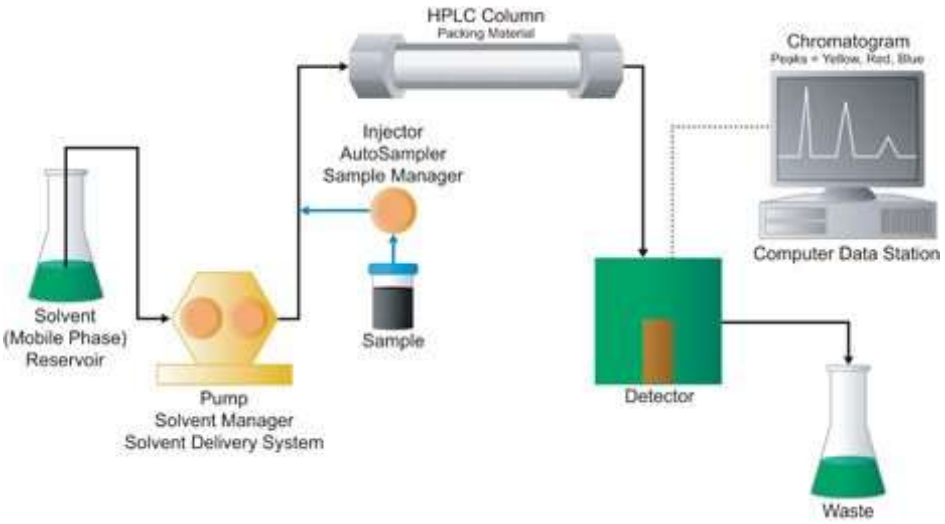

Figure 3.4 Components of HPCL system, adapted from Waters.

ii. Mechanism of protein/peptide retention

The retention mechanism in reversed phase chromatography depends on the hydrophobic binding interaction between the solute molecule in the mobile phase and the immobilized hydrophobic ligand, i.e. the stationary phase. Proteins and peptides possess some degree of hydrophobicity that allows them to be adsorbed by the stationary phase, Figure 3.5. The net interaction caused by this hydrophobic adsorption is very strong resulting in the protein remaining adsorbed to the surface. Much of the proteins are large when compared to the thickness of the hydrophobic surface. This makes them to lie above the surface and be permanently in contact with the mobile phase. The mobile phase constitutes the organic solvent. At a specific concentration of the solvent, proteins are desorbed from the surface and elutes from the column. The amount of organic solvent is unique to each protein. Elution can proceed either by isocratic conditions where the concentration of organic solvent is constant, or by gradient elution whereby the amount or organic solvent is increased over time. In this last case, a gradual increase in the concentration of organic solvent compared to water increases the hydrophobicity of the mobile phase and determines the competition between it and the stationary phase, resulting in a loss of the analyte.[84] Separation is accomplished by the single adsorption/desorption process, although there is some interaction with the surface as the protein moves down the column. The sample should ideally be dissolved in the initial mobile phase in a way to provide a reproducible and homogeneous solution. This solution must be relatively free of interferences to do not cause any damage in the column and be prepared accordingly to the solvent system that will be employed.

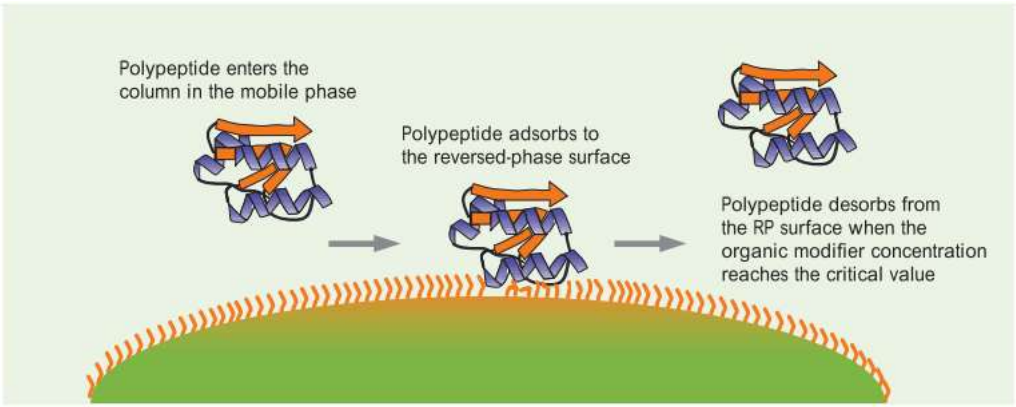

Figure 3.5 Hydrophobic interactions and protein adsorption inside the column in RP-HPLC.[84]

iii. Column characteristics

The column is selected depending on the nature of the solute and the information about the analyte. Proteins and peptides are separated by interacting with the hydrophobic surface of particles packed in columns. The particles in the column are usually made of silica because silica is physically robust, it is stable under most solvent conditions (except at pH greater than 6.5), and can be made into spherical particles of various sizes with pores of different diameters. The silica is modified with a hydrocarbon molecule to create a hydrophobic surface. A C8 or C18 column made from specially purified, less acidic silica, and designed specifically for the separation of basic compounds is generally suitable for all samples and is strongly recommended. Columns with 5 μm particle size give the best compromise of efficiency, reproducibility, and reliability. Using small pore diameter (~100 Å) silica results in inferior proteins separations. Wide pore silica diameter (~300 Å) gives much better separation of proteins. The interaction between column and proteins/peptides occurs near the top of the column, thus, columns length is not important in protein separations.[85]

iv. Mobile phase

The mobile phase usually contains strong acids at low pH with large concentrations of organic solvent. The most popular organic modifier employed for separating peptides is acetonitrile. This solvent is essentially UV transparent. Most peptides only absorb at low wavelengths in the UV spectrum (typically less than 225 nm), and acetonitrile provides much lower background absorbance that other common solvents at low wavelengths. Acetonitrile is also used because it is volatile and it can be easily removed from the sample. The RP chromatography of proteins and peptides requires a reagent, called an “ion-pair”, added to the mobile phase intended to achieve good peak shape. It is believed that metal impurities on the silica surface are responsible for poor protein/peptide peak shape in the absence if an ion-pair reagent. The most commonly used ion-pair reagent is TFA. The TFA concentration may affect peptide selectivity. TFA added to the mobile phase at a concentration of ~0.1% results in good peak shape on most columns.[85]

3.2.3 Plasma polymer deposition through Atmospheric Pressure Plasma Jet (APPJ)

Specialists define plasma as "partially or completely ionized gas that comprises free electrons, ions, radicals and atoms or molecules of non-ionized neutral gas". Plasma deposition, also known as plasma activation or plasma functionalization, is a method employed for modifying or coating surfaces, aiming to improve the adhesion properties of the material. Plasma deposition has applications for the modification of surfaces, depositions of thin films, sterilization, or surface modification of polymer fibres, with utility in the biomedical, environmental, and technological fields. The goal of surface functionalization is to deposit chemical functionalities, independently of the substrate, to promote linkage with other substances added in a second moment, such as biomolecules. Amongst the several plasma modification techniques, Atmospheric Pressure Plasmas (APPs) are one of the most preferred techniques. APP treatments do not require complex and expensive vacuum systems and have shorter processing time.

The working principle of APPJ is based on the ionization of a gas through an electrical discharge. The present work used the method and device described in the patent U.S. Pat. No. 2016/0295676 by Patelli *et al.*, for generating plasma at atmospheric-pressure and under low-temperatures conditions. Low-pressure and low-temperature plasmas benefit the process of surface coating because they generate high concentrations of reactive species that can etch, and deposit thin films, and the thermally sensitive substrates are not damaged. This device is intended for treating surfaces and for deposition of surface coating by means of the introduction of a precursor in a channel situated inside and coaxial with respect to the duct with the plasma. This device comprises: a first pair of electrodes, each of which separated by a dielectric layer, arranged in a way that connects to a High-Frequency (HF) power supply, and externally positioned with respect to a tubular duct where the gas flows; a second pair of electrodes equally separated by a dielectric layer, arranged to connect with a Radio-Frequency (RF) power supply and with respect to said tubular duct where the same gas flows downstream with respect to the first pair and the direction of the flow. A HF excitation is applied to the first pair of electrodes. RF excitation is applied to the second pair of electrodes. The coupling of a HF power supply with RF power supply, and the possibility to operate with pulse trains is designed to obtain cold and self-sustained plasma in a wide range of work conditions and mixtures. The filamentary plasma generated in this manner emerges from the gas flow at the outlet of the transport duct, Figure 3.6. Filamentary plasma is a result of an applied electric field that is greater than the strike voltage, to the gas. This produces electrons' acceleration, causing avalanche ionization along the direction of the electric field itself, forming a filament that then dies out. Helium, hydrogen, neon, nitrogen, argon, oxygen or mixtures thereof can be used as operating gas in any ratio, resulting in a wide array of chemically active species in the plasma. These species can be either organic, inorganic, nano-composites, among others. Chemical precursors and reagents can be added to the plasma as vapours or aerosols.[86]

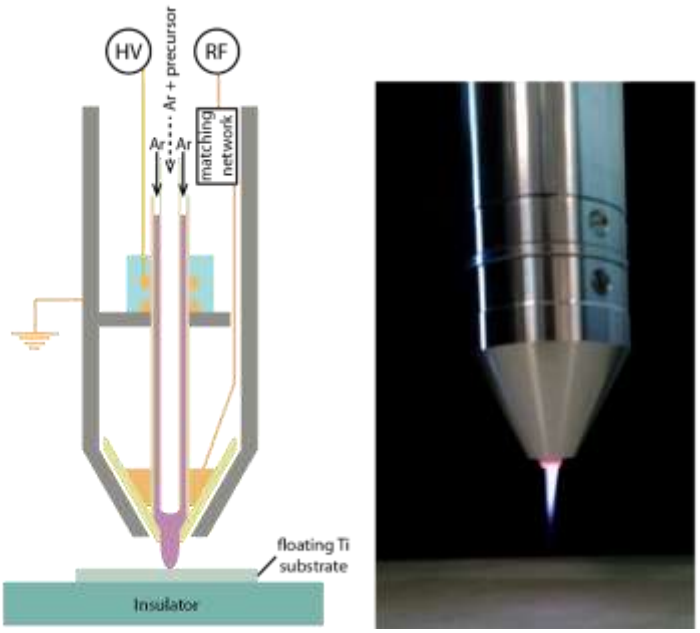

Figure 3.6 On the left, components and APPJ system; on the right, APPJ equipment with a filamentary jet.[86]

3.2.4 Chemo-selective ligation

Chemo-selective ligation is a term employed to describe a site-specific modification to facilitate the assembly of biomolecules. Often presented as chemical bio-conjugation, or simply bio-conjugation, chemo-selective ligation is the process of linking or connecting a biological molecule with another moiety under mild aqueous conditions. These moieties may include other biomolecules, synthetic polymers, and small molecules such as ligands, drugs, or fluorescent dyes, among others.

Bio-conjugation can happen through multiple chemical reactions. The choice of method of conjugation depends on the native functional groups presented in the target biomolecules. These groups are the primary sites for bio-conjugation and are generally nucleophiles or electrophiles. The most typical methods in chemo-selective ligation are the reaction of an amino group with activated carboxylic acids, isothiocynates, and carbonyls, such as ketones or aldehydes, although aldehydes are substantially more reactive than ketones, followed by *in situ* reductive amination.[87,88] Primary amines groups (R-NH_2) are one of the most common nucleophiles in biomolecules, and represent an ubiquitous key functional group found in many biological systems, such as in free amino acids. The reaction between an amine and a carbonyl is highly chemo-selective and is compatible with other functional groups present in biomolecules. Primary amines will spontaneously react with aldehydes and ketones to form imines, also known as Schiff bases, Figure 3.7 a). The resulting imine bond is covalent but reversible, and both its stability and dynamics strongly depend on the nature of the amine and the carbonyl. To address this shortcoming, reductive amination is usually carried out either as one-pot or two-step reaction with sodium cyano-borohydride, yielding a stable secondary amine, Figure 3.7 b).[89]

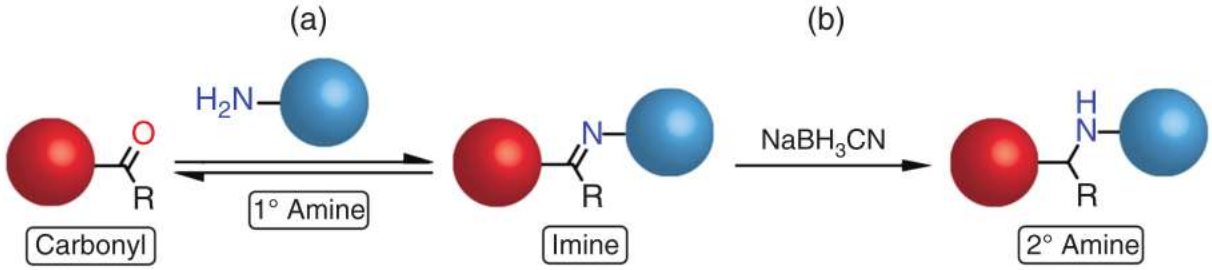

Figure 3.7 a) Primary amine reacting with aldehyde to for an imine; b) Reductive amination with $NaBH_3CN$, yielding a secondary amine, (adapted).[89]

3.3 Methods of analysis

3.3.1 Contact angle

Contact angle is employed to determine the wettability of a surface. The contact angle is defined as the angle formed in the point where solid, liquid, and vapour co-exist, also referred as the "three-phase contact line". The contact angle is geometrically acquired by applying a tangent line from the contact point along the liquid-vapour interface in the droplet profile. The angle, θ, between the surface and the static drop deposited indicates the wettability of the sample. Small contact angles (« 90º) correspond to high wettability, while large contact angles (» 90º) correspond to low wettability, Figure 3.8. Specifically, a contact angle less than 90º indicates that wetting of the surface is favourable, and the fluid will spread over a large area on the surface; while contact angle greater than 90º generally means that wetting of the surface is unfavourable so the fluid will minimize its contact with the surface and form a compact liquid droplet. Complete wetting occurs when the contact angle is 0º.[90]

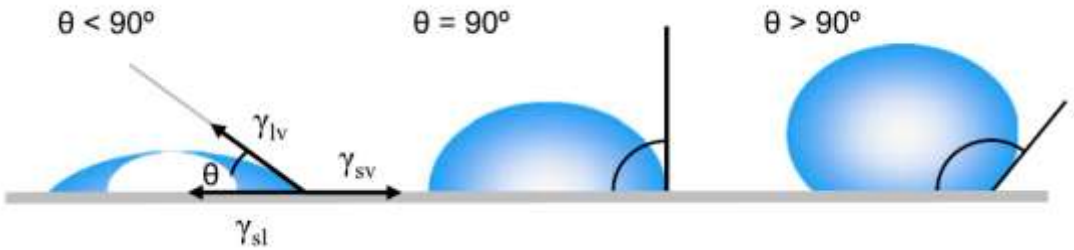

Figure 3.8 From left to right, contact angles indicating high wettability (θ<<90º), low wettability (θ=90º), and unfavourable wettability.[90]

3.3.2 Total Kjeldahl Nitrogen

The Kjeldahl method was developed by Johann Kjeldahl in 1883, and is usually considered to be the standard method to determine protein concentration. The method is based on a preliminary transformation of all the compounds of total nitrogen, organic and inorganic, to nitrate by digestion of an alkaline with a strong acid. Upon digestion, nitrogen is released and can be determined by a suitable titration technique. The total nitrogen in the sample is liberated at high temperature. UV-visible spectrophotometry constitutes one of the several techniques that can be used to measure the total nitrogen using Kjeldahl method. First, a calibration curve of absorbance versus nitrate concentration is prepared using a series of nitrate solutions of known concentration. The absorbance of the solution being analysed is then measured at the same wavelength, and its nitrate concentration determined from the calibration curve.[91]

3.3.3 Cell viability assay: MTT test

3-(4,5-dimethylthiazole-2-yl)-2,5-diphenyl tetrazolium bromide, is a yellow water-soluble tetrazolium salt, commonly represented by MTT. MTT assay is a colorimetric cell viability test, mainly used for spectrophotometric assessment of the metabolic activities of microorganisms, due to the colour yielded upon its enzymatic reduction. The yellow tetrazolium MTT is metabolically reduced by active cells, in part by the action of dehydrogenase enzyme, to yield a water-insoluble purple formazan crystal, which can be solubilized and quantified spectrophotometrically. The total amount of formazan produced is directly proportional to the number of viable cells in the culture; thus, the MTT assay represents a standard method for the indirect estimation of cell's viability. MTT dye is light sensitive; thus, the assays are usually done in the dark. MTT is currently the most employed method to assess cell proliferation; however, tetrazolium dye assays can also be used to measure cytotoxicity (loss of viable cells) or cytostatic activity (shift from proliferation to quiescence) of potential medicinal agents and toxic materials. The reason for its usage relies in its advantage to be performed using microplates and automated reading, significantly improving the test in terms of time and cost.[92,93]

CHAPTER 4 – EXPERIMENTAL PART

4.1 Peptide Synthesis and Characterization

4.1.1 Synthesis of EAK 16-II

The synthesis of EAK 16–II, amide terminal (H–Ala–Glu–Ala–Glu–Ala–Lys–Ala–Lys–Ala–Glu–Ala–Glu–Ala–Lys–Ala–Lys–NH_2), followed standard *Fmoc* chemistry SPPS method. The synthesis used Syro I synthesizer (MultiSynTech GmbH, Witten, Germany) with reaction mixing by vigorous vortex, performed in two reactors. The Syro I used fully automated HBTU/HOBt *in situ* cycles, in DMF.

For each reactor, the synthesis was carried out on 0.36 mmol g^{-1} (resin load) of Rink Amide MBHA resin. The synthesis scale was 0.125 mmol, given by the product between the resin load and the resin amount (347.2 mg). It is always used an excess of 10% in the resin amount calculated by the synthesizer. The resin was swallowed in DMF for 15 min. The quantities of the condensation reaction and every performed step are intrinsic to the synthesis and depend on the protocol followed. The overall volume (in mL) was displayed by the calculation protocol given by the synthesizer, and all the solutions were prepared in excess. The loading of the first amino acid (Lys) was carried out with double coupling. The following insertions were carried out with single couplings, and with double couplings from the 6^{th} cycle till the end of the synthesis. The calculation protocol estimated a synthesis time of 1 day, 13 hours and 29 minutes.

At each cycle, the α-amino function of the growing peptide suffered a reaction of *Fmoc*-de-protection, which comprises a three-step procedure:

1. Reaction with 1mL of a solution of 40% (V/V) of piperidine in DMF for 3 minutes;
2. Reaction with 1.8 mL of a solution of 20% (V/V) of piperidine in DMF for 12 minutes;
3. 6 washing steps, for reaction, with DMF, emptying the reactor of the liquid phase.

The resin is the first compound to be *Fmoc*-de-protected and is followed a piperidine test to evaluate the resin loading. The piperidine test was performed by taking a sample of the functionalized resin with a weight in the range of 4–8 mg. The sample was washed several times with methanol and left to dry under vacuum for 1 hour. Once dried, the sample was carefully weighted (must fit in the same range), and treated with 0.5 mL solution of 20% piperidine in DMF. The solution was left in contact with the resin for 15 minutes by shaking it manually. The deprotection of the amine group bound to the solid support generates the DBF intermediate which absorbs at a wavelength (λ) of 301 nm. The mixture is brought to a final volume (*V*) of 50 mL with DMF, and the absorbance at λ=301 nm is measured using the double-beam spectrophotometer UV/Vis Lambda 2, Perkin Elmer (Waltham, Massachusetts, USA). Absorption values measured at absorbance maxima can be used, in

combination with the respective molar absorption coefficient (ε=7800 $M^{-1}cm^{-1}$), to calculate the load of resins and amino acids, Equation 1:

$$load_{resin} = \frac{(A_{301} \times V)}{\varepsilon \times wt}, \qquad \text{(Eq. 1)}$$

where $load_{resin}$ is expressed in mmol g^{-1} and it represent how many moles (mmoles) of reactive sites (for coupling) are present in 1 g of resin. A_{301} is the absorbance at 301 nm, *V* is the volume of the solution in [mL], ε is the molar absorptivity in [$M^{-1}cm^{-1}$], and *wt* is the weight of the sample after dried in [g]. Eq. 1 gives the result for an experimental resin load. The yield of loading is given by Equation 2:

$$\eta\ (\%) = \frac{Experimental\ loading}{Theoretical\ loading} \times 100, \qquad \text{(Eq. 2)}$$

The activation of the carboxylic group was carried out using coupling reagents HBTU/HOBt/DMF. HBTU is the condensing reagent and HOBt is the coupling reagent that activates the carboxylic group. This activation uses a two-step procedure:

1. 45 minutes reaction of resin-peptidyl in the reactor with a mixture of:
   - 5 equivalents (in solution) of α-protected amino acids in DMF (1 mL of a 0.62 M solution);
   - 1.4 mL solution of 0.45 M HBTU/HOBt/DMF;
   - 10 equivalents (in solution) of DIPEA/NMP (0.625 mL of a 2 M).
2. 5 washing steps for reaction with DMF.

In a first attempt, the resin load resulted in 86%. Although this shortcoming conditioned the success of the remaining synthesis, it is a typical problem found when synthesizing self-assembling peptides. This can be controlled substituting the coupling reagents and performing more than one coupling per amino acid. The coupling reagents HBTU/HOBt were substituted by HATU/Oxima pure in the same proportions.

To determine the presence of free amino groups, and consequently the yield of the reaction, a *Kaiser* test is performed, usually at the end of all coupling reactions. The procedure for this test constituted in the following steps: take a sample of resin in the range of 2–8 mg, which was firstly washed 3 times with methanol and then, 2–3 drops of acetic acid was added (to avoid eventual *Fmoc*-removal). The sample was dried under vacuum for 1 hour and weighted again. Prepare Monitor 1, Monitor 2, and Monitor 3.

- Monitor 1 (solution of 76% (w/w) of Phenol/Ethanol);
- Monitor 2 (solution of 0.2 mM of KCN/Pyridine);
- Monitor 3 (solution of 0.28 M of Ninhydrin/Ethanol).

In the tube containing the resin was orderly added 75 μL of Monitor 1, 100 μL of Monitor 2, and 75 μL of Monitor 3. In another tube, was prepared for reference the same solution excluding the resin. Both mixtures were heated at 100ºC for 5 minutes and added to a 4.8 mL of a solution of methanol at 60%. After centrifugation,

the absorbance of the liquid phase was measured at 570 nm (ε=15000 $M^{-1}cm^{-1}$). The quantity of free amino function is calculated using Equation 3:

$$\mu mol/g \text{ of aminic groups} = \frac{(A \times V \times 10^{-6})}{\varepsilon \times P}, \qquad \text{(Eq. 3)}$$

where, A is the difference between the value of absorbance of the sample and the value of absorbance of the reference solution a 570 nm; *V* is the volume of the sample expressed in [mL]; and P is the weight of the sample in [mg].

The yield of the coupling reactions is given by Equation 4:

$$\eta\ (\%) = \left\{1 - \left[\frac{\mu mol/g \text{ of aminic groups}}{load_{resin} \times 10^{-3}}\right]\right\} \times 100, \qquad \text{(Eq. 4)}$$

The peptide cleavage from the resin and the removal of the side chain protecting groups was done under acidic conditions, using TFA as the strong acid, and TES as *scavenger* to avoid undesired secondary reactions. The procedure included the following six steps:

1. Once the synthesis was accomplished, the N-terminal function of the *Fmoc*-protecting group was automatically removed treating the resin-peptidyl with a solution of 20% piperidine in DMF for 20 min;

2. The resin-peptidyl without the *Fmoc* group was washed with DCM, and dried under vacuum for 2 hours;

3. The resin-peptidyl was transferred to a flask and treated with a solution of 95% TFA, 2.5% H_2O milliQ, and 2.5% TES (v/v/v);

4. The mixture was kept under magnetic stir at room temperature, for 1 hour and 30 minutes;

5. The resin was separated by filtration with gooch G3, and the solution containing the peptide was transported to a rotary evaporator;

6. Once added cold diethyl ether (~4ºC), the peptide precipitated, and was filtrated with a gooch G4, dried, dissolved in H_2O MilliQ, frozen, and lyophilized using Labconco FreeZone® 2.5 (Terra Universal, Inc, Fullerton, CA).

4.1.2 Characterization of EAK 16–II

Peptide purification was conducted using semi-preparative (SP) RP–HPLC. SP uses the same principle of protein/peptide retention as the one described in *section 3.2.2*.

The total amount of crude peptide (144.36 mg) was divided in four parts: SP1=35 mg, SP2=35 mg, SP3=34.7 mg, and SP4=39.6 mg. For each quantity, the peptide (mg) was dissolved in around the same quantity of Eluent A (mL). Magnetic stirrer and ultrasonic bath were used to complete the dissolution for around 5 minutes, each. The solution was filtered. SP was carried out using NovaPack® HR C18 Column (6 µm, 60 Å,

7.8x300 mm), Waters 600 E System Controller, and Waters 2487 Dual λ Absorbance Detector at λ=214 nm, all provided by Waters (Milford, Massachusetts, USA). The machine was set for a 4 mL min^{-1} flow, with a gradient from 7 to 17% of Eluent B in A for 40 minutes. The results were carefully analysed, and the best fractions were selected for HPLC, Figure 4.1.

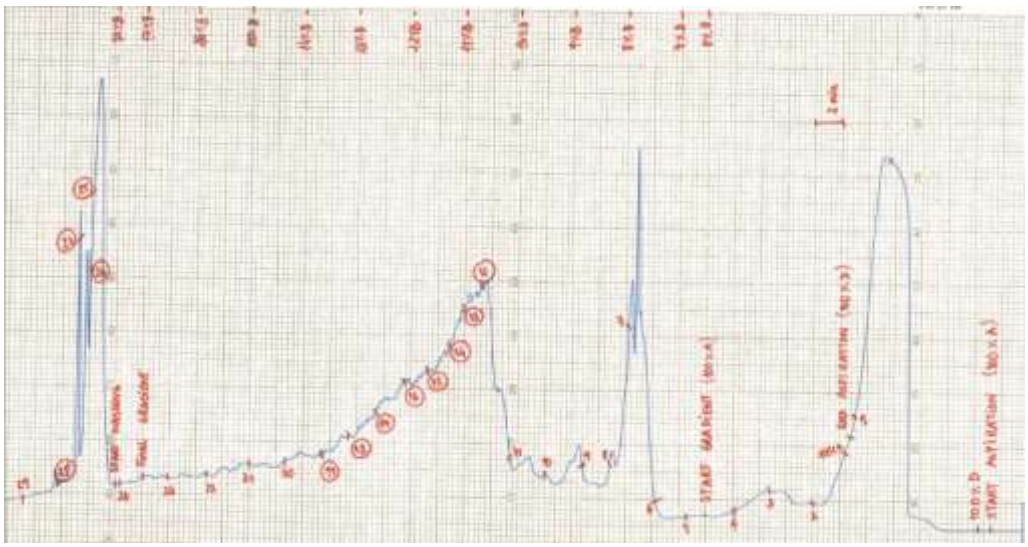

Figure 4.1 Chromatogram for SP1. The numbers in red represent all the fractions obtained. The numbers rounded represent the fractions selected for analytical HPLC. From right to left: the first peak represents the conditioning of the column, that may suffer some instabilities, resulting in this peak; when gradient starts (0% of Eluent B), a peak appears for the same reason; at ~10% of Eluent B, the target, and purest, peptide (named core) elutes from the column; the last peak results from the washing of the column, where there must elute some leftovers of the target peptide.

Were selected fractions 12, 13, 14, 15, 16, 17, 18, 19, 25, 26, 27, and 28, from SP1. From each selected fraction, samples of, no more than, 150 µL±10% were collected and analysed using Jupiter C18 Column (5 µm, 300 Å, 250x10 mm), from Phenomenex® (Torrance, California, USA), HPLC Waters 600 E System Controller for chromatographic analysis, Waters 2487 Dual λ Absorbance Detector at λ=214 nm, and the Empower software for acquisition and integration, all provided by Waters. The machine was set for a 1 mL min^{-1} flow, with a gradient from 7 to 27% of Eluent B in A for 20 minutes, with initial method using partial loop. Figure 4.2 shows the resultant chromatogram for fraction 13. It is verified a large peak at retention time (RT) of 11.238 min with a purity of ~87%. A second small peak is verified with less purity percentage (~12.93%) which refers to the presence of some impurities in this fraction, since it was absorbed at a lower absorbance (AU, adimensional unit).

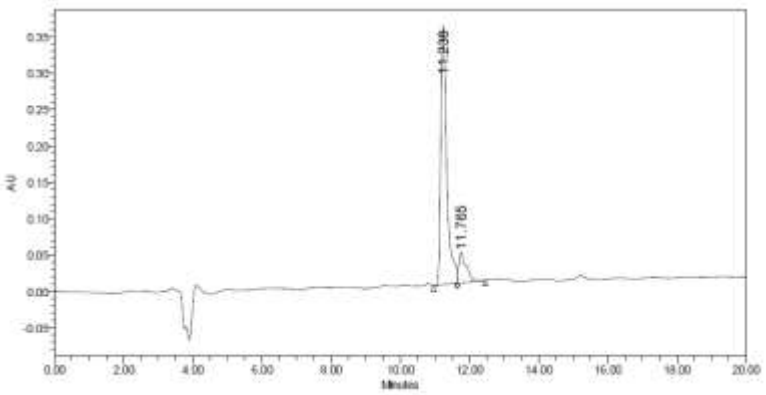

Figure 4.2 HPLC chromatogram for fraction 13 of SP1.

Table 2 % Area giving the purity for each peak observed in the chromatogram of Figure 4.2, and the respective RT.

	RT	% Area
1	11.238	87.07
2	11.765	12.93

The procedure was repeated for all parts of the divided peptide. The purest peptide fractions obtained were placed into polls (core, Table 3), and purified over again according to the described methodology. This time, for HPLC analytics, was used Vydac® 238EV54 (Everest) HR C18 Column by Grace Davison Discovery Sciences™ (Columbia, MD, USA), with the same gradient, Figure 4.3. After freeze-drying, it resulted in a final quantity of 10.66 mg of peptide, with a purity of ~91%.

Table 3. All fractions selected from each SP as the purest fractions containing the target peptide.

FRACTIONS				PEPTIDE
SP1	SP2	SP3	SP4	**(mg)**
13,14	12,13	6	3	10.66

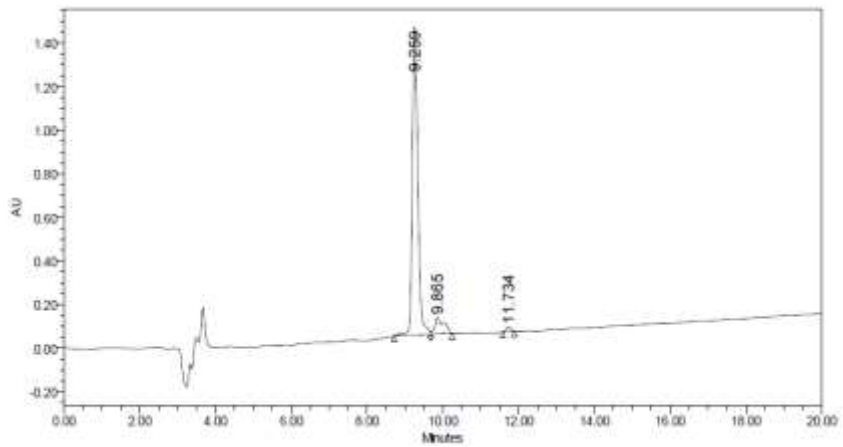

Figure 4.3 HPLC chromatogram resultant from the purification of all the fractions of Table 3.

Table 4. % Area giving the purity for each peak observed in the chromatogram of Figure 4.3, and the respective RT.

	RT	% Area
1	9.259	91.07
2	9.865	7.83
3	11.734	1.10

Molecular weight was confirmed by mass analysis using AB Sciex – 4800 MALDI TOF/TOF Analyzer (Sciex, USA), and the software 4000 series. A small quantity of peptide, in the range of 0.3–0.7 mg, was weighted and dissolved in the same quantity of H_2O MilliQ. The samples were in a plate and covered with the MALDI matrix. The range of masses used for all the fractions was 800–5000 Da, being the expected mass 1615.80 Da. EAK 16-II resulted in an experimental mass of 1614.45 Da, considered equal to the theoretical value.

4.1.3 Synthesis of HVP–CHO

The synthesis of HVP–CHO, aldehyde terminal, (H–Phe–Arg–His–Arg–Asn–Arg–Lys–Gly–Tyr–x–Phe–CHO) followed standard *Fmoc* chemistry SPPS method. The synthesis used Syro I synthesizer with reaction mixing by vigorous vortex. The Syro I used fully automated HBTU/HOBt *in situ* cycles, in DMF.

The synthesis was carried out on 0.18 mmol g^{-1} (resin load) of H–Phe–H NovaSyn® TG resin. The synthesis scale was 0.094 mmol, given by the product between the resin load and the resin amount (500 mg). It is always used an excess of 10% in the resin amount calculated by the synthesizer. The resin was swallowed in DMF for 15 min.

HVP–CHO synthesis used the same protocol for *Fmoc*-de-protection, carboxylic activation, ninhydrin test, and peptide cleavage and side chain protecting groups removal, as the one described in the *section 4.1.1*. This synthesis doesn't require a test to evaluate the load of the resin (piperidine test), because the first amino acid in the sequence (Phe) comes with the resin. The 7-aminoheptanoic acids act as a spacer for the molecule. The loading of the first amino acid was carried out with double coupling. The following insertions were carried out with single couplings, and with double couplings from the 5th cycle till the end of the synthesis. The calculation protocol estimated a synthesis time of 22 hours and 1 minute.

4.1.4 Characterization of HVP–CHO

HVP–CHO is a peptide which usually yields high levels of purity even before fractioning. Before SP, the crude peptide (4.68 mg) was analysed with RP-HPLC given a purity of ~85%, Figure 4.4.

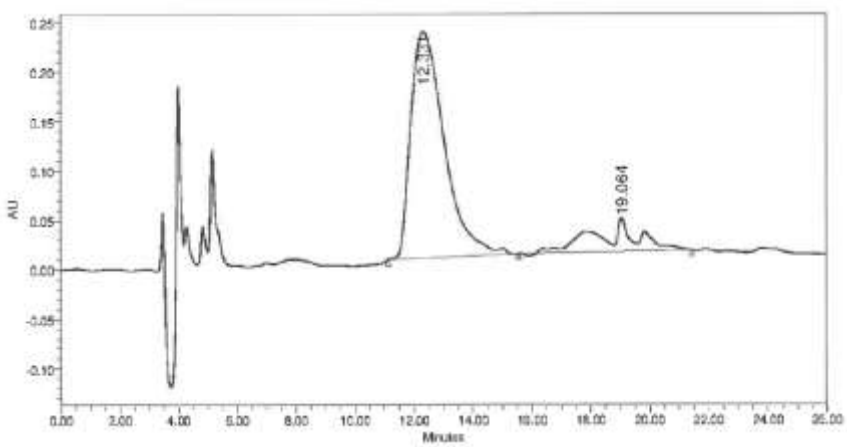

Figure 4.4 HPLC chromatogram resultant from crude HVP peptide.

Table 5. % Area giving the purity of HVP before SP.

	RT	% Area
1	12.331	84.84
2	19.064	15.16

To avoid loss of material, it wasn't conducted any fractioning of this molecule, since it is not needed for the level of purity obtained. Crude peptide was lyophilized resulting in a final quantity of 3.98 mg of pure peptide. Molecular weight was confirmed using mass analysis, resulting in an experimental value of 1472.69 Da, relatively close to the theoretical value of 1507.76 Da.

4.2 PCL matrices production

The electrospinning apparatus was composed by a syringe of 2.5 mL, a 27G needle from Terumo (Tokyo, Japan) assembled on the syringe, a volumetric pump from New Era Pimp Systems Inc. (Farmingdale, New York, USA) on which the syringe was set up, a high voltage generator from Gamma High Voltage (Ormond Beach, Florida, USA), a rectangular collector (8 cm x 8 cm) wrapped with an aluminium foil to facilitate the removal, an air tube collected to a barometer, and a HD 2301.0 Thermohygrometer from Delta Ohm (Caselle di Selvazzano, Padua, Italy).

Spherules of PCL were dissolved in HFIP at different concentrations, to obtain different viscosities. Initially, few experiments were conducted dissolving PCL spherules in DCM (cheaper solvent); however, weren't formed any fibres, resulting only in beads deposition. This fact can be explained with the resultant low viscosity of the solution. Processing parameters were tuned to obtain submicro- and nano-fibres of PCL at very low flow rate. Air was used as shell flow, providing more energy to the jet and helping the solvent to evaporate earlier.

The samples were divided in two batches. The first batch includes the experiments in which the processing and solution parameters were based in the ones used by Zavattin, D. *et. al.*, that has obtained successful results in producing fibres in the range of micro- and nano-dimensions.[94] Table 6 shows the parameters that were varied: polymer concentration of 25% and 30% PCL in HFIP (w/v) and presence/absence of air flow, labelled respectively as A (air) and NA (no air). Temperature and relative humidity (RH) are two difficult parameters to control, depending on several local and environment conditions. The variety presented in Table 6 for these two parameters are explained with the difficulty in stabilizing them. For all cases studied, the collector was located at 22 cm from the syringe, was applied a voltage of 20 kV to the fluid with a flow rate of 0.2 mL h^{-1}.

Table 6. Processing parameters: variation of PCL concentration and presence/absence of coaxial air flow.

PCL sample	PCL conc. (w/v) [%]	Temperature [ºC]	RH [%]	Flow rate [mL h^{-1}]	Distance [cm]	Voltage [kV]	Air flow [bar]
PCL25% NA	25	21–22	75	0.2	22	20	0
PCL25% A	25	23	55	0.2	22	20	0.2
PCL30% NA	30	21–22	63	0.2	22	20	0
PCL30% A	30	21–22	63	0.2	22	20	0.2

The second batch includes a group of samples with the polymer concentration of 30% PCL in HFIP. This concentration was selected based on the type and quality of fibres after naked eye and SEM observations. In this case, all the experiments used coaxial air flow at different pressures, and the applied voltage still the

same. This batch intends to evaluate the effect verified with a decrease in the flow rate from 0.2 to 0.1 mL h^{-1} and varying the distance between the syringe and the collector, from 22 to 30 cm, as shown in Table 7.

Table 7. Processing parameters: variation in the flow rate, distance of the collector and air flow pressure for a concentration of 30% PCL in HFIP.

PCL sample	PCL conc. (w/v) [%]	Temperature [ºC]	RH [%]	Flow rate [mL h^{-1}]	Distance [cm]	Voltage [kV]	Air flow [bar]
PCL30%	30	18–19	63–66	0.2	30	20	0.2
PCL30%	30	21–22	65–66	0.2	30	20	0.4
PCL30%	30	21–22	68–71	0.1	22	20	0.4

4.3 Matrices silanization

The silanization of the matrices was performed using the APPJ technique described in the *section 3.2.3*. APPJ used the argon driven plasma jet Stylu Plasma provided by Nadir (Mestre, Venice, Italy) to deposit (3–aminopropyl)triethoxysilane (APTES), which structure can be seen in Figure 4.5.

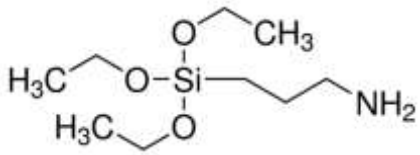

Figure 4.5 APTES structure (adapted from Sigma-Aldrich).

APTES films on the electrospun PCL matrices are intended to enrich the surface with amine (NH_2) groups. APTES is an aminosilane frequently used in the process of silanization, the functionalization of surfaces with organofunctional alkoxysilane molecules. Surface amine groups on APTES thin films promote physical adsorption increasing affinity between silicon substrates and biomolecules. Through the addition of APTES, reactive hydroxyl groups were converted into amino-terminal groups. APTES functionalization can be done with plasma treatment technique. The use of this kind of functionalization in PCL hydrophobic matrices, enhance the hydrophilicity of the fibre mats. Hence, it allows the interactions between the mat and the surrounding environment.[72] The amine functionality of APTES has been used to immobilize polymers and proteins, as well as to promote cell adhesion.[95]

APPJ was conducted by tuning several working parameters to obtain different concentrations of the chemical precursor APTES, and, hence, different concentration of amino groups deposited in the substrates. The working parameters presented in Table 8 were based in the studies done by Maffei, A. *et. Al.*, in which they have varied high voltage, radio-frequency, impulse, distance, different atmospheres for cooling (air and N_2),

and the number of scans done for one sample at a time. They have performed five different functionalizations. The values were selected according to the results obtained for each silanization, such as the film thickness and the concentration of atoms of nitrogen (N) present after deposition that had influenced the chemo-selective ligation with bioactive molecules. In this case, Argon (Ar) was the gas selected as plasma gas, and as carrier for APTES molecules. The inclusion of the chemical precursor implies the passage of Ar gas through a bubbler at room temperature. An atmosphere of nitrogen (N_2) was created to control both: the cooling of the RF electrode and the atmosphere close to the plasma jet. The substrates were fixed, one at a time, on a planar platform that moved simultaneously along X and Y axes with controlled velocity of 300 mm s^{-1}. This allows the torch to scan all the sample area. Samples were cut in square forms of (2 x 2 ± 0.05 cm^2) and located at 2 mm from the torch. Every sample was scanned 40 times (~3 minutes). Was applied a high voltage of 9.6 kV peak to peak, the radio-frequency varied from 12 to 20 W, with a pulsed jet of 50% d.c. (duty cycle) [hz], or continuous plasma jet.

Table 8 Working parameters used for silanization of surfaces with APTES by APPJ.

Sample [2x2 cm^2]	**HV [9.6 kV p.p]**	**RF [W]**	**Impulse 50% d.c. [hz]**	**Ar flow [L min^{-1}]**	**Ar bubbler [L min^{-1}]**	**Dist. [mm]**	**Cool flow [L min^{-1}]**	**Stage Velocity [mm s^{-1}]**	**Nº of Scans**
PCL_01	50	12	None	4.5	2.5	2	5 N_2	300	40
PCL_03	50	20	1000	4.5	2.5	2	5 N_2	300	40
PCL_04	50	15	None	4.5	2.5	2	5 N_2	300	40

4.4 Contact angle measurements

The surface wettability was traced by measuring the static water contact angle, after ~72 hours of treatment. An OCA30 instrument (DataPhysics Instruments GmbH, Filderstadt, Baden-Württemberg, Germany), equipped with a CCD camera for the dropshape analysis, was at 25ºC and 65% of relative humidity. The electrospun layers were fixed on glass coverslips by double-sided tape. 2 µL of ultra-pure water were applied on different areas of the surface. The static contact angles were then measured on both sides of the two-dimensional projection of the droplet by digital image analysis.

4.5 Scanning Electron Microscopy

The morphology of electrospun PCL fibres was examined using an environmental Scanning Electron Microscope (SEM) (Zeiss EVO 50, Carl Zeiss AG, Oberkochen, Germany), with an electron accelerating voltage of 20 kV, without coating the samples. Was used a SEM with low vacuum to prevent charging of the samples. The average fibre diameter of the electrospun fibres was measured by ImageJ 1.52a software (National Institute of Health, USA) from the SEM pictures in original magnification.

4.6 Selective immobilization of HVP on the silanized matrices

The synthesis of HVP using a polymeric support with a Phe amino acid incorporated gives an aldehyde group in the resultant molecule free for ligation, marked in red in Figure 4.6.

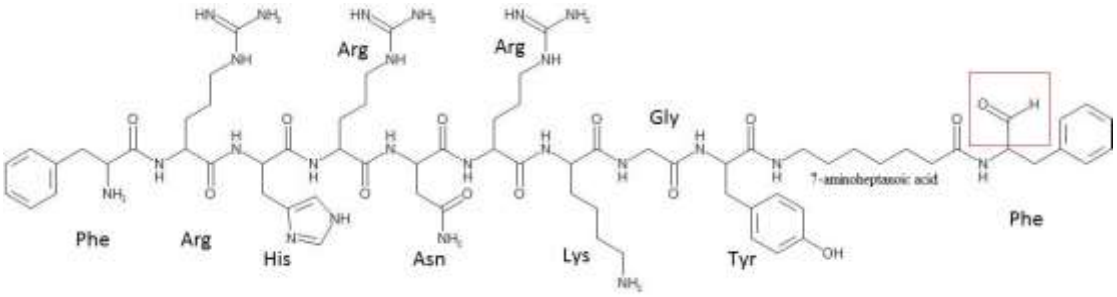

Figure 4.6 HVP molecule, on the right is the polymeric support with a Phe amino acid incorporated.

This allows the biochemical conjugation, described in *section 3.2.4*, between the amino groups present in the surface, obtained from the previous surface treatment, with the aldehyde group. This is a specific functionalization since the peptide bond is exploited only by the aldehyde group, supporting an ordered deposition of the biomolecule on the surface. The spacer included in the HVP sequence during the synthesis gives a degree of freedom to the molecule, so it can have flexibility to move and perform it functions, Figure 4.7.

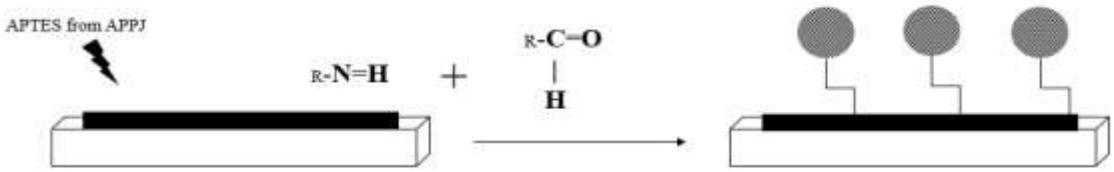

Figure 4.7 *In situ* bio-functionalization of the matrices.

For the bio-functionalization of the silanized surfaces were cut PCL layers in circles with diameter of ~6.4 mm. Were cut three samples for each treatment to perform bio-conjugation with HVP peptide, labeled PCL_01_F, PCL_03_F, and PCL_04_F, three samples for each treatment without bio-functionalization for comparison, labelled PCL_01, PCL_02, and PCL_03, and 3 samples without any surface modification. The samples were distributed in the wells of a treated tissue culture plate of 96 wells (well diameter 6.4 mm, well volume 360 μL, well working volume 75–200 μL) provided by Sigma-Aldrich (Corning®, Turin, Italy). Was prepared a *buffer* solution of sodium dihydrogen phosphate monohydrate ($NaH_2PO_4.H_20$) with a concentration of 20 mM, and sodium chloride (NaCl) with a concentration of 200 mM, in H_2O milliQ. This solution was stabilized at pH 7.5, measured with sensiON – pH3 provided by Hach® (Lange, Milano Linate, Italy). The reductive agent sodium cyanoborohydride ($NaBH_3CN$) was added to the *buffer* solution in a concentration of 3 mg mL^{-1}. The resultant solution was filtered with a filter of polyvinylidene difluoride (PVDF). The peptide was

dissolved in this solution at a concentration of 1 mg mL^{-1}. The solution was placed in every well prepared for bio-functionalization 100 μL of this solution. It was left to react with the silanized surface overnight, and removed after 24 hours. Then, the surfaces were rinsed three times with H_2O milliQ, and dried at room temperature.

4.7 Surface chemistry analysis

Surface chemistry was analysed by measuring the total nitrogen with the method described in the section *3.3.5*. This method permits the measurement of total N in the range of 0.1-0.7 mg/L. PCL silanized and bio-functionalized samples were weighted and dissolved in 100 μL of HFIP. This solution was brought to a volume of 50 mL with milliQ H_2O. Was added 7 mL of oxidant solution Antimony potassium tartrate ($KOOC(CHOH)_2COOSbO$), and 0.3 g of Potassium Persulfate ($K_2S_2O_8$) to 50 mL sample solution. The same quantities of potassium tartrate and potassium persulfate were added to 50 mL of bare deionized water for reference. The samples were heated at 120 ºC for 30 minutes, and the cooling was done at room temperature. The analysis was conducted after withdrawal of 10 mL of digested sample and acidification with 0.15 mL of sulfuric acid (H_2SO_4). The digestion is strongly alkaline at the outset, which promotes oxidation of nitrogen to nitrate. Absorbance was detected at λ=200 nm, retrieving the total nitrogen concentration through a calibration curve.

4.8 Biological assays

In this section is described the procedure to test the viability of the multi-layer scaffold to incorporate cells and allow them to perform their functions of proliferation and migration within. First, the scaffold was assembled with a 3D gradient obtained from the combination of bio-functionalized electrospun fibre mats with hydrogel from self-assembling peptides. This first trial was important to perceive the limitations of both systems when combined. In the hydrogel was incorporated the growth factor human recombinant Fibroblast Growth Factor (rh−FGF), and the inflammatory cytokine, Interleukin-6 (IL−6). In a second approach, the scaffold was 'disassembled' aiming to study each component separately and where was possible to evaluate the cell adhesion on the bio-functionalized surfaces. The biological assay comprises the cell culture and the cell seeding.

4.8.1 Cell culture

We opted for a culture using primary cells instead of a cell line. Primary cells are not immortalized cells (cancer like phenotype) and are believed to be better for this type of experiments since measurement of replication is like normal cells.

Human bone cells were obtained from explants of cortical mandible bone collected by surgery. The patient was a 37 years old, healthy man. The study was approved by the local ethics committee, and informed

consent was obtained from the patient. Bone fragments were initially cultured in D-MEM/F12 (1:1) supplemented with 20% v/v fetal bovine serum, 1% v/v sodium pyruvate, 1% v/v nonessential amino acids, 1% v/v antibiotic-antimycotic solution, and 1 U/mL insulin, until cells migrated from tissue. At confluence, cells were detached by trypsin-EDTA and cultured in complete medium supplemented with 50 μg mL^{-1} ascorbic acid, 10 nM dexamethasone, and 10 mM β-glycerophosphate. For the separation using trypsin, the residual culture media containing a trypsin inhibitor needs to be firstly removed. The cells were washed with 0.1 % v/v of Phosphate *Buffer* Saline (PBS), and trypsin was added, centrifuging the cells with 1600 rpm for 6 minutes.

4.8.2 Cell adhesion

To evaluate cell adhesion to the bio-functionalized layers of PCL, we use the tissue culture plate referred in the *section 4.7*. The samples of electrospun layers were sterilized in 20% (v/v) ethanol for 10 minutes, including the layers for control. After sterilization, samples were washed in PBS for 5 minutes. Was seeded a solution of 100 μL, containing ~1×10^4 cells of human *h*-osteoblasts per well, for an incubation time of 2 hours, at 37 ºC. At the end of the incubation, culture medium was discharged, and non-adherent cells were removed by extensive washes in PBS, and cellular viability was assessed by using the MTT assay already described herein. Samples were then incubated for 4 hours at 37 ºC with 100 μL of fresh complete medium containing MTT (5 mg/mL). The reaction was stopped by adding a 10% w/v sodium dodecyl sulphate (SDS) solution acidified with 0.01 M HCl, and samples were stirred for 12 hours. To quantify the number of cells, a standard curve was obtained for each experiment by culturing a known number of *h*-osteoblasts in complete medium. At the end, cellular lysate (100 μL) were transferred to a new 96-well tissue culture plate to determine the absorbance at λ=620 nm, using a microplate reader (Sunrise, Tecan, Milan, Italy).

4.8.3 Scaffold assembly and cell seeding

Scaffold assembly proceed with manual bottom-up layer-by-layer building stack. Two scaffolds were prepared: one where the PCL layers were conveniently functionalized, and one for control, where the layers were only submitted to plasma treatment. PCL layers were first sterilized with an exposition to UV radiation for 5 minutes, including the layers for control. PCL membranes were placed between two frames of polycarbonate (PC) with thickness in the range of 0.1-0-3, obtained by a machine press. The films were cut into 4x4 cm^2 frames, with a centred square 1x1 cm^2 hole. Hydrogels with concentration of 1% (w/v) were prepared by dissolving 10 mg/mL of EAK 16-II in PBS. For the functionalized scaffold, three layers of hydrogel were prepared labelled as Hydrogel 1, Hydrogel 2, and Hydrogel 3. For each layer were prepared a mixture with 15 μL (0.15 mg of SAP) of EAK-hydrogel, 11 μL of PBS, 2 μL of rhFGF, and 2 μL of IL−6, these last two at different concentration, and differing the concentration from layer to layer, as shown in Table 9. This mixture was prepared on time in Eppendorf and placed on top of PCL membranes, Figure 4.8.

Table 9 Concentration of HVP, rhFGFG, and IL-6 for each layer.

Samples	HVP % (w/v)	Samples	rhFGF % (w/v)	IL–6 % (w/v)
PCL 1	8.6	Hydrogel 1	0.016	0.00064
PCL 2	6	Hydrogel 2	0.0032	0.0032
PCL 3	3.4	Hydrogel 3	0.00064	0.016

From bottom to top, the assembly was done by placing PCL layers from highest to lowest concentration of HVP, labelled, respectively, as PCL 1, PCL 2, and PCL 3, Table 9.

The scaffold for control used the same procedure for stacking, but in its turn the hydrogel layers included only 10 μL of EAK–hydrogel.

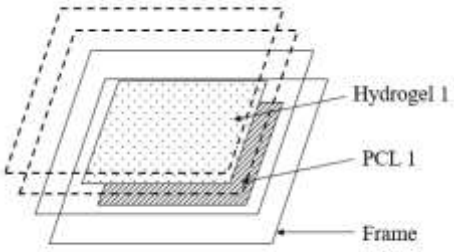

Figure 4.8 Scaffold assembly: the frame fixing the PCL layers, and hydrogel placed between the layers.

After assembling, a 40 μL solution, containing ~3×10^5 cells, was implanted on top of the functionalized scaffold, repeating the procedure for the control scaffold. Both scaffolds were immersed in culture media. After 3 days, scaffolds were rinsed several times using PBS. Human *h*-osteoblasts cells were fixed for 10 minutes with a solution of 4% (w/v) of PFA in PBS at room temperature, pH 8. After washing it three times with Tris-*Buffered* Saline (TBS) for 5 minutes each, the samples were incubated with 0.05 M of ammonium chloride in PBS for 10 minutes, to reduce auto-florescence. Then, three additional 5 minutes washes were performed with TBS; and a solution consisting of 2% v/v of Bovine Serum Albumin (BSA) and of 0.3% v/v of Triton X-100 in TBS was added for 30 minutes, to block non-specific bonds and permeabilize the cells. The samples were then incubated for 30 minutes at room temperature with the p-FAK antibody generated in rabbit and diluted 1:500 in TBS containing BSA 2% w/v and Triton X-100 0.3% v/v. At the end of the incubation, the samples were washed and then incubated again for 45 minutes with a second antibody conjugated to the fluorophore Alexa Fluor 488, which emits in the green. After incubation, the samples were washed with TBS three times and then prepared for analysis under confocal microscopy, by adding a drop of 70% glycerol and sealed with a coverslip. All this procedure was performed within a class II microbiological safety cabinet. Image acquisition was performed using Leica TCS-NT/SP2 fluorescence confocal microscope and the matching Leica software, provided by Leica Microsystems GmbH (Wetzlar, Germany). Scaffold's thickness was measured using a digital micrometre.

CHAPTER 5 – RESULTS AND DISCUSSION

5.1 Contact angle analysis

Silanized samples using the conditions for treatment 03, PCL_03 and PCL_03_ F, where the last one received an additional bio-functionalization with a covalent immobilization of HVP at the surface, were submitted for contact angle measurements. Data are reported as the average of five separate measurements. The water contact angle measurements showed that both samples drastically improved their wettability, as shown in Table 10, since they were characteristically hydrophobic before treatment. The contact angle for samples only submitted to silanization (PCL_03) present complete wettability (θ=0º), while samples that were bio-functionalized show a slightly decrease in the wettability (θ=25º).

Table 10 Wettability. Contact angle value of water, as average value obtained from 5 measurements.

Samples	Contact angle, θ (º)
PCL_03	0
PCL_03_F	~25

The present values for contact angle after plasma treatment demonstrated a strongly increase in wettability suggesting that the plasma-treated PCL surfaces contain many hydrophilic groups, thus indicating the generation of functional groups and/or morphological changes on the PCL surfaces. Bio-functionalized samples present less favourable wettability, a fact that can be explained by the presence of more molecules on the surface, affecting the disposal of the water drop, and, consequently, affecting the contact angle measure. Usually, untreated PCL has a contact angle above of 90º, indicating the natural hydrophobic characteristic of this polymer. The introduction of Ar-containing polar groups in the fibres surface resulted in a significant change of hydrophilicity. After treating the PCL fibres, the water contact angle decreased meaning that APTES-precursor hydrolysed the amide bonds resulting in amine functional groups on the PCL surfaces. These functional groups, deposited by plasma, increased the surface energy of the fibres, contributing to the lower water contact angle, thus making the fibre surface less hydrophobic. After APP treatment, the water droplet was absorbed into the fibres immediately, showing complete wettability, and a water contact angle of 0º was observed.

5.2 Morphological characterization of PCL fibres

In this study, we explored the electrospinning capability to produce micro- and nanofibres of PCL to generate 3D scaffolds for tissue engineering. First, we focused in the control of the working parameters ideal

for obtaining fibres in the required dimensional range. Second, we selected the best fibres for coating the surface to improve their biocompatibility. We selected the fibres based on their fibre diameter and porosity like the ones of ECM tissues, and with morphologies suitable for cell attachment and proliferation.

5.2.1 Effect of coaxial air flow and polymer concentration

A series of experiments were carried out when the initial polymer concentration was varied, in presence or absence of coaxial air flow. Solutions were processed with PCL concentrations varying from 25 to 30% in HFIP, and varying the pressure of coaxial air flow from 0 to 0.2 bar, at a flow rate of 0.2 mL/h, a tip-target distance of 22 cm, and an applied voltage of 20 kV. SEM micrographs were used to analyse the influence of both parameters on the resulting morphology, and results are shown in Figure 5.1.

For 25% PCL, electrospinning process produced primarily polymer beads, and sparse fibres, (Figure 5.1 A, B, and C). This situation is improved when at the same concentration, the process is carried with the presence of coaxial air flow (0.2 bar), (Figure 5.1 D, E, and F). At concentration of 30% PCL beads were still visible, (Figure 5.1 G, H, and I). However, in the presence of coaxial air flow, the number of beads significantly decreased, resulting in fibres with almost consistent morphology (Figure 5.1 J, K, and L). SEM micrographs showed that the presence of air flow has a positive influence in reducing beads for both concentrations. Results for 30% PCL were favourable than for 25% PCL. Changing the polymer concentration could alter the solution viscosity. For 25% PCL is expected a solution with lower viscosity than 30% PCL and it has been proven that continuous and smooth fibres cannot be obtained in very low viscosity. The unfavourable results given for 25% PCL fibres may be explained by this fact, and by the insufficiency of chain entanglements to stabilize the jet. The results allowed the selection of fibres using 30% PCL in presence of coaxial air flow for further studies.

5.2.2 Effect of tip-target distance and flow rate

Electrospun fibres for concentration of 30% PCL were used to vary the tip-target distance from 22 to 30 cm; however, tip-target distance had no significant effect on the electrospun fibres morphology, as shown in Figure 31, where the micrographs were practically undistinguishable. The morphological structure can be slightly changed by changing the solution flow rate, as shown in the same Figure 5.2. At the flow rate of 0.1 mL/h, a few big beads were observed on the fibres. The flow rate could affect electrospinning process. Generally, lower flow rate is more recommended as the polymer solution will get enough time for polarization, oppositely to high flow rate that usually leads to beaded fibres with thick diameters. Contrary to what was expected, the presence of beads and beaded fibres was decreased for higher flow rate (0.2 mL h^{-1}). For the results using lower tip-target distance, it was assumed that solution jets were elongated and solidified quickly after they flowed out of the needle tip. Lower distances are usual responsible for thinner fibre diameters, as can be observed. However, due to the presence of beads, the fibres respected to higher flow rate and tip-target distance, (Figure 5.2 D, E, and F), were the ones selected for surface treatment.

Air Flow [bar]	(%) PCL	SEM images
-	25	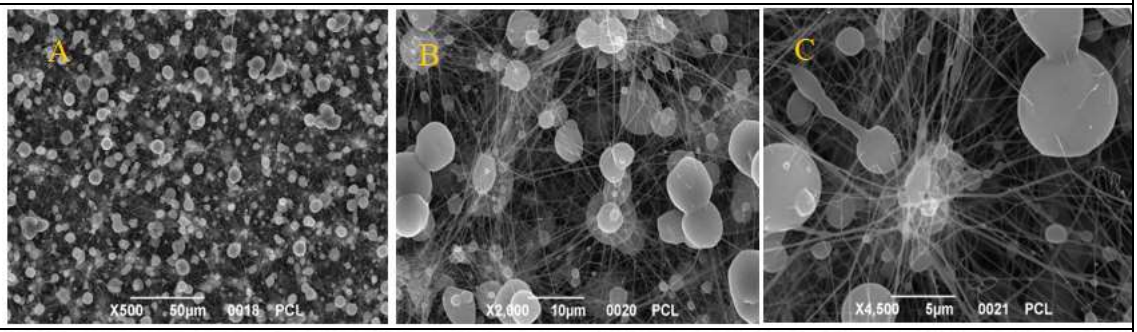
0.2	25	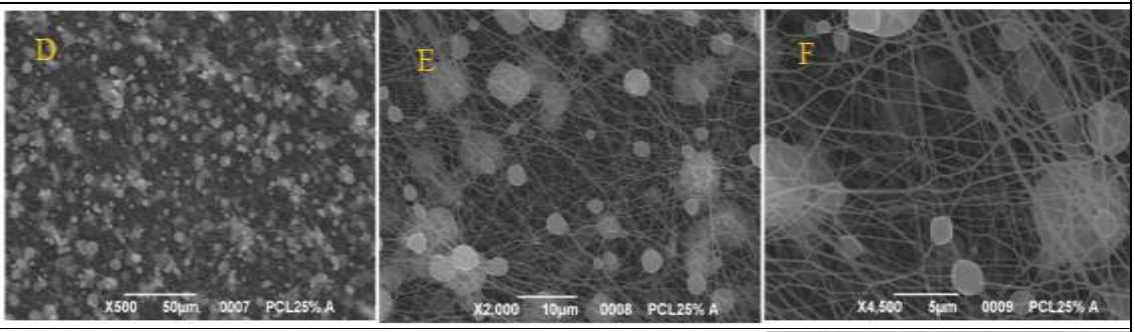
-	30	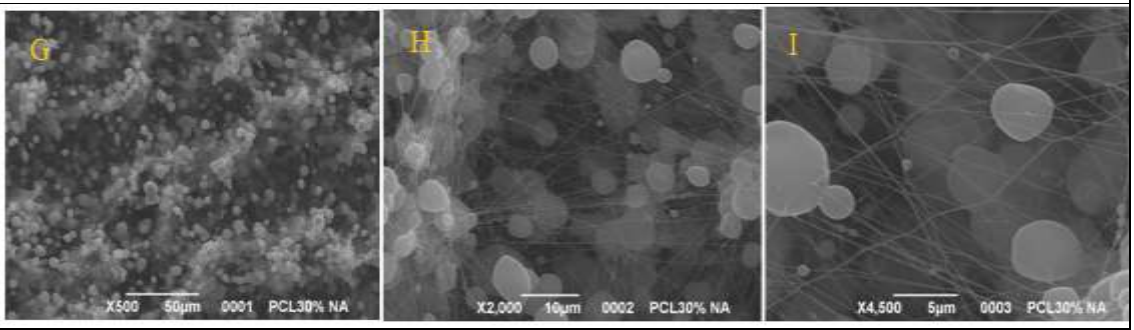
0.2	30	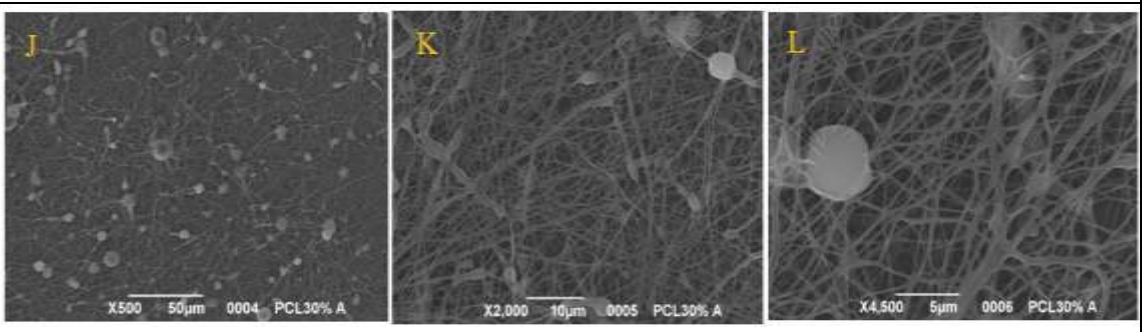

Figure 5.1 Scanning electron micrographs of PCL electrospun nanofibres depicting the effect of different polymer concentration (25 and 30% of PCL in HFIP), and the influence of coaxial air flow, while the other parameters remain equal.

Flow rate (mL h^{-1})	Distance (cm)	SEM images
0.1	**22**	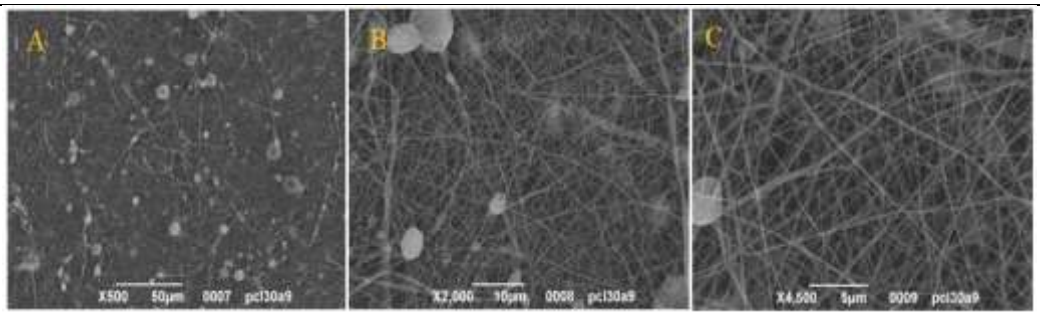
0.2	**30**	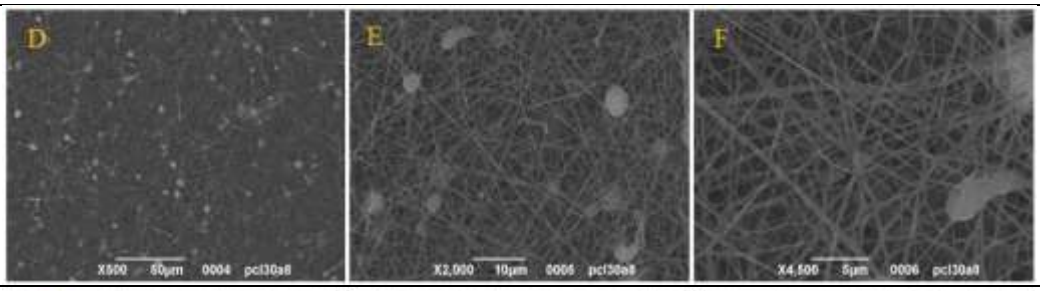
0.1	**30**	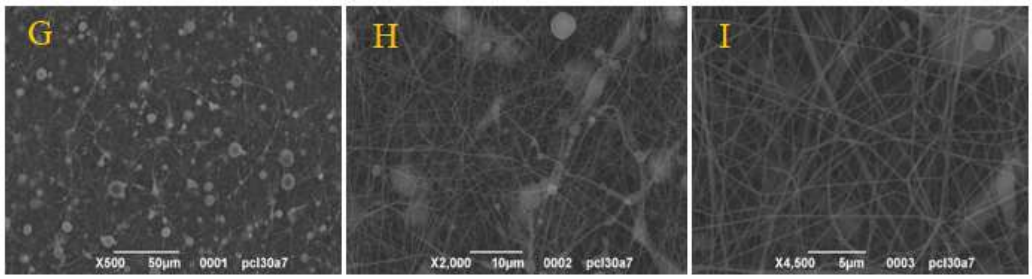

Figure 5.2 Scanning electron micrographs of PCL electrospun nanofibres depicting the effect of tip-target distance (22 and 30 cm), and the influence of variety in low flow rates (0.1 and 0.2 mL h^{-1}), while the other parameters remain equal.

5.2.3 Effect of surface treatment

The change in surface topography on PCL nanofibres before and after plasma modification by argon-driven plasma was determined by SEM. Three samples: a matrix without coating, a matrix coated with treatment 03 (PCL_03), and a matrix coated with treatment 04 (PCL_04), were selected for SEM examination. PCL fibres with 30% polymer concentration, collected at 30 cm of tip-target distance, at a flow rate of 0.2 mL h^{-1} were selected for surface treatment using plasma polymer deposition with APP method. The results were compared with surfaces without being treated, and the results are shown in Figure 5.3. Based on the SEM micrographs, plasma treatment had no significant effect on the surface morphology of PCL fibres. All samples present a smooth surface topography, with reduce quantity of beads. Based on the micrographs for not-coated (Figure 5.3 A, B, and C) and coated-PCL_03 (Figure 5.3 D, E, and F), plasma treatment did not change the porosity of the fibres. Both have highly porous structures with interconnected pores. However, for PCL_04 (Figure 5.3 G, H, and I) open porosity in the fibres, point-bounded junctions, and melting of thinner fibres can be observed.

Plasma Treatment	SEM images
Not coated	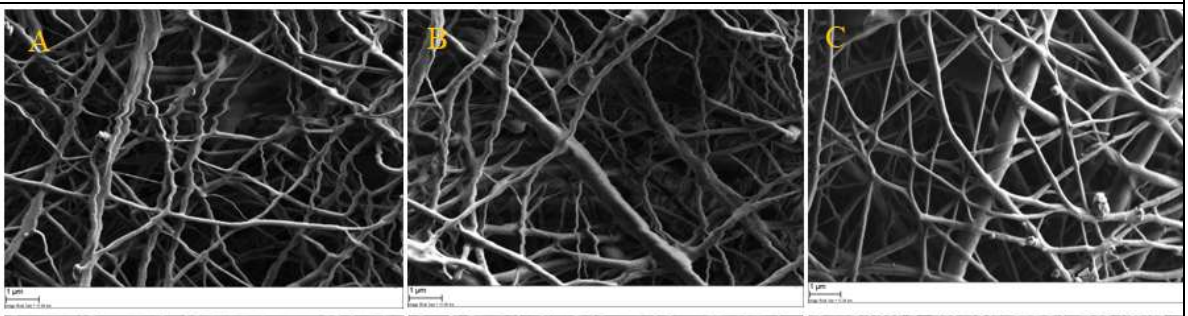
PCL_03	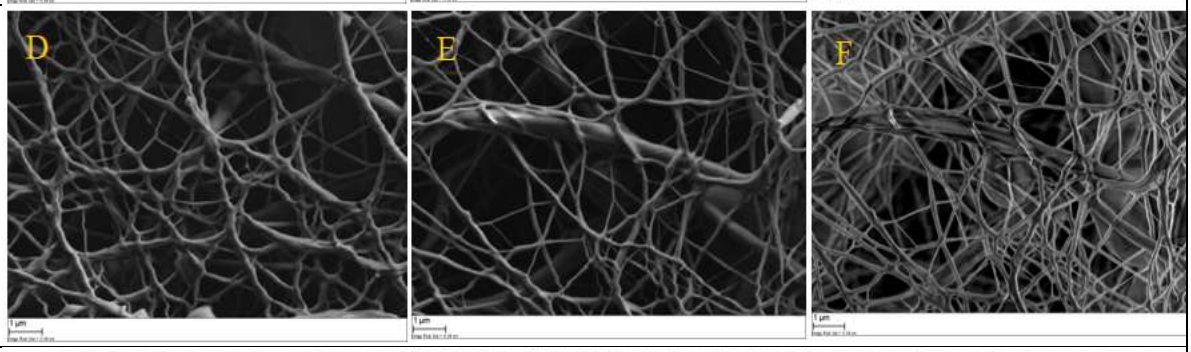
PCL_04	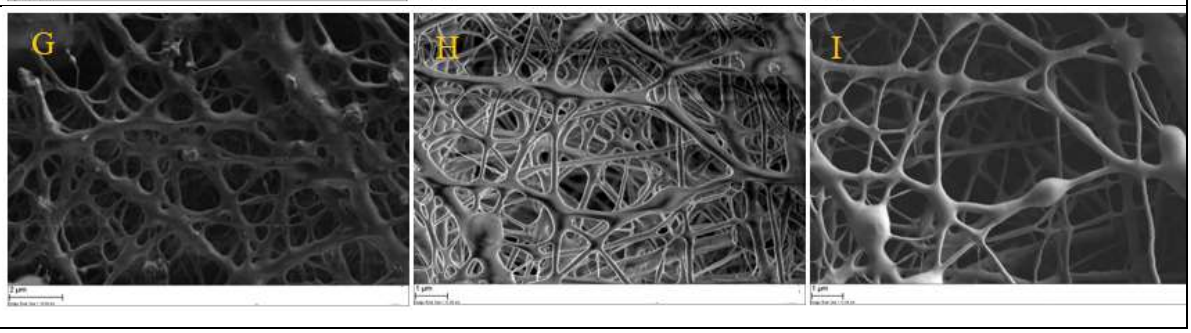

Figure 5.3 Scanning electron micrographs of PCL electrospun nanofibres depicting the effect of plasma surface treatment, for treatments 03 and 04, and comparing with non-coated surfaces.

The average diameter of the collected electrospun PCL fibres was 190 nm, with fibres ranging from 16 to 696 nm, which indicates their dimensional characteristics as micro- and nanofibres. For each case, fibre diameter was obtained with an average of ~200 measurements, and the fibres distribution is shown in Figure 5.4. There's more frequency of fibres ranging from 100 to 200 nm for all the matrices.

Normally the fibre diameter of the matrices conform to the structural properties of the ECM are on the order of 80–500 nm. The diameter of electrospun PCL nanofibres was around 190 nm, suggesting their potential applications as tissue engineering scaffolds, capable to provide ECM-like morphologies. SEM images showed that obtained fibres were continuous and almost bead free, with interconnected microfibre and web-like nanofibre formation between. High scaffold porosity is preferable for cell seeding, adhesion and tissue in-growth because of high surface area-to-volume ratio, which elicits better diffusion of oxygen and nutrients into the scaffolds. Ideally, the structure of the scaffold must be highly porous, with open pores and fully

interconnected. Depending upon the cell type, the optimal pore diameters are 20−100 μm. The percentage of porosity and the pore size were not measured due to the low resolution of the images for segmentation computing methods; however, it can be perceptible by the SEM micrographs the presence of large and interconnected pores, that may favour the cell's movement.

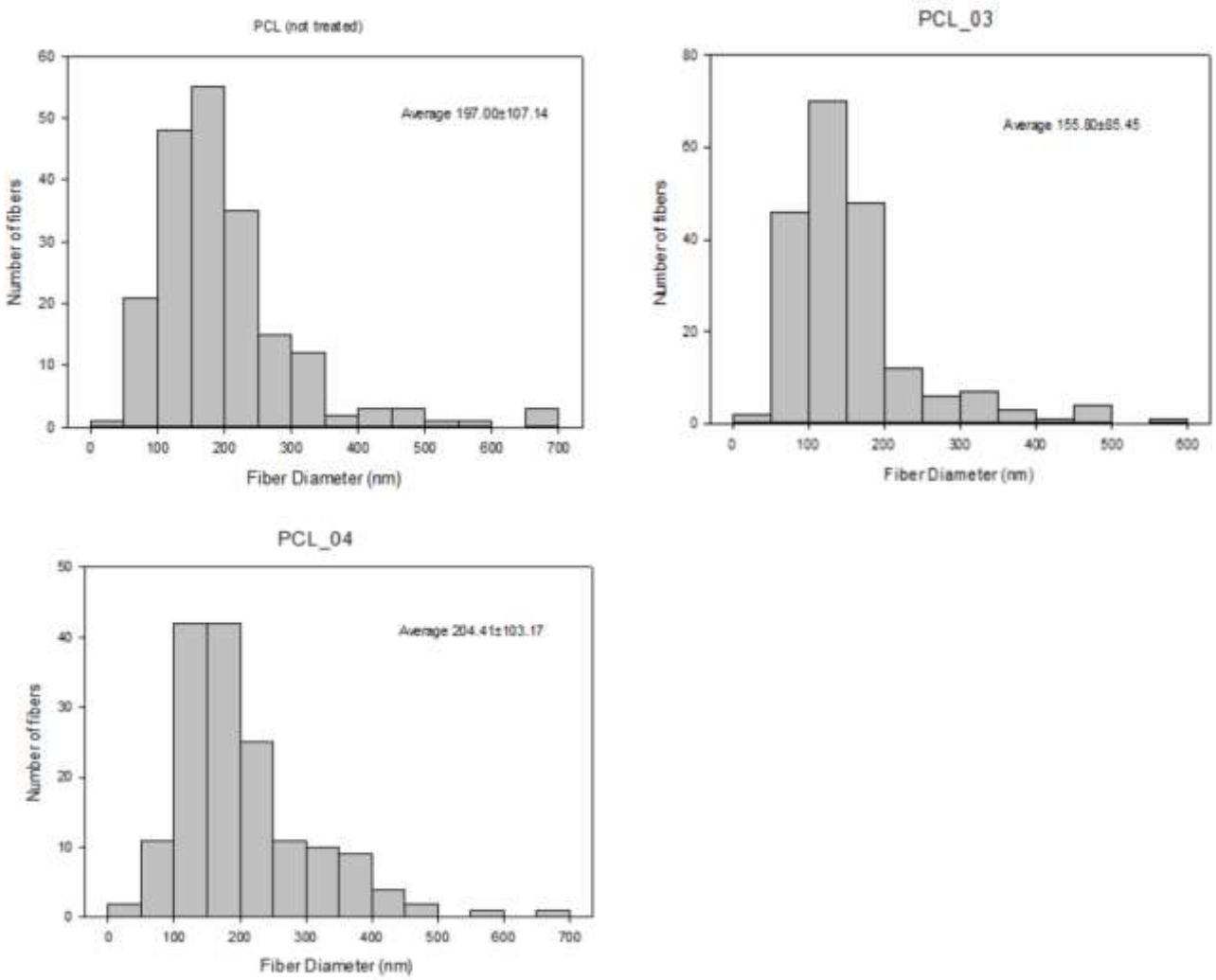

Figure 5.4 Fibre diameter distribution of nano-fibrous membrane. Top left: surfaces without treatment, Top right: surfaces with treatment number 03, Bottom: surfaces with treatment number 04. For each case is presented the result as mean ± standard deviation.

5.3 Surface chemistry analysis

The properties of the organic layer deposited by plasma, such as density and orientation of the molecules within the layer, are directly influenced by the choice of alkoxysilane. APTES represents a popular choice as it allows for further attachment of molecules through its terminal amines and exhibits self-assembly. The silanization reaction aim to provide a more uniform monolayer surface with an aminopropyl-terminal, resulted from the anhydrous conditions where it happens. There are several reactions in the silanization process that will

result in a combination of the final configuration of the amine groups, Figure 5.5. Ideally, the amine group should point toward the liquid phase, leaving free amine groups available for further functionalization.[96]

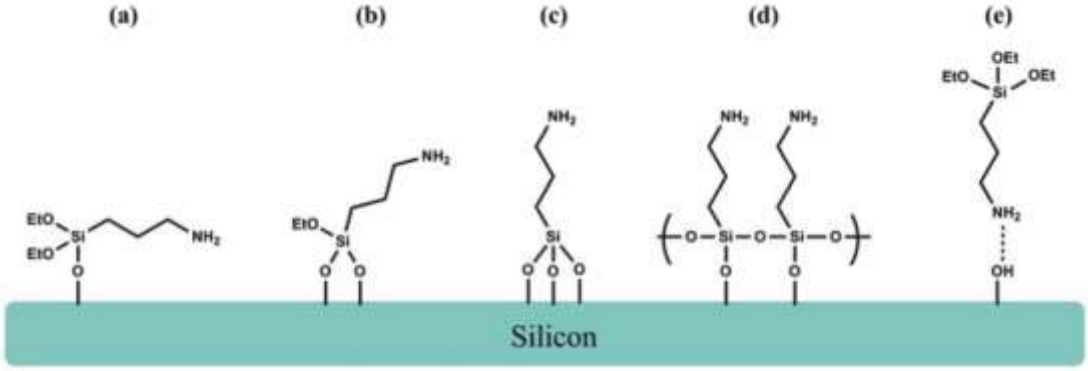

Figure 5.5 Possible orientation of the APTES molecule at the silicon surface: a) reaction of only one, or b) two of the ethoxy groups with the silanol-terminated silicon; c) reaction of the all three ethoxy groups with the silanol-terminated silicon; d) crosslinking of the APTES molecules; and, e) attachment of the NH_2 group of the APTES molecule to the surface.[96]

However, obtaining a uniform monolayer with amine groups oriented away from the underlying substrate can be a complex issue, as APTES is very sensitive to many reaction conditions, such as induced condensation reactions. Hydrogen bonding can result in unhydrolyzed APTES molecules with intact ethoxy groups adsorbing on the initial covalently bound APTES layer, resulting in vertical multilayering. In this case, APTES molecules physisorb to each other on an already APTES-treated surface, as seen in Figure 5.6. The film continuous to increase in density with further deposition leading to hydrogen bonding with previous deposited APTES, compressing the layer closest to the substrate.[97]

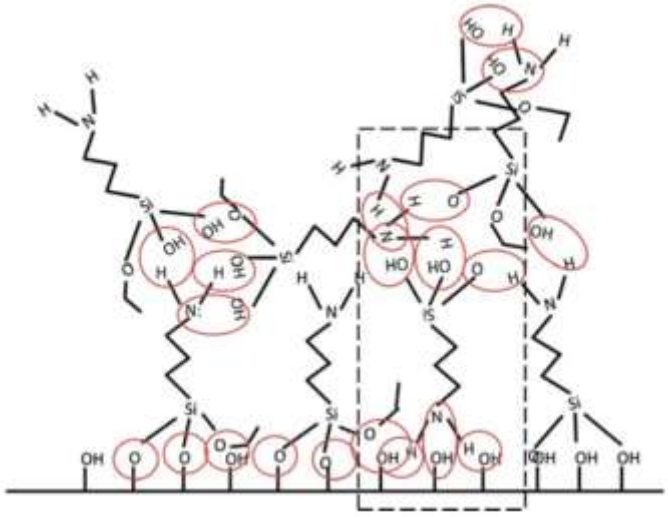

Figure 5.6 Schematic structure of APTES films under anhydrous deposition conditions. Some condensation may occur between APTES molecules and the native interface. Red circles denote bonding (both covalent and hydrogen bonding) while the highlighted section is meant to demonstrate that APTES molecules are bound at multiple sites through the film.[97]

This fact suggests that the thickness of the deposited layer can disfavour the silanization process, as a thicker film may come from condensation of APTES at the surface. Furthermore, a higher concentration of the APTES molecule does not mean that all these molecules are available for further functionalization, indicating the necessity for two types of chemical analysis at the surface to prove the efficiency of the plasma treatment. One to evaluate the quantity of APTES, and another to evaluate it configuration on the surface.

The efficiency of plasma on the surfaces was studied by Maffei, A. *et al.*, where they conducted X-ray photoelectron spectroscopy (XPS) analysis.[94] This is a surface sensitive quantitative spectroscopic technique, used to analyse the surface chemistry of a material, by measuring the elemental composition, chemical state, and electronic state. In their studies, the atomic ratios Si/C=O and N/Si were measured, and the results are presented in Table 11. N/Si ratio indicates the integrity of the APTES molecules after plasma treatment and the efficiency of the functionalization after treatment with HVP; while Si/C=O ratio gives indications about the concentration of the APTES molecules on the surface. They determined the Si/C=O ratio allowing the selection of PCL_01, PCL_03, and PCL_04 as the matrices with ideal APTES concentration for creating a gradient. The ratio N/Si was expected to have a variety as the one observed in the Si/C=O ratio, and if the APTES is intact, the N/Si ratio must be 1. Based on these principles, PCL_01 would indicate a higher efficient rate of functionalization, followed by PCL_03, and the last would be PCL_04. Film thickness matched with the Si/C=O ratio, but it can be understood as an aftermath of the APTES condensation at the surface, as described herein. They proceeded with the selective HVP immobilization on the layers where the results were equally expected to have the same variety from layer to layer. A significant increase in the N/Si ratio was expected, to support the idea that APTES molecules were oriented in a way to allow functionalization with HVP. The results were unsatisfactory, indicating a negative influence of the HVP on the functionalization of the PCL_04 layer observed from the ΔN/Si, and did not match with the primary Si/C=O ratio.

Table 11 Si/C=O and N/Si atomic ratios for plasma treated PCL samples. N/Si ratio for HVP-functionalized samples, and ΔN/Si.

Samples (area [cm^2])	**Plasma Treatment**			**Functionalization with HVP**	**ΔN/Si**
	Si/C=O	**N/Si**	**film thickness (nm)**	**N/Si**	
PCL_01 [2x2]	0.91	0.74	30-40	1.06	0.32
PCL_03 [2x2]	0.36	0.76	7-10	1.53	0.77
PCL_04 [2x2]	0.09	0.67	<5	0.65	-0.2

Based on these results, a colorimetric assay was conducted to confirm the total nitrogen content in the coated and bio-functionalized layers, using the protocol described in *section 4.7*, and the results are presented in Table 12. The analysis of the content of nitrate in the dissolved silanized and functionalized layers by the Total Kjeldahl Nitrogen method confirmed the concentration of APTES obtained with the Si/C=O ratio from XPS results. The nitrate content in the silanized layers comes from the titration of the nitrogen provided by the amino groups presented in the APTES molecules, while the nitrate content in the bio-functionalized layers, labelled PCL_01_F, PCL_03_F, and PCL_04_F, comes from the nitrogen provided by the amino groups present in the APTES molecules and present in the peptide sequence. For this reason, was expected an increase in the N/Si ratio.

Table 12 Total nitrogen content in silanized vs. functionalized surfaces.

Samples	N [w/w]	Samples	N [w/w]	ΔN
Pure PCL (2.28 mg)	*0.0016*			
PCL_01 (0.55 mg)	0.020	PCL_01_F (0.23 mg)	0.086	0.066
PCL_03 (0.33 mg)	0.016	PCL_03_F (0.25 mg)	0.060	0.044
PCL_04 (1.01 mg)	0	PCL_04_F (0.32 mg)	0.034	0.034

The colorimetric assay verified that PCL_01 was the more functionalized layer, supporting the previous XPS results. Unexpectedly, PCL_04 resulted in a zero value for functionalization, and Pure PCL (layers not submitted to any kind of treatment) presented a content of N atoms, contradicting it hydrophobic character. However, the nitrogen content analysis for the layers with posterior functionalization with protein immobilization has increased; a measurement that had given inconclusive results in the XPS analysis. It suggested the presence of well-oriented amino groups able to covalently link to HVP. The concentration of APTES is proportional to the concentration of the immobilized molecules at the surface. The functionalization resulted, in terms of HVP present at the surface, from an increase to a decrease in it concentration, in PCL_01_F, PCL_03_F, and PCL_04_F, with positive influence in all cases, allowing to create a gradient from adhesive molecules at the surface for further studies.

5.4 Cell adhesion

A covalent binding method was used to immobilize HVP on the surface of electrospun layers. The film created was used to test the adhesion activity of osteoblastic cells. Cell adhesion properties of the silanized and bio-functionalized were compared and are shown in Figure 5.7. Adhesion of cultured osteoblasts on PCL nanofibres was evaluated by MTT assay after incubating cells for 2 hours. Data are reported as mean and standard deviation (SD) of three measurements. Figure 5.7 a) illustrates the number of cells that adhere to the control PCL matrix (C) and the number of cells that adhere to the PCL matrices after plasma treatment 01, 03, and 04 (PCL_01, PCL_03, and PCL_04, respectively). Figure 5.7 b) illustrates the comparison in cell adhesion

between the matrices submitted to different plasma treatment and the matrices with further functionalization with HVP peptide. This graph reported the (number of cells on HVP functionalized electrospun matrix measured with MTT assay/number of cells seeded on electrospun matrix)×100. Data is reported as mean±SD. Statistical analysis was performed using the paired Student's *t*-test, using Graph-Pad Prism 3.03 (San Diego, California, USA). *P* values <0.05 (Figure 5.7 a)) and *P* values <0.01 (Figure 5.7 b)) were considered statistically significant. Plasma treatment improves osteoblast adhesion, but the different plasma treatments do not modify cell adhesion. The increase in the case PCL_01 (Figure 57 b) is significant with respect to its control. The trend is an improvement of osteoblast adhesion due to functionalization. The anchoring of HVP is important and scaffold treated differently by plasma give the possibility to modify HVP concentration and osteoblast are influenced by different peptide concentration.

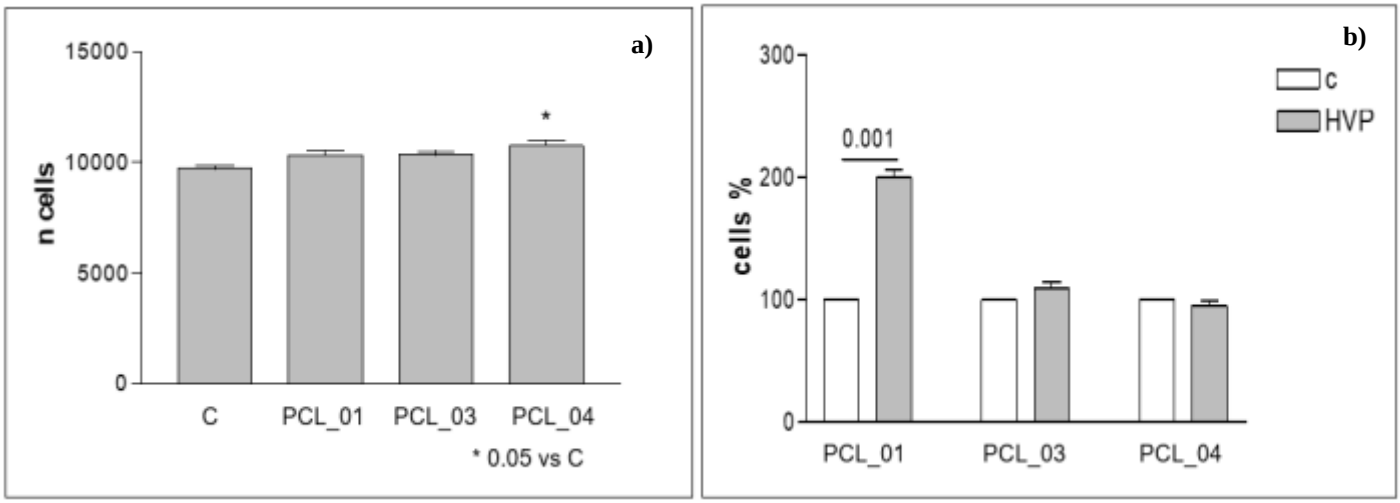

Figure 5.7 a) Comparison of cell adhesion on control matrix and matrices submitted to different plasma treatments. Data are reported as mean ± standard error of three independent experiments. * *P* < 0.05 vs. Control surface; b) Comparison of number of cells between matrices with different plasma treatments and the matrices bio-functionalized with HVP. Data are expressed as mean ± standard error of three independent experiments. P < 0.01 vs. silanized surfaces.

Cell adhesion onto the layers enriched with HVP was greater than silanized layers, excepting for 04. It was verified the highest adhesion in the substrate 01, the same sample that had also resulted in the substrate with higher concentration of APTES. This permits to conclude that cells recognized the surface chemistries provided by the silanization, which had influenced their attachment. When comparing both functionalized with HVP layers and layers only submitted to plasma treatment, it gives an important result indicating that the cell adhesion does not depend on the surface treatment, but in the concentration of HVP immobilized. In fact, plasma treatment had no significant effect on cell adhesion; however, it directs the immobilization of adhesive proteins, inducing an increase of the adherent cells through protein immobilization. Cells were more prone to adhere to the substrate presenting HVP at its surface, even if an uncommon situation happened for 04 layers, where cells adhere more to the layer without bio-functionalization. This confirms the previous idea that cell adhesion not only depends in the presence of HVP, but it is also concentration-dependent of this molecule. Adhesion in plasma treated samples was poor, yet, cells reflected some cellular adhesion.

It was first observed that in two cases the presence of HVP favoured the cell adhesion, indicating that cells recognized the properties of the molecule as a chemotactic cue. But, it does not allow the creation of a well-defined gradient along the scaffold. The concentration of HVP should increase along the scaffold as the driving forces for cells to migrate and proliferate within are expected to decrease due to the restrictions imposed by the structure itself. Since it was not possible to prove the efficiency of this method for all layers, the desired gradient will be always susceptible to failure. Plasma surface treatment through APP has been demonstrated as a well suitable technique to develop interfaces capable to improve cell adhesion at the implant surfaces.[98,99] However, the unfavourable results can be assigned to an inaccurate surface treatment using this method. Some of the main factors to explain the poor cell adhesion in the bio-functionalized layers can be related to an inadequate selection of the PCL silanized layer, as a result obtained from the operating parameters used in the APPJ, to a possible formation of a vertical multi-layering created with APTES deposited, compromising the silanization and leaving less functional groups to react with HVP, to the time for incubation, that may have not been enough for cells to detect the presence of surface chemistries and stablish interactions with them, to the number of cells seeded. Although, these results have given important indications point for further functionalization. Nevertheless, PCL layers were used to perform the assembly of the scaffold to evaluate their influence in cells functions and to complement, or contradict, the results described in this section.

5.5 Cell migration into designed 3D scaffold

To observe cell attachment and proliferation on/within the scaffolds, fluorescent images were taken on the 3rd day of seeding by confocal microscope immediately after fixing the cells. Both scaffolds, functionalized and control were investigated. Confocal microscope permits to obtain images with reduced blurring, in the perpendicular and parallel optical sections. Confocal microscope can penetrate the sample and scan it with a maximum depth of 50 μm. The scaffold resulted in a thickness of 0.229 ± 0.005 (mm) and 0.320 ± 0.005 (mm) for functionalized and control, respectively. Since confocal microscope was not able to scan all the thickness of the matrix, was first examined the top of the scaffold (where the cells were seeded), collecting the images until possible depth, and then, was examined the bottom (where is supposed to start the regeneration process), until the depth where the presence of the first cells could be detectable.

After 3 days of seeding, the cells could migrate, at least, till a depth of 50 μm. Functionalized scaffold presented, at this depth, significant cell's populations (in green), as showed in Figure 5.8. The images were taken from different regions of the same *xy* plane. Comparing with the control scaffold, it is notable the increase in cell number, indicating the benefits of rhFGF in sustaining cell proliferation in the functionalized architecture. The presence of cells at this depth can also demonstrate and prove the existence of sufficient and interconnected porosity allowing cells to travel within the structure. It is important to note the presence of cells in the control scaffold at 40 μm, evidencing the existence of some hydrophobic character and cell's ability to perform their functions, yet narrowly, in environments with the same characteristics.

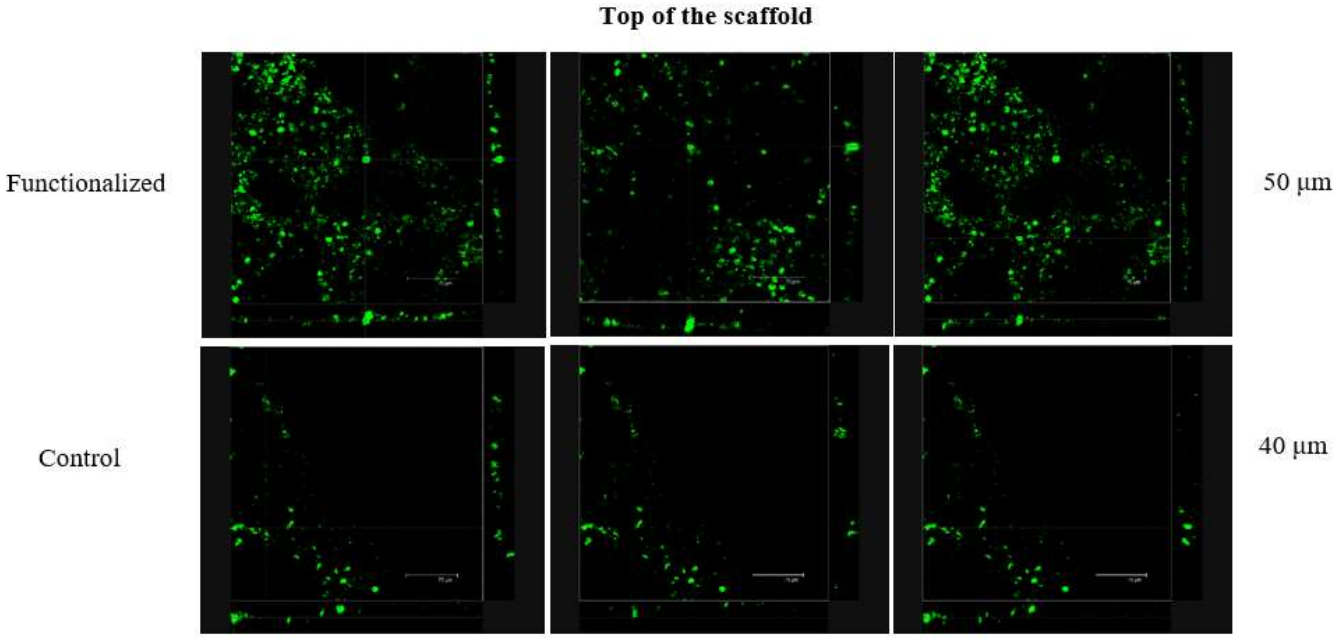

Figure 5.8 Confocal microscope images for the top of the scaffold. Above, cell migration at a depth of 50 μm in the functionalized scaffold, after 3 days of culture. Below, cell migration at a depth of 40 μm in control scaffold, after 3 days of culture.

While examining the bottom of the scaffold, a substantial difference in cell number could be distinguished. Fluorescent signals at the bottom of the scaffold were barely detectable, indicating the absence of cellular populations at the bottom. Images were taken along the *z*-axis (from bottom to top) and the first cells were observed at a depth of 30 μm and 17 μm for functionalized and control scaffolds, respectively, were scarce cells appeared, and the concentration of cell's populations is practically inexistent, Figure 5.9. Morphological restrictions, low porosity or porosity conditioned by the insertion and immobilization of biological moieties, and well as inappropriate concentrations of these molecules to create the gradient, are the basic findings to explain the break in cell proliferation and migration. Also, the insufficient seeding period, hydrogel concentration, and the fact of the assembly of the scaffold had been done manually are aspects that can influence the migration of the cells within the structure. Cells were closer to the bottom in the scaffold for control. This fact does not guarantee more efficiency when compared to the functionalized scaffold, since the seeding was

done in an open petri dish and cells could have been detached from the structure and reached these regions through the culture medium.

The scaffold's thickness presents a contradictory result. It was expected a thickness in the range of 0.30 to 0.50 mm, with a thicker structure for the functionalized scaffold. However, the assembly faced some problems in the stacking due to the vulnerability of the system that may had influenced the final thickness.

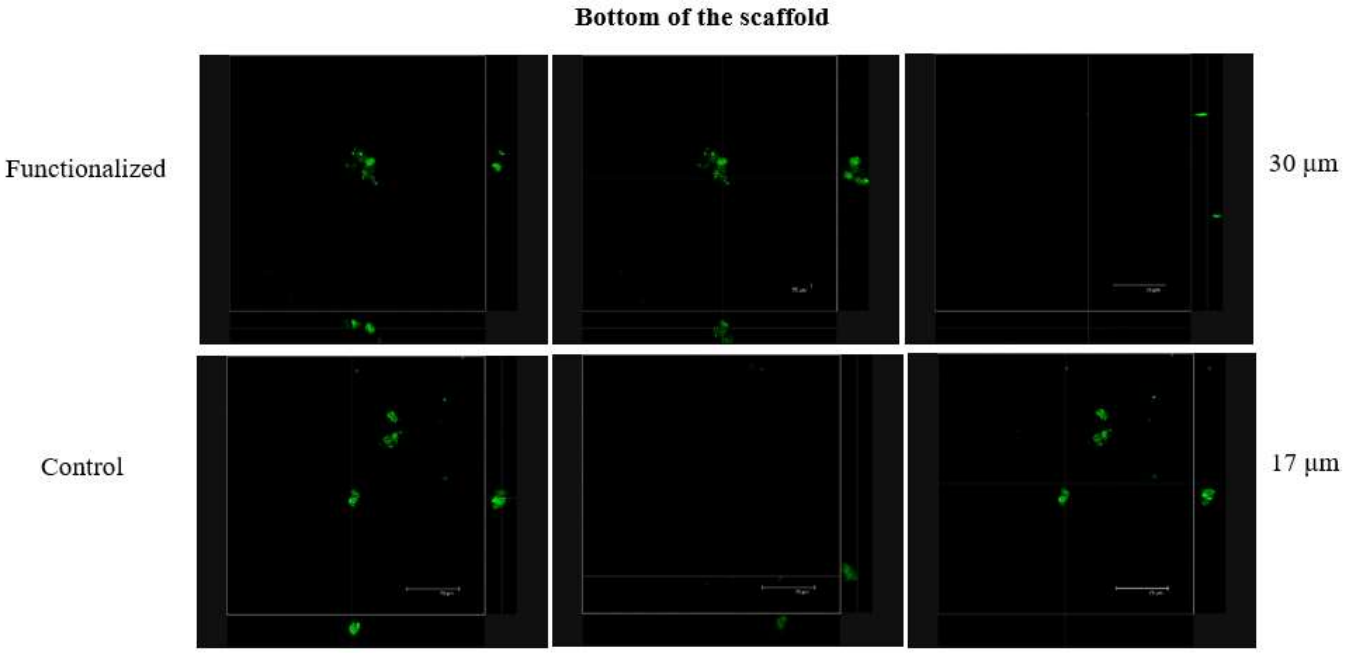

Figure 5.9 Confocal microscope images for the bottom of the scaffold. Above, presence of cells at 30 µm from the bottom in the functionalized scaffold. Below, presence of cells at 17 µm from the bottom, in the control scaffold, after 3 days of culture.

When assembling, we faced two major problems: a trouble in stack the PCL bio-functionalized layers in the frames, and the difficulty to produce hydrogels in appropriate concentration. Hydrogel concentration was selected based on the experiments of Koutsopoulos, S. *et al.*, where they studied the release kinetics for a variety of proteins in a wide range of molecular mass, hydrodynamic radii, and isoelectric point.[100] The release studies consisted in the determination of the diffusion coefficients of lysozyme, trypsin inhibitor, BSA, and IgG presented inside a nanofibre SAP-hydrogel scaffold and released into solution, using the single-molecule approach. The release kinetics suggested that protein diffusion through nanofibre hydrogels depended primarily on the size of the protein. rhFGF and IL–6 are in the same range of molecular mass and size of the proteins used in this study, where the release was performed through 1% (wt/vol) peptide hydrogel. This concentration was adopted to build the EAK 16–II hydrogel; however, when assembling, the hydrogel formed a single dense drop on the PCL surfaces, which was then spread out of the matrix when the next PCL layer was placed on its top. In the following layers, 0.5% (wt/vol) peptide hydrogel was produced, but the material was completely absorbed by the PCL layers. These observations demonstrate unsuitable hydrogel concentration for incorporating the soluble molecules and to form interwoven nanofibre controlled structure. It was not perceptible if the failure to

obtain the hydrogel was due to its concentration, or if it is related to the concentration of the growth factors/inflammatory cytokines. On other hand, the problem with PCL nanofibres is due to is vulnerability to rupture after functionalization. As the available material was not enough to produce samples bigger than 1x1 cm^2, at this area, the samples easily bend, and it is difficult to place them straight on the frames. These problems directly influenced the success of the final 3D structure, and, consequently, cell migration since the layers were not concentric, neither intact along the scaffold.

CHAPTER 6 – CONCLUSIONS

A nano-fibrous biomimetic scaffold was developed by assembling PCL nanofibres layers with hydrogels from self-assembling peptides into a 3D structure. PCL nanofibres were obtained by electrospinning, where the working parameters were studied and tuned to obtain fibres with diameters in the nano-range. Nano-fibres with average diameter of 190 nm were obtained for a concentration of 30% of PCL in HFIP, at a flow rate of 0.2 mL h^{-1} in the presence of coaxial air flow (0.2 bar), at a tip-target distance of 30 cm. The collected fibres were submitted to a surface plasma treatment and the SEM analysis verified that this treatment had no significant effect on the PCL matrices in terms of porosity and fibre topography. However, PCL surface treatment by Ar-driven APP successfully resulted in a significant increase of the surface hydrophilicity, allowing the anchor of the bioactive molecule HVP at different concentrations. Plasma treatment improves osteoblast adhesion, but the different plasma treatments do not modify cell adhesion. *h*-osteoblast adhesion on the surfaces has revealed to be concentration-dependent of HVP molecules. Control and bio-functionalized scaffolds manifested limitations for cell migration from the top to the bottom after a super attack of 3 days. The introduction of chemical guidance molecules permitted a better cell proliferation in the bio-functionalized scaffold, where it could be seen the presence of considerable cell's populations until a depth of 50 μm, from the top to the bottom.

It was expected to develop a novel bone substitute capable to promote osteoblasts penetration along the entire bony support. The experiment presented some barriers along the process, although some remarkable conclusions could be taken from what was investigated. First, it was confirmed the efficiency of APP as a successful surface plasma treatment to contradict the original hydrophobic character of PCL. This fact contributed to the immobilization of HVP that, even though it has not been possible to determine it precise concentration, was capable to enhance cell attachment for some of the treatment conditions studied. Cell attachment, proliferation and migration is essential for long-term success of the implant. The provided scaffold offered some constraints to the cell's functions through it thickness. An excessive density of hydrogel, after incorporation of rhFGF was point out as one of the reasons for unaccomplished scaffold design.

6.1 Future perspectives

Once it was not possible to demonstrate the efficiency of the designed scaffold for cell proliferation and migration, future studies are recommended to optimize both individual systems that constitute the idea here presented. In author's opinion, the first step should be optimizing APP parameters and perform new XPS studies to obtain correct silanization of the matrices, in a way to guarantee a more suitable immobilization of the adhesive molecules. In a first approach, plasma surface treatment seemed to enhance the surfaces capability to immobilize bioactive molecules, however, the silanization performed was not successful to obtain a coherent gradient able to be employed in the scaffold as it was firstly thought. After obtaining a coherent and efficient

gradient, biological assays should be investigated. For these studies, at least three replicates per sample should be done to confirm the results. The author suggests that should be created, besides a control scaffold as the one described, a scaffold in which was possible to investigate the influence of each single molecule, HVP, rh-FGF and IL-6, in the cell's viability. The comparison of all these structures will allow to conclude about the most valuable cues for signalize cells and establish a more accurate regeneration process.

ACKNOWLEDGEMENTS

The author is grateful to Alessandro Maffei for having studied the Electrospinning and the APPJ operating parameters, to Professor Alessandro Patelli from Physics Department in University of Padua and Dr. Paolo Scopece from Cà Foscari University, Mestre, Venice, for their help in surface treatment with APPJ and SEM analysis, to Professor Paola Brun from Department of Molecular Medicine in University of Padua, for having conducted all the biological assays, and to Department of Chemistry from University of Catania for having performed the contact angle measurements.

REFERENCES

1. Zamuner, A. *et al.* Smart biomaterials: Surfaces functionalized with proteolytically stable osteoblast-adhesive peptides. *Bioact. Mater.* **2,** 121–130 (2017).
2. Woolf, A. D. & Pfleger, B. Burden of major musculoskeletal conditions. *Bull. World Health Organ.* **81,** 646–656 (2003).
3. Reeder, S. B., Hu, H. H., Sirlin, C. B., Group, L. I. & Diego, S. HHS Public Access. **36,** 1011–1014 (2016).
4. Yu, X., Tang, X., Gohil, S. V. & Laurencin, C. T. Biomaterials for Bone Regenerative Engineering. *Adv. Healthc. Mater.* **4,** 1268–1285 (2015).
5. O'Brien, F. J. Biomaterials & scaffolds for tissue engineering. *Mater. Today* **14,** 88–95 (2011).
6. Matassi, F., Nistri, L., Paez, D. C. & Innocenti, M. New biomaterials for bone regeneration. *Clin. Cases Miner. Bone Metab.* **8,** 21–24 (2011).
7. Jin, L. *et al.* Electrospun Fibres and Tissue Engineering. *J. Biomed. Nanotechnol.* **8,** 1–9 (2012).
8. Ahmed, E. M. Hydrogel : Preparation , characterization , and applications : A review. *J. Adv. Res.* **6,** 105–121 (2015).
9. Suwantong, O. Biomedical applications of electrospun polycaprolactone fibre mats. *Polym. Adv. Technol.* **27,** 1264–1273 (2016).
10. Yang, J. Peptide-directed self-assembly of hydrogels q. **5,** 805–816 (2009).
11. Habibi, N. *et al.* HHS Public Access. **11,** 41–60 (2017).
12. Ravaglioli, A. & Krajewski, A. *Bioceramics: materials, properties and applications*. *London: Chapman & Hall* (1992).
13. (US), O. of the S. G. Bone Health and Osteoporosis: A Report of the Surgeon General. (2004).
14. Nakamura, H. Morphology , Function , and Differentiation of Bone Cells. *J. Hard Tissue Biol.* **16,** 15–22 (2007).
15. Asha Shekaran, A. J. G. Repair. *J. Biomed. Mater. Res.* **96,** 261–272 (2012).
16. Mathews, S., Bhonde, R., Gupta, P. K. & Totey, S. Extracellular matrix protein mediated regulation of the osteoblast differentiation of bone marrow derived human mesenchymal stem cells. *Differentiation* **84,** 185–192 (2012).
17. Zreiqat, H., Dunstan, C. & Rosen, V. *A Tissue Regeneration Approach to Bone and Cartilage Repair*. *Springer* (2015). doi:10.1007/978-3-319-13266-2
18. Dirckx, N., Van Hul, M. & Maes, C. Osteoblast recruitment to sites of bone formation in skeletal development, homeostasis, and regeneration. *Birth Defects Res. Part C - Embryo Today Rev.* **99,** 170–191 (2013).
19. Ten Cate, A. *Histologia Oral. Desarollo, estrutura y funcion*. (1986).

20. Ziats, N., Miller, K. & Anderson, J. In vivo and in vitro interactions of cells with biomaterials. *Biomaterials* **9,** 5–13 (1988).
21. Rodan, G. Introduction to bone biology. *Bone* **13,** 3–6 (1992).
22. Articles, R. Osteoblast Differentiation at a Glance. 95–106 (2016). doi:10.12659/MSMBR.901142
23. Sela, J. J. & Bab, I. A. *Principles of bone regeneration*. *Principles of Bone Regeneration* (2012). doi:10.1007/978-1-4614-2059-0
24. Schneider, R. & Helms, J. The cellular and molecular origins of beak morphology. *Science (80-.).* **299,** 565–568 (2003).
25. Bagorda, A. & Parent, C. A. Eukaryotic chemotaxis at a glance. *J. Cell Sci.* **121,** 2621–2624 (2008).
26. Sanchez-Fernandez, M. A., Gallois, A., Riedl, T., Jurdic, P. & Hoflack, B. Osteoclasts control osteoblast chemotaxis via PDGF-BB/PDGF receptor beta signaling. *PLoS One* **3,** (2008).
27. Wang, X. *et al.* Growth factor gradients via microsphere delivery in biopolymer scaffolds for osteochondral tissue engineering. *J. Control. Release* **134,** 81–90 (2009).
28. Babensee, J. E., McIntire, L. V. & Mikos, A. G. Growth factor delivery for TE. *Pharmacol. Res.* **17,** 497–504 (2000).
29. Chung, Y. I. *et al.* Enhanced bone regeneration withe BMP-2 loaded functional nanoparticle-hydrogel complex. *J. Control. Release* **121,** 91–99 (2007).
30. Bergmann, C. P. & Stumpf, A. Dental ceramics: Microstructure, properties and degradation. *Dent. Ceram. Microstruct. Prop. Degrad.* 1–84 (2013). doi:10.1007/978-3-642-38224-6
31. Loh, Q. L. & Choong, C. Three-Dimensional Scaffolds for Tissue Engineering Applications: Role of Porosity and Pore Size. *Tissue Eng. Part B Rev.* **19,** 485–502 (2013).
32. Jiang, T., Carbone, E. J., Lo, K. W. H. & Laurencin, C. T. Electrospinning of polymer nanoFibres for tissue regeneration. *Prog. Polym. Sci.* **46,** 1–24 (2015).
33. Bhardwaj, N. & Kundu, S. C. Electrospinning: A fascinating fibre fabrication technique. *Biotechnol. Adv.* **28,** 325–347 (2010).
34. Goh, Y. F., Shakir, I. & Hussain, R. Electrospun Fibres for tissue engineering, drug delivery, and wound dressing. *J. Mater. Sci.* **48,** 3027–3054 (2013).
35. Eslahi, N., Abdorahim, M. & Simchi, A. Smart Polymeric Hydrogels for Cartilage Tissue Engineering: A Review on the Chemistry and Biological Functions. *Biomacromolecules* **17,** 3441–3463 (2016).
36. De Mori, A., Peña Fernández, M., Blunn, G., Tozzi, G. & Roldo, M. 3D Printing and Electrospinning of Composite Hydrogels for Cartilage and Bone Tissue Engineering. *Polymers (Basel).* **10,** 285 (2018).
37. Horii, A., Wang, X., Gelain, F. & Zhang, S. Biological designer self-assembling peptide nanofibre scaffolds significantly enhance osteoblast proliferation, differentiation and 3-D migration. *PLoS One* **2,** 1–9 (2007).
38. Bokhari, M. A., Akay, G., Zhang, S. & Birch, M. A. The enhancement of osteoblast growth and differentiation in vitro on a peptide hydrogel - PolyHIPE polymer hybrid material. *Biomaterials* **26,** 5198–5208 (2005).

39. Danesin, R. *et al.* Self-assembling peptide-enriched electrospun polycaprolactone scaffolds promote the h-osteoblast adhesion and modulate differentiation-associated gene expression. *Bone* **51,** 851–859 (2012).
40. Khorshidi, S. & Karkhaneh, A. A review on gradient hydrogel/fibre scaffolds for osteochondral regeneration. *J. Tissue Eng. Regen. Med.* 1–17 (2018). doi:10.1002/term.2628
41. Zhang, X. *Science and Principles of Biodegradable and Bioresorbable Medical Polymers: Materials and Properties*.
42. Brun, P. *et al.* Acta Biomaterialia Mechanisms underlying the attachment and spreading of human osteoblasts : From transient interactions to focal adhesions on vitronectin-grafted bioactive surfaces. *Acta Biomater.* **9,** 6105–6115 (2013).
43. Iucci, G. *et al.* Novel immobilizations of an adhesion peptide on the TiO2 surface: An XPS investigation. *Mater. Sci. Eng. C* **27,** 1201–1206 (2007).
44. Visser, R., Rico-Llanos, G. A., Pulkkinen, H. & Becerra, J. Peptides for bone tissue engineering. *J. Control. Release* **244,** 122–135 (2016).
45. Wichterle, O. & Lím, D. Hydrophilic Gels for Biological Use. *Nature* **185,** 117–118 (1960).
46. Bahram, M., Mohseni, N. & Moghtader, M. An Introduction to Hydrogels and Some Recent Applications. *Emerg. Concepts Anal. Appl. Hydrogels* (2016). doi:10.5772/64301
47. Fichman, G. & Gazit, E. Acta Biomaterialia Self-assembly of short peptides to form hydrogels : Design of building blocks , physical properties and technological applications q. *Acta Biomater.* **10,** 1671–1682 (2014).
48. Maitra, J. & Shukla, V. K. Cross-linking in Hydrogels - A Review. *Am. J. Polym. Sci.* **4,** 25–31 (2014).
49. Loo, Y., Zhang, S. & Hauser, C. A. E. From short peptides to nanofibres to macromolecular assemblies in biomedicine. *Biotechnol. Adv.* **30,** 593–603 (2012).
50. Eskandari, S., Guerin, T., Toth, I. & Stephenson, R. J. Recent advances in self-assembled peptides : Implications for targeted drug delivery and vaccine engineering ☆. *Adv. Drug Deliv. Rev.* **110–111,** 169–187 (2017).
51. Tsutsumi, H. & Mihara, H. Soft materials based on designed self-assembling peptides: from design to application. *Mol. Biosyst.* **9,** 609 (2013).
52. Xu, D., Samways, D. S. K. & Dong, H. Bioactive Materials Fabrication of self-assembling nano fi bers with optimal cell uptake and therapeutic delivery ef fi cacy. *Bioact. Mater.* 1–9 (2017). doi:10.1016/j.bioactmat.2017.09.001
53. Mendes, A. C., Baran, E. T., Reis, R. L. & Azevedo, H. S. Self-assembly in nature: Using the principles of nature to create complex nanobiomaterials. *Wiley Interdiscip. Rev. Nanomedicine Nanobiotechnology* **5,** 582–612 (2013).
54. Zhang, S., Lockshin, C., Herbert, a, Winter, E. & Rich, a. Zuotin, a putative Z-DNA binding protein in Saccharomyces cerevisiae. *EMBO J.* **11,** 3787–3796 (1992).

55. Holmes, T. C. *et al.* Extensive neurite outgrowth and active synapse formation on self-assembling peptide scaffolds. *Proc. Natl. Acad. Sci.* **97,** 6728–6733 (2000).
56. Chen, P. Self-assembly of ionic-complementary peptides: A physicochemical viewpoint. *Colloids Surfaces A Physicochem. Eng. Asp.* **261,** 3–24 (2005).
57. Mandal, D., Nasrolahi Shirazi, A. & Parang, K. Self-assembly of peptides to nanostructures. *Org. Biomol. Chem.* **12,** 3544–3561 (2014).
58. Pauling, L. & Corey, R. B. Configurations of Polypeptide Chains with Favored Orientations Arounf Single Bonds. *Proc. Natl. Acad. Sci. USA* **37,** 729–740 (1951).
59. Schweitzer-Stenner, R. *Protein and Peptide Folding, Misfolding and Non-Folding*. (2012). doi:10.1002/9781118183373
60. Misawa, H. *et al.* PuraMatrix facilitates bone regeneration in bone defect of calvaria in mice. *Cell Transpl.* **15,** 903–910 (2006).
61. Zhang, S., Ellis-behnke, R. & Zhao, X. PuraMatrix : Self-assembling Peptide Nanofibre Scaffolds. 1–31
62. Ramakrishna, S., Fujihara, K., Teo, W.-E., Lim, T.-C. & Ma, Z. *An Introduction to Electrospinning and NanoFibres*. (World Scientific, 2005).
63. Deitzel, J. M. *et al.* Generation of Polymer NanoFibres Through Electrospinning. (1999).
64. Garg, K. & Bowlin, G. L. Electrospinning jets and nanofibrous structures. *Biomicrofluidics* **5,** 1–19 (2011).
65. Uchko, C. J., Chen, L. C., Shen, Y. & Martina, D. C. Processing and microstructural characterization of porous biocompatible protein polymer thin films. *Polymer (Guildf).* **40,** 7397–7407 (1999).
66. De Vrieze, S. *et al.* The effect of temperature and humidity on electrospinning. *J. Mater. Sci.* **44,** 1357–1362 (2009).
67. Jarusuwannapoom, T. *et al.* Effect of solvents on electro-spinnability of polystyrene solutions and morphological appearance of resulting electrospun polystyrene Fibres. *Eur. Polym. J.* **41,** 409–421 (2005).
68. Li, D. & Xia, Y. *Advanced Materials*. (2004).
69. Azimi, B., Nourpanah, P., Rabiee, M. & Arbab, S. Poly (lactide -co- glycolide) Fibre : An Overview. *J. Eng. Fibre. Fabr.* **9,** 74–90 (2014).
70. Woodward, C. S. The intracellular degradation of poly (epsilon-caprolactone). *J. Biomed. Mater. Res.* **19,** 437–444 (1985).
71. Mann, B. K. & West, J. L. Cell adhesion peptides alter smooth muscle adhesion, proliferation, migration and matrix protein syntheis on modified surfaces and in polymer scaffolds. *J. Biomed. Mater. Res.* **60,** 86–93 (2002).
72. Wulf, K. *et al.* Surface functionalization of poly(ε-caprolactone) improves its biocompatibility as scaffold material for bioartificial vessel prostheses. *J. Biomed. Mater. Res. - Part B Appl. Biomater.* **98 B,** 89–100 (2011).

73. Dettin, M. *et al.* Electrospun scaffolds for osteoblast cells: Peptide-induced concentration-dependent improvements of polycaprolactone. *PLoS One* **10,** 1–23 (2015).
74. Yamaguchi, M. *et al.* Surface modification of poly(L-lactic acid) affects initial cell attachment, cell morphol-ogy, and cell growth. *J. Artif. Organs* **7,** 187–193 (2004).
75. Gregory A. Grant. *Synthetic Peptides - A user's guide*. (2002).
76. Pires, D. A. T., Bemquerer, M. P. & Do Nascimento, C. J. Some mechanistic aspects on Fmoc solid phase peptide synthesis. *Int. J. Pept. Res. Ther.* **20,** 53–69 (2014).
77. Amblard, M., Fehrentz, J.-A., Martinez, J. & Subra, G. Methods and Protocols of Modern Solid Phase Peptide Synthesis. *Mol. Biotechnol.* **33,** 239–254 (2006).
78. Luna, O. F. *et al.* Deprotection Reagents in Fmoc Solid Phase Peptide Synthesis : Moving Away from Piperidine ? 1–12 doi:10.3390/molecules21111542
79. Hood, C. A. *et al.* Fast conventional Fmoc solid-phase peptide synthesis with. 97–101 (2008). doi:10.1002/psc
80. Friedman, M. Applications of the Ninhydrin Reaction for Analysis of Amino Acids, Peptides, and Proteins to Agricultural and Biomedical Sciences. *J. Agric. Food Chem.* **52,** 385–406 (2004).
81. Support, T. Technical Support Information Bulletin 1188. **289,** 2–3 (1997).
82. Online, V. A., Dagaut, P. & Shahla, R. RSC Advances An alternative to trial and error methodology in solid phase extraction : an original automated solid phase extraction procedure for analysing PAHs and. **19,** 33636–33644 (2014).
83. Waters. Waters. The science of what's possible. (2018).
84. Vydac, G. The handbook of analysis and purification of peptides and proteins by reversed-phase HPLC. *Hesperia, CA, USA Grace Vydac* **0924,** 36 (2002).
85. Carr, D. A Guide to the Analysis and Purification of Proteins and Peptides by Reversed-Phase HPLC. *A Guid. to Anal. Purif. Proteins Pept. by Reversed-Phase HPLC* (2005).
86. Patelli, A., Verga Falzacappa, E., Scopece, P., Pierobon, R. & Vezzu′, S. Method for generating an atmospheric plasma jet and atmospheric plasma minitorch device. *Wo2015071746* 18 (2016).
87. Manuscript, A. & Oxime, R. NIH Public Access. **19,** 2543–2548 (2009).
88. Elahipanah, S., O'Brien, P. J., Rogozhnikov, D. & Yousaf, M. N. General Dialdehyde Click Chemistry for Amine Bioconjugation. *Bioconjug. Chem.* **28,** 1422–1433 (2017).
89. Algar, W. R. A Brief Introduction to Traditional Bioconjugate Chemistry. *Chemoselective Bioorthogonal Ligation React.* 1–36 (2017). doi:10.1002/9783527683451.ch1
90. Bracco, G. & Holst, B. *Surface science techniques*. *Springer Series in Surface Sciences* **51,** (2013).
91. Reagents, I. Nitrogen Determination by Kjeldahl Method. 2–11 (2015).
92. Life, T. No Title. **26,** 111–120 (2015).
93. Ozkan, O. & Turkoglu Sasmazel, H. Effects of nozzle type atmospheric dry air plasma on L929 fibroblast cells hybrid poly (ε-caprolactone)/chitosan/poly (ε-caprolactone) scaffolds interactions. *J. Biosci. Bioeng.* **122,** 232–239 (2016).

94. Zavattin, D. Matrici elettrofilate ibride per l'ingegneria del tessuto osseo: valutazione dell'arrichimento progressivo della fibre con peptide auto-aggreganti. (2014).
95. Zhang, Z. L., Crozatier, C., Le Berre, M. & Chen, Y. In situ bio-functionalization and cell adhesion in microfluidic devices. *Microelectron. Eng.* **78–79,** 556–562 (2005).
96. Acres, R. G. *et al.* Molecular structure of 3-aminopropyltriethoxysilane layers formed on silanol-terminated silicon surfaces. *J. Phys. Chem. C* **116,** 6289–6297 (2012).
97. Argekar, S. U., Kirley, T. L. & Schaefer, D. W. Determination of structure-property relationships for 3- aminopropyltriethoxysilane films using x-ray reflectivity. *J. Mater. Res.* **28,** 1118–1128 (2013).
98. Mussano, F. *et al.* In vitro characterization of two different atmospheric plasma jet chemical functionalizations of titanium surfaces. *Appl. Surf. Sci.* **409,** 314–324 (2017).
99. Liu, W. *et al.* Effects of plasma treatment to nanoFibres on initial cell adhesion and cell morphology. *Colloids Surfaces B Biointerfaces* **113,** 101–106 (2014).
100. Koutsopoulos, S., Unsworth, L. D., Nagai, Y. & Zhang, S. Controlled release of functional proteins through designer self-assembling peptide nanofibre hydrogel scaffold. **106,** (2009).
101. Alford, A. I., Kozloff, K. M. & Hankenson, K. D. Extracellular matrix networks in bone remodeling. *Int. J. Biochem. Cell Biol.* **65,** 20–31 (2015).
102. Jun, S. *et al.* Self-Assembly of the Ionic Peptide EAK16 : The Effect of Charge Distributions on Self-Assembly. **87,** 1249–1259 (2004).
103. Aguiar, L. Síntese de Péptidos Antimicrobianos e Penetradores Celulares. (2014).